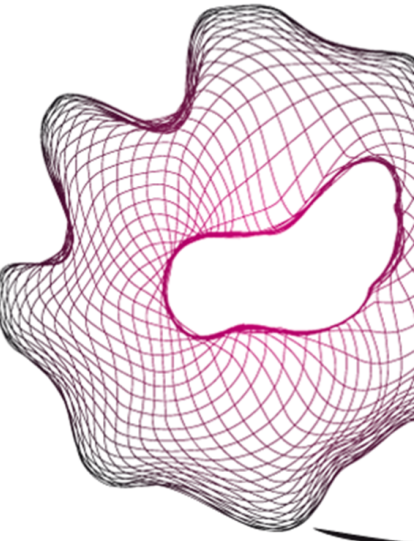


# UNIVERSITY OF TWENTE.

Faculty of Engineering Technology,  
Civil Engineering & Management



## The influence of a grid structure on hydraulic river modelling outcomes of river meanders

Master thesis

Eray Bilgili  
October 2020



---

**Head graduation committee:**  
prof.dr. S.J.M.H. Hulscher

**Supervisors:**  
dr.ir. A. Bomers  
dr. F. Huthoff  
ir. J.G.W. van Lente

Faculty of Engineering Technology  
Civil Engineering & Management  
University of Twente  
7522 NB Enschede  
The Netherlands

---



## Preface

Before you lies the thesis report 'The influence of a grid structure on hydraulic river modelling outcomes of river meanders'. This thesis finalises my master study in Water Engineering & Management at the University of Twente. The research is carried out in cooperation with HKV lijn in water. From April 2020 to October 2020, I was engaged in researching and writing this thesis report. Due to the Coronavirus, I was forced to conduct the research in my home office in Hengelo (Overijssel). Nonetheless, I am grateful to HKV lijn in water for their online support in those difficult circumstances.

I would like to extend my deepest gratitude to the entire graduation committee, Jan-Willem van Lente, Anouk Bomers, Freek Huthoff and Suzanne Hulscher for their interest and feedback during the research. Jan-Willem, thank you for your strong commitment, enthusiasm and for providing help during the research. Anouk, thank you for helping me setting up my research plan, and for assisting me to write an academical thesis report. Freek, thank you for your practical help and for the discussions we had from time to time. Suzanne, thank you for the guidance and support during the research.

I am also very grateful to Jurjen de Jong from Deltares and Pieter Roos from the University of Twente. Jurjen, thank you for your passion, which helped my to gain different insights of the topic and for providing me feedback, inspiring ideas and tools during my research. Pieter, thank you for your enthusiasm and delivered insights with respect to the involving mathematics in this topic.

Finally, I would like to thank my family and friends for being supportive and patient during my study and this research. Special thanks go to my sister. Pelin, thank you for your mental support and distracting me from the thesis when I needed it.

I hope that you enjoy reading this thesis report and if you still have any questions left, do not hesitate to contact me.

*Eray Bilgili*

*Hengelo, October 2020*

## Abstract

To evaluate the efficacy and impact of river interventions, a detailed insight in flow patterns in rivers is essential. A common approach to investigate such processes is by making use of hydrodynamic simulations, which solve the (depth-averaged) shallow water equations. In these models, fully triangular and fully curvilinear grids are commonly applied to discretise study areas. A combination of both grid shapes is also possible, which is known as a hybrid grid. Previous studies have shown that the accuracy and computation time of depth-averaged models is substantially influenced by the grid structure.

It has been highlighted that in river models, grid coarsening and poor alignment between grid and the direction of the flow have a diffusive-like appearance, resulting in lower depth-averaged flow velocities and hence higher water depths. These generated numerical effects by a grid are referred to as respectively numerical diffusion and false diffusion. According to previous studies, the former depends on grid resolution, depth-averaged flow velocity and rapid flow changes, whereas the latter relies on the orientation of the grid lines with respect to the flow direction as well as grid resolution and depth-averaged flow velocity. Nonetheless, in previous studies, grid effects are interrelated with how well the bathymetry is captured by a grid. Consequently, it is unclear to what extent effects by grid generation choices influence hydraulic river modelling outcomes, especially in river bends. The objective of this study is to understand under which conditions effects by grid generation choices affect hydraulic river modelling outcomes of river meander bends.

In this study, we performed simulations for hypothetical river meanders and the Grensmaas river, which is a section of the Meuse River, the Netherlands. The hypothetical rivers helped to isolate the effects by grid generation choices on hydraulic modelling outcomes in river meanders and are set up based on the characteristics of the Grensmaas river. The Grensmaas river consists of both mild and sharp bends with large local variations in floodplain width. To capture the extremes of these geometrical characteristics in the Grensmaas river, four hypothetical river schematisations are set up which can be differentiated by a mild or sharp bend and the presence/absence of floodplains.

For the hypothetical cases with floodplains, a constant floodplain height is considered with respect to the bed level of the main channel. Except for the transition between main channel and floodplains, a constant bed level in transverse flow direction is used. All four rivers are forced at the upstream boundary with a constant discharge until similar water levels are obtained between the cases. Three flow scenarios are calculated with each lasting 10 days: (i) low; (ii) mid and (iii) high discharge range. The downstream boundary conditions are set by predefined rating curves based on steady uniform flow considerations. Curvilinear and triangular grids are considered with three different grid resolutions (high, medium and low) in the hypothetical cases with only a main channel. Regarding the resolution in the main channel of the curvilinear grids, 20, 10 and 5 grid cells are placed in the transverse flow direction for respectively the high, medium and low resolution. For the triangular grids, 8, 4 and 3 cells in the transverse flow direction are placed for respectively the high, medium and low resolution. In hypothetical cases where floodplains are present, curvilinear and triangular grids, as well as hybrid grids, are used with only a high and medium grid resolution. For the Grensmaas river, similar grid shapes are constructed as for the hypothetical cases with floodplains. Three levels of grid resolution are examined for the different grids shapes: (i) a high; (ii) a medium grid resolution; and (iii) a locally refined medium resolution grid. D-Flow FM is used as the software to perform the computations.

In terms of the general flood patterns, it was found that an elevated water surface near the outer bank was simulated by all grids in both the hypothetical river meanders as well as in the Grensmaas river. Higher depth-averaged flow velocities are obtained close to

the inner bank at the bend entrance and apex in the main channel of the hypothetical rivers. The opposite occurred at in the river bends of the Grensmaas river, where higher depth-averaged flow velocities are simulated close to the outer bank due to the bed topography. The latter is generally asymmetrical with a shallow (sometimes nearly flat) section extending from the centre of the channel towards the inner bank and a deep portion (pool) located at the outer bank.

The analysis showed that lower depth-averaged flow velocities and hence higher water depths are obtained with coarser grids in the hypothetical river meanders in the absence of floodplains. Even larger deviations are simulated in the sharper bend, as rapid flow changes have to be captured by the grids. These differences are more evident at higher discharges. Regarding the differences between grid shapes, greater numerical effects are obtained with curvilinear grids at lower resolutions than triangular grids. The opposite is observed at highest resolution of both grids.

In contrast to the cases without floodplains, negligible differences are obtained in terms of the water depth in the hypothetical cases with floodplains. This is a consequence of relatively less deviations in depth-averaged flow velocity differences throughout the spatial domain even though considerable differences are present in the main channel.

The results showed that the generated numerical effects become larger in the case with higher discharges and hence higher depth-averaged flow velocities, and under circumstances in which rapid flow changes occur (i.e. for cases with sharp river bends). Furthermore, the results also indicated that numerical effects are proportional to grid resolution, as coarser grids generated lower depth-averaged flow velocities and higher water levels.

In Grensmaas river, greater differences in simulated water levels and depth-averaged flow velocities are obtained compared to the hypothetical river meanders. This showed that the discretisation of the bathymetry plays a more dominant role than numerical effects. In order to simulate water levels and depth-averaged flow velocities accurately, executing a calibration is necessary. Thereby, it is important to address that coarse grids contain larger bed level discretisation errors and hence are more sensitive to calibration.

The influence of the generated numerical effects and the bed level discretisation are dampened by the presence of large floodplains. This indicates that the numerical effects and discretisation errors are both proportional to the discharge per unit width due to relatively less deviations in depth-averaged flow velocity differences throughout the river bend.

The use of a locally refined grid contributed to have water levels and depth-averaged flow velocities which converges towards those of a higher grid resolution. This was a result of better representation of the bathymetry. In terms of the calibration, it is preferable to first carry out a local grid refinement before executing a calibration procedure, as generated numerical and discretised bathymetry errors can differ for locally refined grids and the coarser grids. In practise, however, it can be time expensive to calibrate various grids after each local grid refinement and unnecessary if the locally refined region is small in comparison to the calibrated roughness trajectory. Nonetheless, if small hydrodynamic differences are expected between a coarse and a fine grid, calibrating after a local grid refinement might have minor influences on the model accuracy. Yet, it is recommended that model results from a grid, which is locally refined after calibration, are analysed carefully.

## Contents

<b>1</b>	<b>Introduction</b>	<b>1</b>
1.1	Background . . . . .	1
1.2	Research gap . . . . .	2
1.3	Research objective . . . . .	3
1.4	Research questions . . . . .	3
1.5	Report outline . . . . .	4
<b>2</b>	<b>Methodology</b>	<b>5</b>
2.1	Hydraulic model . . . . .	5
2.1.1	Governing equations . . . . .	5
2.1.2	Discretisation . . . . .	6
2.2	Case study . . . . .	9
2.2.1	Model domain . . . . .	9
2.2.2	Boundary and initial conditions . . . . .	10
2.3	Hypothetical river meanders . . . . .	12
2.3.1	Model domain . . . . .	12
2.3.2	Boundary and initial conditions . . . . .	13
2.4	Grids . . . . .	17
2.4.1	Aspects in grid generation choices . . . . .	17
2.4.2	Constructed grids . . . . .	19
<b>3</b>	<b>Results</b>	<b>29</b>
3.1	Hypothetical river meanders . . . . .	29
3.1.1	Mild river meander (main channel case) . . . . .	29
3.1.2	Sharp river meander (main channel case) . . . . .	32
3.1.3	Floodplain involvement . . . . .	35
3.2	Case study . . . . .	39
3.2.1	River bend (small floodplain areas) . . . . .	39
3.2.2	River bend (wide floodplain areas) . . . . .	41
3.2.3	Local grid refinement . . . . .	44
3.2.4	Computation time . . . . .	46
<b>4</b>	<b>Discussion</b>	<b>47</b>
4.1	Influences of the grid generation choices . . . . .	47
4.1.1	Numerical effects . . . . .	47
4.1.2	Bed level discretisation effects . . . . .	48
4.1.3	Computation time . . . . .	48
4.2	Limitations . . . . .	49
4.3	Implications . . . . .	50
<b>5</b>	<b>Conclusion</b>	<b>53</b>
<b>6</b>	<b>Recommendations</b>	<b>55</b>
6.1	Future research . . . . .	55
6.2	Practical usage . . . . .	56
	<b>References</b>	<b>58</b>
	<b>Appendices</b>	<b>61</b>

---

<b>A</b>	<b>Modified equation one-dimensional advection problem</b>	<b>61</b>
<b>B</b>	<b>Derivation of the pre-defined rating curves</b>	<b>63</b>
<b>C</b>	<b>Grid properties</b>	<b>65</b>
C.1	Hypothetical cases: grids (main channel case) . . . . .	65
C.2	Hypothetical cases: grids (main channel & floodplains case) . . . . .	66
C.3	Close-up locally refined grids . . . . .	67
C.4	Grids case study . . . . .	68
<b>D</b>	<b>Results: hypothetical river meanders</b>	<b>69</b>
D.1	Mild river meander (main channel case) . . . . .	69
D.2	Sharp river meander (main channel case) . . . . .	71
D.3	Mild river meander (main channel and floodplain case) . . . . .	73
<b>E</b>	<b>Results: case study</b>	<b>75</b>
E.1	River bend (small floodplain areas) . . . . .	75
E.2	River bend (wide floodplain areas) . . . . .	77

## List of Figures

2.1	An example of the orthogonality principle for a hybrid grid where the red and blue lines represent respectively the flow links and net links. The angle between the lines is given with $\alpha$ . The red and black dots are the cell centers and nodes respectively. The green dotted lines are the circumscribed circle for a grid cell. . . . .	9
2.2	Shortened model-domain of the pre-release Meuse-model. The trajectory between km-15 and km-55 is the Grensmaas river. The model-domain ranges from km-2 Eijsden till km-64 (Maasbracht). The blue and green colour represent respectively the main channel and floodplains. The computed hydrodynamics in the red regions are considered for the evaluation of the grids. The black lines illustrate the cross-sectional areas we focused on. . . . .	11
2.3	The applied cross-sections in the hypothetical river meander cases with only the main channel. Here, $h$ stands for the water depth in the main channel and $W_m$ for the main channel width. . . . .	14
2.4	The applied cross-sections in the hypothetical river meander cases with the main channel and floodplains. Here, $h$ stands for the water depth in the main channel, $h_f$ for the water depth in the in the floodplains, $W_m$ for the main channel width and $W_f$ for the width of a single floodplain. The distinction in cross-sections is used for deriving the boundary conditions (see Section 2.3.2 and Appendix B). . . . .	15
2.5	A top-view of the four hypothetical river meanders. The land boundaries are given in black. The computed hydrodynamics in the red regions are considered for the evaluation of the grids. The blue lines illustrate the cross-sectional areas. . . . .	16
2.6	An illustration of how the bed level is discretised in (a) the cases with the main channel and (b) the cases with the main channel and floodplains. The solid black lines and filled black circles represent respectively the borders and nodes of the grid cells. The bed level at the cell faces are computed at the red filled circles. The green filled dots symbolise the bed level of a grid cell at the grid center. . . . .	18
2.7	A cross-section view of the bed level in case of the hypothetical river meanders with floodplains. The solid black line is the original bed level. The dotted black line represent the grid lines. The black and green filled circles denote the bed level at the grid nodes and cell faces respectively. The bed level at the cell center positions are given with the red circle. (a) illustrates an increase in the discharge capacity of the main channel when the bed level is discretised on the grid nodes, whereas (b) results in a lower discharge capacity. (De Jong, 2020). . . . .	18
2.8	The six considered grids in the second bend of hypothetical mild river meander without floodplains. The names of the grids are given between brackets: M stands for mild; MC for main channel; Cur and Tri for respectively curvilinear and triangular; and HR, MED and LR for high, medium and low resolution respectively. . . . .	20
2.9	The six considered grids in the second bend of the hypothetical sharp river meander without floodplains. The names of the grids are given between brackets: S stands for sharp; MC for main channel, Cur and Tri for respectively curvilinear and triangular; and HR, MED and LR (see next page) for high, medium and low resolution respectively. . . . .	20

2.9	(continued)	21
2.10	The six considered grids in the second bend of the hypothetical mild river meander with floodplains. The names of the grids are given between brackets: M stands for mild; MCFL for main channel & floodplains; Cur, Tri and Hybr for respectively curvilinear, triangular and hybrid; and HR and MED for high and medium resolution respectively.	22
2.11	The six considered grids in the second bend of the hypothetical sharp river meander with floodplains. The names of the grids are given between brackets: S stands for sharp; MCFL for main channel & floodplains; Cur, Tri and Hybr for respectively curvilinear, triangular and hybrid; and HR and MED for high and medium resolution respectively.	23
2.12	The six considered grids for the case study in the river bend (area of interest) with almost no floodplains (see Figure 2.2). The names of the grids are given between brackets: Grensmaas stands for the Grensmaas river; Cur, Tri and Hybr for respectively curvilinear (as much as possible), triangular and hybrid (see next page); and HR and MED for high and medium resolution respectively.	25
2.12	(Continued)	26
2.13	The three locally refined grids for the case study in the river bends (areas of interest) with almost no and wide floodplains (see Figure 2.2). The names of the grids are given between brackets: Grensmaas stands for the Grensmaas river; Cur, Tri and Hybr for respectively curvilinear (as much as possible), triangular and hybrid (see next page); HR and MED for high and medium resolution respectively; and Loc and Ref for locally and refined respectively.	27
2.13	(Continued)	28
3.1	Cross-sectional view of the simulated water depth for the mild river meander (main channel case) with the highest discharge range at CS 1, CS 2 and CS 3 by the six considered grids. Regarding the names: M stands for mild; MC for main channel; Cur and Tri for respectively curvilinear and triangular; and HR, MED and LR for high, medium and low resolution respectively.	30
3.2	Map-plots of the simulated depth-averaged flow velocities for the mild river meander (main channel case) with the highest discharge range by the six considered grids. Regarding the names: M stands for mild; MC for main channel; Cur and Tri for respectively curvilinear and triangular; and HR, MED and LR for high, medium and low resolution respectively.	31
3.3	Cross-sectional view of the simulated water depth in the sharp river meander (main channel case) for the highest discharge range at CS 1, CS 2 and CS 3 by the six considered grids. Regarding the names: S stands for sharp; MC for main channel; Cur and Tri for respectively curvilinear and triangular; and HR, MED and LR for high, medium and low resolution respectively.	33
3.4	Map-plots of the simulated depth-averaged flow velocities for the sharp river meander (main channel case) with the highest discharge range by the six considered grids. Regarding the names: S stands for sharp; MC for main channel; Cur and Tri for respectively curvilinear and triangular; and HR, MED and LR for high, medium and low resolution respectively.	34
3.5	Cross-sectional view of the simulated water level in the sharp river meander (main channel and floodplain case) for the highest discharge range at CS 1, CS 2 and CS 3 by the six considered grids. Regarding the names: S stands for sharp; MCFL for main channel & floodplains; Cur, Tri and Hybr for respectively curvilinear, triangular and hybrid; and HR and MED for high and medium resolution respectively.	36

3.6	Cross-sectional view of the simulated depth-averaged flow velocity in the sharp river meander (main channel and floodplain case) for the highest discharge range at CS 1, CS 2 and CS 3 by the six considered grids. Regarding the names: S stands for sharp; MCFL for main channel & floodplains; Cur, Tri and Hybr for respectively curvilinear, triangular and hybrid; and HR and MED for high and medium resolution respectively. . . . .	37
3.7	Cross-sectional view of the simulated water levels and depth-averaged flow velocities for the highest discharge range at CS 1.1, CS 1.2 and CS 1.3. Regarding the names: Grensmaas stands for the Grensmaas river; Cur, Tri and Hybr for respectively curvilinear (as much as possible), triangular and hybrid; and HR and MED for high and medium resolution respectively. . .	40
3.8	Cross-sectional view of the simulated water levels and depth-averaged flow velocities for the highest discharge range at CS 2.1, CS 2.2 and CS 2.3. Regarding the names: Grensmaas stands for the Grensmaas river; Cur, Tri and Hybr for respectively curvilinear (as much as possible), triangular and hybrid; and HR and MED for high and medium resolution respectively. . .	42
A.1	An illustration of the induced numerical diffusion in an explicit first-order upwind scheme for the one-dimensional advection problem. The initial value is given by Gaussian function ( $u_0 = \exp(-200(x - 0.25)^2)$ ). The exact and approximated solutions are the velocities profiles after a certain time. . . .	62
B.1	The pre-defined rating curves (Qh-relationships) for the hypothetical river meanders and Grensmaas river at km-55 and km-64. In the legend, mild and sharp refer to respectively the mild and sharp hypothetical river meanders.	64
C.1	Close-up for the three locally refined grids for the case study in the river bend (area of interest) with almost no floodplains (see Figure 2.2). The close-up is focused on the transition between the medium and locally refined bend, which is upstream of river bend. The names of the grids are given between brackets: Cur, Tri and Hybr for respectively curvilinear (as much as possible), triangular and hybrid; HR and MED for high and medium resolution respectively; and Loc and Ref for locally and refined respectively.	67
D.1	Cross-sectional view of the simulated water depth for the mild river meander (main channel case) with the lowest discharge range at CS 1, CS 2 and CS 3 by the six considered grids. Regarding the names: M stands for mild; MC for main channel; Cur and Tri for respectively curvilinear and triangular; and HR, MED and LR for high, medium and low resolution respectively. . .	69
D.2	Map-plots of the simulated depth-averaged flow velocities for the mild river meander (main channel case) with the lowest discharge range by the six considered grids. Regarding the names: M stands for mild; MC for main channel; Cur and Tri for respectively curvilinear and triangular; and HR, MED and LR for high, medium and low resolution respectively. . . . .	70
D.3	Cross-sectional view of the simulated water depth for the Sharp river meander (main channel case) with the lowest discharge range at CS 1, CS 2 and CS 3 by the six considered grids. Regarding the names: S stands for sharp; MC for main channel; Cur and Tri for respectively curvilinear and triangular; and HR, MED and LR for high, medium and low resolution respectively. . . . .	71
D.4	Map-plots of the simulated depth-averaged flow velocities for the Sharp river meander (main channel case) with the lowest discharge range by the six considered grids. Regarding the names: S stands for sharp; MC for main channel; Cur and Tri for respectively curvilinear and triangular; and HR, MED and LR for high, medium and low resolution respectively. . . . .	72

D.5 Cross-sectional view of the simulated water level in the mild river meander (main channel and floodplain case) for the highest discharge range at CS 1, CS 2 and CS 3 by the six considered grids. Regarding the names: M stands for mild; MCFL for main channel & floodplains; Cur, Tri and Hybr for respectively curvilinear, triangular and hybrid; and HR and MED for high and medium resolution respectively. . . . . 73

D.6 Cross-sectional view of the simulated depth-averaged flow velocity in the mild river meander (main channel and floodplain case) for the highest discharge range at CS 1, CS 2 and CS 3 by the six considered grids. Regarding the names: M stands for mild; MCFL for main channel & floodplains; Cur, Tri and Hybr for respectively curvilinear, triangular and hybrid; and HR and MED for high and medium resolution respectively. . . . . 74

E.1 Cross-sectional view of the simulated depth-averaged flow velocities for the medium discharge range of the six grids for the case study at CS 1.1, CS 1.2 and CS 1.3. Regarding the names: Grensmaas stands for the Grensmaas river; Cur, Tri and Hybr for respectively curvilinear (as much as possible), triangular and hybrid; and HR and MED for high and medium resolution respectively. . . . . 75

E.2 Cross-sectional view of the bathymetry of the six grids for the case study at CS 1.1, CS 1.2 and CS 1.3. Regarding the names: Grensmaas stands for the Grensmaas river; Cur, Tri and Hybr for respectively curvilinear (as much as possible), triangular and hybrid; and HR and MED for high and medium resolution respectively. . . . . 76

E.3 Cross-sectional view of the simulated depth-averaged flow velocities for the medium discharge range of the six grids for the case study at CS 2.1, CS 2.2 and CS 2.3. Regarding the names: Grensmaas stands for the Grensmaas river; Cur, Tri and Hybr for respectively curvilinear (as much as possible), triangular and hybrid; and HR and MED for high and medium resolution respectively. . . . . 77

E.4 Cross-sectional view of the bathymetry of the six grids for the case study at CS 2.1, CS 2.2 and CS 2.3. Regarding the names: Grensmaas stands for the Grensmaas river; Cur, Tri and Hybr for respectively curvilinear (as much as possible), triangular and hybrid; and HR and MED for high and medium resolution respectively. . . . . 78

## List of Tables

2.1	The imposed semi-stationary discharges in the model domain of the case study. . . . .	10
2.2	The imposed semi-stationary discharges in the hypothetical river meanders. Mild and sharp refer to respectively the mild and sharp hypothetical river meanders. . . . .	16
3.1	The computation time of all six grids for the mild river meander (main channel case). Here T stands for the computation time, $\Delta t$ for the average time step and $T_{ref}$ for the reference computation time, which is chosen to be the computation time of M_MC_Cur_HR. Regarding the names: M stands for mild; MC for main channel; Cur and Tri for respectively curvilinear and triangular; and HR, MED and LR for high, medium and low resolution respectively. . . . .	32
3.2	The computation time of all six grids for the sharp river meander (main channel case). Here T stands for the computation time, $\Delta t$ for the average time step and $T_{ref}$ for the reference computation time, which is chosen to be the computation time of S_MC_Cur_HR. Regarding the names: S stands for sharp; MC for main channel; Cur and Tri for respectively curvilinear and triangular; and HR, MED and LR for high, medium and low resolution respectively. . . . .	35
3.3	The computation time of all six grids for the sharp river meander (main channel & floodplain case). Here T stands for the computation time, $\Delta t$ for the average time step and $T_{ref}$ for the reference computation time, which is chosen to be the computation time of M_MCFL_Cur_HR. Regarding the names: M stands for mild; MCFL for main channel & floodplains; Cur, Tri and Hybr for respectively curvilinear, triangular and hybrid; and HR and MED for high and medium resolution respectively . . . . .	38
3.4	The computation time of all six grids for the sharp river meander (main channel & floodplain case). Here T stands for the computation time, $\Delta t$ for the average time step and $T_{ref}$ for the reference computation time, which is chosen to be the computation time of S_MCFL_Cur_HR. Regarding the names: S stands for sharp; MCFL for main channel & floodplains; Cur, Tri and Hybr for respectively curvilinear, triangular and hybrid; and HR and MED for high and medium resolution respectively . . . . .	38
3.5	Predicted water levels in the main channel at the bend apex (CS 1.2) for the three discharges ranges by the six grids. Regarding the names: Grensmaas stands for the Grensmaas river; Cur, Tri and Hybr for respectively curvilinear (as much as possible), triangular and hybrid; and HR and MED for high and medium resolution respectively. . . . .	41
3.6	The flow area through the main channel at the bend entrance (CS 1.1), apex (CS 1.2) and exit (CS 1.3) for the six grids and the bathymetry data directly from the baseline-maas-j14_6-w14 database. Regarding the names: Grensmaas stands for the Grensmaas river; Cur, Tri and Hybr for respectively curvilinear (as much as possible), triangular and hybrid; and HR and MED for high and medium resolution respectively. . . . .	41
3.7	Predicted water levels in the main channel at the bend apex (CS 2.2) for the three discharges ranges by the six grids. Regarding the names: Grensmaas stands for the Grensmaas river; Cur, Tri and Hybr for respectively curvilinear (as much as possible), triangular and hybrid; and HR and MED for high and medium resolution respectively. . . . .	43

3.8	The flow area through the main channel at the bend entrance (CS 2.1), apex (CS 2.2) and exit (CS 2.3) for the six grids and the bathymetry data directly from the baseline-maas-j14_6-w14 database. Regarding the names: Grensmaas stands for the Grensmaas river; Cur, Tri and Hybr for respectively curvilinear (as much as possible), triangular and hybrid; and HR and MED for high and medium resolution respectively. . . . .	44
3.9	The flow area through the main channel at the bend entrance (CS 1.1), apex (CS 1.2) and exit (CS 1.3) for the three locally refined grids. Regarding the names: Grensmaas stands for the Grensmaas river; Cur, Tri and Hybr for respectively curvilinear (as much as possible), triangular and hybrid; HR and MED for high and medium resolution respectively; and Loc and Ref for locally and refined respectively. . . . .	44
3.10	The flow area through the main channel at the bend entrance (CS 2.1), apex (CS 2.2) and exit (CS 2.3) for the three locally refined grids. Regarding the names: Grensmaas stands for the Grensmaas river; Cur, Tri and Hybr for respectively curvilinear (as much as possible), triangular and hybrid; HR and MED for high and medium resolution respectively; and Loc and Ref for locally and refined respectively. . . . .	45
3.11	Predicted water levels in the main channel at the bend apex (CS 1.2) for the three discharges ranges by the three locally refined grids. Regarding the names: Grensmaas stands for the Grensmaas river; Cur, Tri and Hybr for respectively curvilinear (as much as possible), triangular and hybrid; HR and MED for high and medium resolution respectively; and Loc and Ref for locally and refined respectively. . . . .	45
3.12	Predicted water levels in the main channel at the bend apex (CS 2.2) for the three discharges ranges by the three locally refined grids. Regarding the names: Grensmaas stands for the Grensmaas river; Cur, Tri and Hybr for respectively curvilinear (as much as possible), triangular and hybrid; HR and MED for high and medium resolution respectively; and Loc and Ref for locally and refined respectively. . . . .	45
3.13	The computation time of all nine grids for the case study. Here T stands for the computation time, $\Delta t$ for the average time step and $T_{ref}$ for the reference computation time, which is chosen to be the computation time of Grensmaas_Cur_HR. Regarding the names: Grensmaas stands for the Grensmaas river; Cur, Tri and Hybr for respectively curvilinear (as much as possible), triangular and hybrid; HR and MED for high and medium resolution respectively; and Loc and Ref for locally and refined respectively. . . . .	46
C.1	Properties of the constructed grids for the hypothetical river meanders with only the main channel. Regarding the names: M and S stands respectively for mild and sharp; MC for main channel; Cur and Tri for respectively curvilinear and triangular; and HR, MED and LR for high, medium and low resolution respectively. Furthermore, min/max stands for minimum and maximum respectively. . . . .	65
C.2	Properties of the constructed grids for the hypothetical river meanders with the main channel and floodplains. Regarding the names: S stands for sharp; MCFL for main channel & floodplains; Cur, Tri and Hybr for respectively curvilinear, triangular and hybrid; and HR and MED for high and medium resolution respectively. Furthermore, min/max stands for minimum and maximum respectively. . . . .	66

---

C.3	Properties of the constructed grids for the Grensmaas river. Regarding the names: Grensmaas stands for the Grensmaas river; Cur, Tri and Hybr for respectively curvilinear (as much as possible), triangular and hybrid; HR and MED for high and medium resolution respectively; and Loc and Ref for locally and refined respectively. Furthermore, min/max stands for minimum and maximum respectively; and transitions for the shift between the medium resolution variant and local refinements. . . . .	68
-----	---	----

# 1 Introduction

This introductory section serves to outline the motivation for this research. Section 1.1 provides background information. Thereafter, the research gap are presented in section 1.2. Section 1.3 elaborates on the research objective, which is followed by the research questions in Section 1.4. Finally, the structure of this report is given in Section 1.5.

## 1.1 Background

A detailed insight in flow patterns in rivers is fundamental as it helps evaluating the efficacy and impacts of river engineering projects regarding flood protection, navigation as well as pollutant dispersion and controlling sediment management. To acquire these insights, two-dimensional (2D) depth-averaged models are generally applied, since the water depths are relatively shallow compared to the width and vertical motions are assumed to be insignificant (see Section 2.1.1) (Altaie & Dreyfuss, 2018; Hardy et al., 1999; Lai, 2010). In 2D depth-averaged models, water motions are described with the Shallow Water Equations (SWEs), which are given by the depth-averaged continuity equations and the momentum equations (Altaie & Dreyfuss, 2018; Deltares, 2019a). In order to obtain flow pattern predictions with 2D depth-averaged models, grids (also known as meshes) can be used to discretise study areas. Nevertheless, various feasible grid shapes are available, while an optimum grid resolution is not specified beforehand (Caviedes-Voullième et al., 2012; Hardy et al., 1999). Additionally, Bomers et al. (2019) concluded that the accuracy and computation time of 2D depth-averaged models is largely influenced by grid shape and grid resolution.

So far, fully curvilinear (structured) or fully triangular (unstructured) grids are generally used to discretise study areas to solve the governing equations in hydraulic river models. A combination of both grid shapes is applicable as well and is referred to as a hybrid grid (see Figure 2.10f for an example).

In rivers, changes in flow velocity in channel length direction are generally smaller in comparison to those in cross direction (Kernkamp et al., 2011). Therefore, Kernkamp et al. (2011) addressed that a curvilinear grid is beneficial of having less grid cells than a triangular grid since the grid cells are elongated and aligned in the main flow direction. Moreover, along a river main channel, the orthogonality (see Section 2.1.2) in a curvilinear grid stays within reasonable bounds (Bomers et al., 2019; Lai, 2010; Tu et al., 2013a). Furthermore, the computation time can be reduced when applying curvilinear grid cells over triangular grid cells as the former results in a larger spatial time step, and hence larger time step to satisfy stability criteria of the numerical solution method (Courant-Friedrich-Lewy condition (see Section 2.1.2))(Bomers et al., 2019). However, curvilinear grid cells do have limitations as applying a curvilinear grid in a (sharp) river bend with large floodplains can lead to unwanted small and overlapping grid cells (see Figure 2.10a for an example). The former decreases the time step (Bomers et al., 2019; Kernkamp et al., 2011).

Triangular grid cells on the other hand, provide more flexibility when it comes to grid point clustering, which can overcome problems in complex boundaries such as river bends, large floodplains or hard structures (Bomers et al., 2019; Lai, 2010; Nabi et al., 2017; Pinho et al., 2015). Moreover, generating a triangular grid is relatively simple. Nevertheless, applying a triangular grid can be at the expense of the model accuracy. Triangular grids commonly have a low orthogonality. Projecting triangular grid cells on the edge normal vector can help to increase orthogonality and hence its model accuracy (Bomers et al., 2019). Furthermore, triangular grid cells will tend to degenerate into lines when these are elongated (Bomers et al., 2019). Consequently, this leads to small area-edge length ratios, which has an adverse effect on the computation time.

In Caviedes-Voullième et al. (2012), it has been highlighted that in depth-averaged river models poor alignment between grid and the direction of the flow, lead to a smoothed hydrograph, resulting in a lower depth-averaged flow velocities and hence higher water depths. Similar findings are obtained by Bomers et al. (2019) as well. This generated effect by a grid has a diffusion-like appearance and is known as "false diffusion" (see Section 2.1.2).

Considering the advantages and disadvantages of both fully curvilinear and fully triangular grids, a hybrid grid can serve as a good alternative. In a hybrid grid, curvilinear grid cells are commonly applied to the main channel, while triangular grid cells are used in the floodplains (Bomers et al., 2019; Lai, 2010). This strategy is beneficial regarding the computational efficiency as the main channel is discretised with stretched grid cells. Furthermore, unnecessary small grid cells in sharp river bends and/or large floodplains are prevented (Bomers et al., 2019; Kernkamp et al., 2011; Lai, 2010). Additionally, hybrid grids do have a relatively lower false diffusion than a triangular grid in the straight rivers (Bomers et al., 2019). In relation to a curvilinear grid, obtaining a lower false diffusion with a hybrid grid is possible as well if the cells in a curvilinear grid are not perfectly orientated in the flow direction. The latter is especially done in cases with large floodplains and/or sharp river bends to avoid overlapping and/or infinitely small grid cells.

Since small details in river bathymetry can sometimes affect large scale flow behaviour (Caviedes-Voullième et al., 2012), a grid should be fine enough to capture important flow features and geometrical structures (Caviedes-Voullième et al., 2012). This is even more highlighted by Bomers et al. (2019), who suggested that hydraulic river models largely depend on how well the bathymetry is discretised. If the cross-sectional area of the river is not captured sufficiently as a result of a strongly schematised bathymetry, it can lead to an overestimation or underestimation of the discharge capacity. Even though a high grid resolution is assumed to be favourable in terms of accuracy, it is at the expense of the computation time.

Last, Caviedes-Voullième et al. (2012) and Bomers et al. (2019) addressed that grid coarsening led to a damping of the discharge wave. Consequently, depth-averaged flow velocities decreased and water depths increased. These numerical effects by the grid resolution have a diffusive-effect similar to the false-diffusion and are referred as "numerical diffusion". Numerical diffusion is a result of a discretisation method and is induced differently compared to the false diffusion (see Section 2.1.2).

## 1.2 Research gap

Fully curvilinear or fully triangular grids are commonly used in hydraulic river models, while hybrid grids are a good alternative as well. Nonetheless, model outcomes and computation time are sensitive to grid shape and grid resolution (Bomers et al., 2019; Caviedes-Voullième et al., 2012). Furthermore, there does not exist a step-by-step plan to generate grids, except some firm rules (Minns et al., 2019).

In Caviedes-Voullième et al. (2012) and Bomers et al. (2019), the importance of the (i) false diffusion, (ii) numerical diffusion and (iii) bathymetry accuracy is discussed. Nonetheless, in these studies the influences of the false diffusion, numerical diffusion and bathymetry accuracy by a grid are interrelated as both studies were case studies. Consequently, it is unclear to what extent effects by grid generation choices or the bathymetry accuracy impact hydraulic river modelling outcomes.

By applying a uniform bed in transverse flow direction, it is possible to exclude the influences/errors by the bathymetry accuracy of grids and thus gain insights in the effects of false diffusion and numerical diffusion separately. Simulations for a straight flat channel with fully curvilinear and fully triangular grids have already been performed by Bilgili (2020), whose findings were in line with Caviedes-Voullième et al. (2012) and Bomers et al.

(2019). Simulations for a curved flume have already been carried out as both Lai (2010) and Nabi et al. (2017) simulated the hydrodynamics in a flat curved flume. However, there is no consensus between these two studies as the findings of Nabi et al. (2017) contradict with those of Lai (2010). In the former study, the predictions by both curvilinear and triangular grids showed a good agreement with experimental and theoretical results, which in the latter was only the case for curvilinear grids. In addition, Lai (2010) and Nabi et al. (2017) simulated the flow through a flume to validate their findings with experiments. Therefore, an extensive comparison between different grids is required for a flat curved channel, which should have the same size as a natural river.

Additionally, an accurate representation of the flow patterns in rivers is crucial regarding the assessment of the efficacy and impacts of river engineering projects. Therefore, grids may require a local increase in grid resolution to accurately schematise the bathymetry and lower the numerical effects. Nevertheless, the effects of a local increase in grid resolution is not yet fully understood as it is currently unknown to what extent a grid resolution influences model outcomes in cases with low and large floodplains or a low and a highly varying bathymetry.

### 1.3 Research objective

The goal of this research was to obtain a better understanding of the influence of the grid generation choices on the hydraulic river modelling outcomes in river meander bends. In this research, model outcomes are expressed in terms of the predictions of water depth, water level and depth-averaged flow velocity in meander bends. Thereby, we aimed to gain additional insights for generating a grid to the already existing guidelines (see Section 2.4.1). To solve the research gap, the following research objective is defined:

- *To understand under which conditions grid generation choices affect hydraulic modelling outcomes in river meanders bends.*

### 1.4 Research questions

To support the research objective, we formulated research questions. First, an insight is required in how influential and under which conditions effects by grid generation choices affect hydraulic river model outcomes if model errors by bathymetry accuracy are excluded. This can best be done by considering a constant bathymetry in the transverse flow direction, which isolates the effects of the false diffusion and numerical diffusion. It is important to consider the fact that natural rivers vary in geometry as some consists of only a main channel, while other rivers include large floodplains as well. Hence, we sought to answer the following two research questions:

- (i) *How do grid generation choices affect hydraulic river modelling outcomes in the main channel of hypothetical river meanders?*
- (ii) *How do grid generation choices affect hydraulic river modelling outcomes if floodplains are included in hypothetical river meanders?*

Afterwards, it is essential to verify if similar effects/errors by grid generation choices are found in natural river meanders:

- (iii) *To what extent do the findings for the hypothetical cases also hold for a case study/natural river meander?*

Last, a local grid resolution increase in a natural river meander contribute to give insight in how a local resolution change in grids influences the hydraulic river modelling outcomes:

- (iv) *How does a local increase in grid resolution affect hydraulic river modelling outcomes in a case study/natural river meander?*

## **1.5 Report outline**

The study is organised as follows. Section 2 describes the methodology. It gives a description of the used hydraulic model to simulate hydrodynamics and it represents the various model setups and considered grids. Section 3 provides the results of the hypothetical river meanders followed by those of the case study. Section 4, 5 and 6 contain the discussion, conclusion and recommendations of the study respectively.

## 2 Methodology

The methodology section starts with introducing the applied numerical method in Section 2.1. Section 2.2 and Section 2.3 focuses on the case study and hypothetical river meanders respectively. This sequence is chosen since the river characteristics of the hypothetical river meanders are chosen such that these are in line with those of the case study. In the end, Section 2.4 discusses the importance of several aspects in grid generation choices and highlights the applied grids in the model domain of the hypothetical river meanders and case study.

### 2.1 Hydraulic model

Section 2.1 starts with discussing the underlying physics in the hydraulic model, by giving a clear view of the governing equations in Section 2.1.1. Afterwards, Section 2.1.2 discusses the implemented discretisation method.

#### 2.1.1 Governing equations

Hydraulic modelling is performed with D-Flow Flexible Mesh (FM) which is a 2D depth-averaged model. The SWEs can be derived by depth-integrating the 3D Navier-Stokes equations (Altaie & Dreyfuss, 2018; Hardy et al., 1999; Lai, 2010). Since the Navier-Stokes equations are derived based on the conservation of mass and momentum (Altaie & Dreyfuss, 2018), the SWEs are given by the depth-averaged continuity equations and the momentum equations in horizontal Cartesian coordinates ( $x$ - and  $y$ -direction) (Altaie & Dreyfuss, 2018; Deltares, 2019a; Lai, 2010):

$$\frac{\partial h}{\partial t} + \frac{\partial hu}{\partial x} + \frac{\partial hv}{\partial y} = 0 \quad (2.1)$$

$$\underbrace{\frac{\partial hu}{\partial t}}_1 + \underbrace{\frac{\partial hu^2}{\partial x} + \frac{\partial huv}{\partial y}}_2 = \underbrace{-gh \frac{\partial \zeta}{\partial x}}_3 + \underbrace{\nu \left[ \frac{\partial}{\partial x} \left( h \frac{\partial u}{\partial x} \right) + \frac{\partial}{\partial y} \left( h \frac{\partial u}{\partial y} \right) \right]}_4 + \underbrace{fhu}_5 + \underbrace{\frac{\tau_u^w}{\rho}}_6 + \underbrace{\frac{\tau_u^b}{\rho}}_7 \quad (2.2)$$

$$\underbrace{\frac{\partial hv}{\partial t}}_1 + \underbrace{\frac{\partial huv}{\partial x} + \frac{\partial hv^2}{\partial y}}_2 = \underbrace{-gh \frac{\partial \zeta}{\partial y}}_3 + \underbrace{\nu \left[ \frac{\partial}{\partial x} \left( h \frac{\partial v}{\partial x} \right) + \frac{\partial}{\partial y} \left( h \frac{\partial v}{\partial y} \right) \right]}_4 - \underbrace{fhv}_5 + \underbrace{\frac{\tau_v^w}{\rho}}_6 + \underbrace{\frac{\tau_v^b}{\rho}}_7 \quad (2.3)$$

In the SWEs,  $t$  represents the time ( $s$ ),  $u$  and  $v$  are the depth-averaged flow velocities ( $m/s$ ) in respectively  $x$ - and  $y$ -direction,  $g$  is the gravitational acceleration ( $m/s^2$ ),  $\zeta$  is the water level ( $m$ ),  $\nu$  is the kinematic viscosity ( $m^2/s$ ).  $\rho$  represents the density of the water ( $kg/m^3$ ), which is assumed to be incompressible.  $f$  is the Coriolis frequency ( $rad/s$ ).  $\tau_u^b$  and  $\tau_v^b$  are respectively bottom friction ( $N/m^2$ ) in  $x$ - and  $y$ -direction.  $\tau_u^w$  and  $\tau_v^w$  are the wind friction acting at the free surface ( $N/m^2$ ) in  $x$ - and  $y$ -direction respectively. Furthermore, it is important to realise that the inertia, advection, hydrostatic pressure, diffusion, Coriolis force, wind and bottom friction terms are represented with respectively terms 1 until 7 in Equations 2.2 and 2.3. In D-Flow FM, the bottom friction is expressed as (Deltares, 2019a):

$$\left( \tau_u^b, \tau_v^b \right) = -\frac{\rho g}{C^2} \left( u, v \right) \sqrt{u^2 + v^2} \quad (2.4)$$

In this expression,  $C$  represents the Chézy coefficient ( $m^{1/2}/s$ ), which is based on the White-Colebrook relationship, and can be expressed as follows (Colebrook, 1939):

$$C = 18 \log_{10} \left( \frac{12R}{k_s} \right) \quad (2.5)$$

Here,  $R$  is the hydraulic radius ( $m$ ), which is the cross-sectional area ( $m^2$ ) divided by the wetted perimeter ( $m$ ) (Vermeulen et al., 2018).  $k_s$  is the Nikuradse roughness coefficient ( $m$ ). Applying the White-Colebrook equation is beneficial as it incorporates the influences of the channel bathymetry and water depth on the friction under constant Nikuradse roughness values. Similarly to the bottom friction, the wind friction acting on the free surface is expressed as (Deltares, 2019a):

$$\left( \tau_u^w, \tau_v^w \right) = \frac{\rho_a g}{C_a^2} \left( u_w, v_w \right) \sqrt{u_w^2 + v_w^2} \quad (2.6)$$

In this expression,  $\rho_a$  is the air density ( $kg/m^3$ ),  $C_a$  the air (or wind) friction coefficient ( $m^{1/2}/s$ ). The friction coefficient is set by a relationship depended value according to Smith and Banke (1975). The Smith and Banke (1975) formulation considers the friction coefficient as a variable of the wind speed. In D-Flow FM,  $u_w$  and  $v_w$  are the wind velocity vectors  $10m$  above the free surface (Deltares, 2019a).

### 2.1.2 Discretisation

In this study, we applied a finite volume method on a staggered scheme to discretise the governing equations. In the staggered scheme, the cells are generally numbered by indices  $i$  and  $j$ , which count cell center positions along the horizontal plane. Half-integer values are used to label the cell boundaries (cell faces). For the SWEs in a staggered scheme, water levels are stored at the cell centers whereas velocity variables are found at the cell boundaries (Harlow & Welch, 1965; Tu et al., 2013b). This approach differs from a collocated scheme, in which all SWEs variables are discretised at the same positions (Meier et al., 1999; Mungkasi et al., 2018; Tu et al., 2013b). The advantage of using a staggered scheme over a collocated scheme, is that the number of grid points is reduced by a factor four. This makes a staggered scheme a more effective discretisation method for the SWEs as the computation time decreases (Stelling, 1983).

In the recent years, triangular and hybrid grids have gained much attention, because these grids are able to handle complex geometries. Nevertheless, a staggered scheme in a triangular grid needs special treatments to retain conservation properties since not all variables are located in the cell centres (Tu et al., 2013b). This problem can be addressed as we adopted orthogonal grid cells, which contribute to preserve conservation laws (Kleptsova et al., 2009; Perot, 2000). The orthogonality principle enforces the criteria that the corners of two adjacent grid cell are placed on a common circle (Figure 2.1: green dotted circles). Secondly, the line segment (flow link (Figure 2.1: red lines)) that connects the circumcenter of two neighbouring cells intersects orthogonally with the interface between (net links (Figure 2.1: blue lines)) them (Bomers et al., 2019; Casulli & Walters, 2000; Kernkamp et al., 2011; Kleptsova et al., 2009). The orthogonality is defined as the cosine angle  $\alpha$  between the flow link that connects the circumcenter of two neighbouring cells and the net links. (The considered orthogonality in this study is addressed in Section 2.4.1).

In order to find the solution to the governing equations, algorithmic descriptions are required. These descriptions contain a process or set of rules to be followed in the calculations. Special attention has to be given to the numerical algorithm for the advection problem in Equation 2.2 and 2.3, since several algorithms regarding this problem inherently induce a certain artificial diffusion. In this study, we discussed the (i) false diffusion and (ii) numerical diffusion.

Despite having a similar effect, false diffusion is induced differently in comparison to numerical diffusion. First of all, false diffusion is a multi-dimensional phenomena, whereas numerical diffusion can be obtained in one-dimensional situations as well. Secondly, false diffusion only exists if the orientation of the grid lines fail to be in line with the true local direction of the flow. This means that the effect is absent if the flow is orthogonal or parallel to grid cells (Patankar, 1980; Patel, 1987).

In cases in which false diffusion is present, the order of magnitude also depends on the applied numerical algorithm, which solves the advection problem. Taylor series expansions are commonly applied to approximate differential equations. The highest term that is omitted from the Taylor series expansions, which is known as the truncation error, indicates the accuracy of these approximations. A larger false diffusion arises if the numerical approximations for the advection problem contain higher truncation errors that can artificially induce a diffusive effect in the numerical solution (Bailey, 2017; Patel, 1987).

In the numerical model for this study, a first-order upwind scheme is adopted as the algorithm to solve the advection problem. This scheme is a combination of a Forward Euler approximation of the time derivative and the upwind discretisation of the space at the same location (Roos, 2019). In a two-dimensional situations, the approximate expressions for the false diffusion coefficient is given by (Patankar, 1980):

$$\Gamma_{false} = \frac{\rho\sqrt{u^2 + v^2}\Delta x\Delta y \sin 2\theta}{4(\Delta y \sin^3 \theta + \Delta x \cos^3 \theta)} \quad (2.7)$$

Where  $\theta$  is the angle between the flow direction and the grid, which ranges between 0 and  $90^\circ$ ). From Equation 2.7, it can be seen that a maximum false diffusion coefficient is obtained when the flow direction makes an angle  $45^\circ$  with the grid lines. Furthermore, the amount of false diffusion is proportional to size of the spatial steps  $\Delta x$  and  $\Delta y$ , which indicates that false diffusion depends on the grid resolution as well.

To give an insight in how the numerical diffusion is induced, we use the one-dimensional advection problem (in Cartesian coordinates) for convenience (Roos, 2019):

$$\frac{\partial u}{\partial t} + u\frac{\partial u}{\partial x} = 0 \quad (2.8)$$

We analyse the numerical solution of this one-dimensional problem by using the method of finite differences. To discretise the one-dimensional advection problem in both space and time, two equidistant grids can be defined: one grid consisting of the space points  $x_j$  and the other consisting of time points  $t_k$ :

$$\begin{cases} x_j = \Delta x, & j = 0, 1, 2, 3, \dots, J \\ t_k = \Delta t, & k = 0, 1, 2, 3, \dots, K \end{cases} \quad (2.9)$$

and consider a two-dimensional flow velocity of numerical values

$$u_{j,k} = u(x_j, t_k), \quad j = 0, 1, 2, 3, \dots, J \quad k = 0, 1, 2, 3, \dots, K \quad (2.10)$$

Applying the upwind scheme to the one-dimensional advection problem results in the following numerical scheme:

$$u_{j,k+1} = u_{j,k} - \frac{u\Delta t}{\Delta x} \left[ u_{j,k} - u_{j-1,k} \right] \quad (2.11)$$

In order to assess the accuracy of the upwind scheme, we compared the approximation of the one-dimensional advection problem by the first-order upwind scheme to its modified equation. The latter represents, aside from the round-off error, the actual partial differential equation solved when a numerical solution is computed using a finite-difference

equations. In our case, we derived the modified equation by first expanding each term in Equation 2.11 by a Taylor-expansion and then eliminating time derivatives higher than the first-order by algebraic manipulations (see Appendix A). This led to the following modified equation, in which third order terms are truncated:

$$\frac{\partial u}{\partial t} + u \frac{\partial u}{\partial x} = \frac{u \Delta x}{2} \left[ 1 - \frac{u \Delta t}{\Delta x} \right] \frac{\partial^2 u}{\partial x^2} + O\left[(\Delta t)^2, (\Delta x)^2\right] \quad (2.12)$$

Comparing the modified equation to the Equation 2.8, we can note that higher order terms are introduced in the former. These higher order terms are introduced due to the truncation error in the first-order upwind scheme. In particular, the term proportional to  $\frac{\partial^2 u}{\partial x^2}$  is diffusive and is known to play a dominant part in the solution. This means that the explicit first-order upwind scheme induces a severe numerical diffusion, which makes the upwind method an advection-diffusion equation. As a result, a function with a (sharp) edge is smeared out over time as it propagates (Figure A.1). The first-order upwind scheme is exact if in the diffusive term  $1 - \frac{u \Delta t}{\Delta x} = 0$ . However, this is not desired, as this compromises with the stability of the solution (see below).

From Equation 2.12, it can be noted that the numerical diffusion in the one-dimensional upwind scheme becomes larger at coarser grids and higher flow velocities, since it is proportional to the spatial step  $\Delta x$  and the depth-averaged flow velocity  $u$ . Since the numerical model in this study is two-dimensional, the spatial step  $\Delta y$  determines the amount of numerical diffusion as well. Furthermore, numerical diffusion is particularly present in regions which lead to sharper flow velocity profiles, which is likely in sharp river meanders (Starikovičius et al., 2006). The latter can be explained by considering the  $\frac{\partial^2 u}{\partial x^2}$  in the diffusive term. This differential becomes larger in more skewed velocity profiles, which leads to a degradation of the accuracy.

To satisfy the stability of the numerical model, we considered the Courant number (Courant et al., 1928):

$$C = \frac{u \Delta t}{\Delta x} \quad (2.13)$$

The Courant number tells us how the flow velocity travels ( $u$ ) over a computational grid cell ( $\Delta x$ ) in a given time step ( $\Delta t$ ) (Roos, 2019). If in an explicit scheme  $C > 1$ , then fluid particles propagate through more than one grid cell at each time step. As a result, the solution becomes unstable with major inaccuracies. The solution is marginally stable if  $C = 1$ , whereas the solution is stable for  $C < 1$ . Since we discretise the governing equations with a grid, the interval length  $\Delta x$  will be set (see Equation 2.13). Consequently, an explicit scheme does have a time step restriction in order to have a stable solution. However, in the hydraulic model, the continuity equation is solved implicitly for all points (Deltares, 2019b). This means that the continuity equation has no time step restriction since the implicit scheme is unconditionally stable. To solve the implicit part, a matrix vector equation in the form of  $Ax = b$  is obtained. This part is for some extent solved by the Gaussian elimination (Deltares, 2019a; Kernkamp et al., 2011). The remaining unknowns are solved with an iterative solver (Deltares, 2019a; Kernkamp et al., 2011). Applying a combined solver is beneficial as the iterative solver, which is the most time consuming part, needs to be executed on less unknowns (Kernkamp et al., 2011). The advection term on the other hand is solved explicitly. The hydraulic model uses a dynamic time step limitation to automatically satisfy the Courant criterium. This basically means that the time step depends on the variable interval length  $\Delta x$  of each specific grid cell (Deltares, 2019b; Minns et al., 2019). In this study, a Courant number of 0.7 is used.

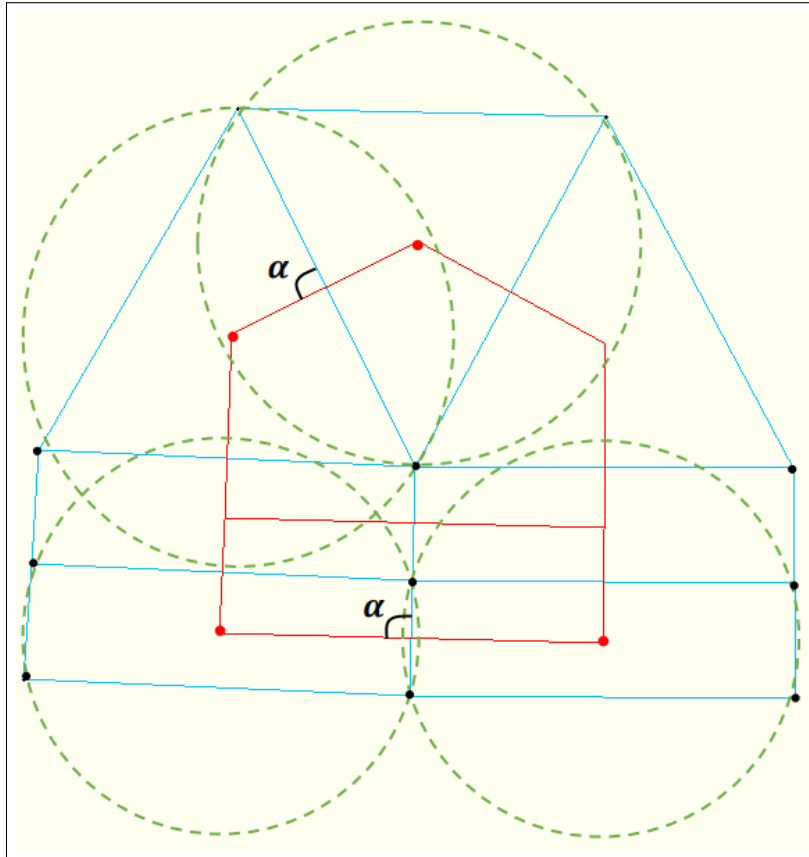


Figure 2.1: An example of the orthogonality principle for a hybrid grid where the red and blue lines represent respectively the flow links and net links. The angle between the lines is given with  $\alpha$ . The red and black dots are the cell centers and nodes respectively. The green dotted lines are the circumscribed circle for a grid cell.

## 2.2 Case study

This section highlights the case study. First, Section 2.2.1 focuses on the considered model domain for the case study, which is followed by the elaboration of the implemented boundary and initial conditions in Section 2.2.2.

### 2.2.1 Model domain

For the case study, a pre-release model of the Meuse River (Maas-j14\_6-w7) is used (De Jong, 2019). The upstream boundary is located at Eijsden (Figure 2.2), where the Meuse river enters the Netherlands. The downstream boundary is at Keizersveer. The study area of this research is the Grensmaas river, which is the trajectory of the Meuse river between 15 and 55 kilometers from the start of the Meuse (km-15 and km-55) (Figure 2.2). The Grensmaas river is used in this study since it is a typical meandering river.

For the pre-release model, geometries for each of the considered grids (see Section 2.4) are derived from Baseline. Baseline consists of an ArcGIS-application and an ArcGIS-database. The latter contains spatial information such as bed roughnesses, bed levels and weirs, of the model domain which are required in the hydraulic river model D-Flow FM. For this study, the baseline-maas-j14\_6-w14 schematisation is used, which is a sixth generation Baseline-schematisation.

To reduce the computation time of our hydraulic model, we shortened the model-domain by shifting the downstream boundary more upstream without influencing the hydrody-

namics in the study area. To satisfy this, we sought for a location which is an adequate distance away from most river bends in the Grensmaas river. Furthermore, the downstream boundary should preferably be placed at a straight part and should be unattached to a lake. In this way, the discharge at the downstream boundary stays more or less constant throughout the simulation period. Consequently, we shifted the downstream boundary from km-247 to km-64, which is slightly upstream of the city Maasbracht (Figure 2.2). This basically means that the model-domain is approximately shortened by a factor 4. The upstream boundary is kept at the same location (km-2).

The model domain consists of the main channel of the Meuse river and its floodplains. The main channel of the Grensmaas river has an average width of  $140m$  and has a length of approximately  $40km$  (Huthoff et al., 2020). No large differences in the main channel width are present. Furthermore, the model-domain stops at higher grounds as the Grensmaas river does not contain much dikes along the ends of the floodplains. Both floodplains together have an average width of  $1110m$  and are on average  $6m$  higher with respect to the main channel (Huthoff et al., 2020). A characteristic bed slope for the Grensmaas river is  $4.49e-4m/m$  (Huthoff et al., 2020). The bottom friction of the Grensmaas river is expressed as the Nikuradse coefficient with an average calibrated value of  $0.15m$  in the main channel and  $0.91m$  in the floodplains (Huthoff et al., 2020).

For the case study, we evaluated two river regions of the Grensmaas river (Figure 2.2: red regions). These regions are selected such that a location with almost no floodplains (Cross-sectional areas (CS) 1.1, CS 1.2 and CS 1.3) can be compared to one with wide floodplains (CS 2.1, CS 2.2 and CS 2.3). To capture the hydrodynamics in longitudinal direction within the river bends, we analysed the bend entrance (CS 1.1 and CS 2.1), bend apex (CS 1.2 and CS 2.2) and bend exit (CS 1.3 and CS 2.3). In order to obtain a view on the hydrodynamics in the transverse flow direction, we evaluated the complete cross-sectional areas at the bend entrance, apex and exit.

### 2.2.2 Boundary and initial conditions

Throughout the entire spatial domain, an initial water level is set which is taken over from the pre-release model. The initial water level corresponds to a discharge of  $250m^3/s$ . The system is forced at km-2 with a semi-stationary discharge. The forcing is subdivided into three categories: (i) low-; (ii) mid- and (iii) high-range semi-stationary discharges (Table 2.1). The model domain is initially forced with a low-range, which is eventually increased to a mid- and high range after each three days (Table 2.1). For the low-, mid-, and high-range semi-stationary discharges  $250$ ,  $2260$  and  $3430m^3/s$  respectively (Table 2.1).

The downstream boundary condition is set by predefined rating curves based on measurements and WAQUA (2D depth-averaged model) simulations (Figure B.1) (Rijkswaterstaat Zuid-Nederland, 2015). The rating curve at km-64 rivers applies to the schematisations of the bathymetry and bottom friction of 2014-2015.

Table 2.1: The imposed semi-stationary discharges in the model domain of the case study.

	low-range ( $m^3/s$ ) (0-3 days)	mid-range ( $m^3/s$ ) (3-6 days)	high-range ( $m^3/s$ ) (6-9 days)
Case study	250	2260	3430

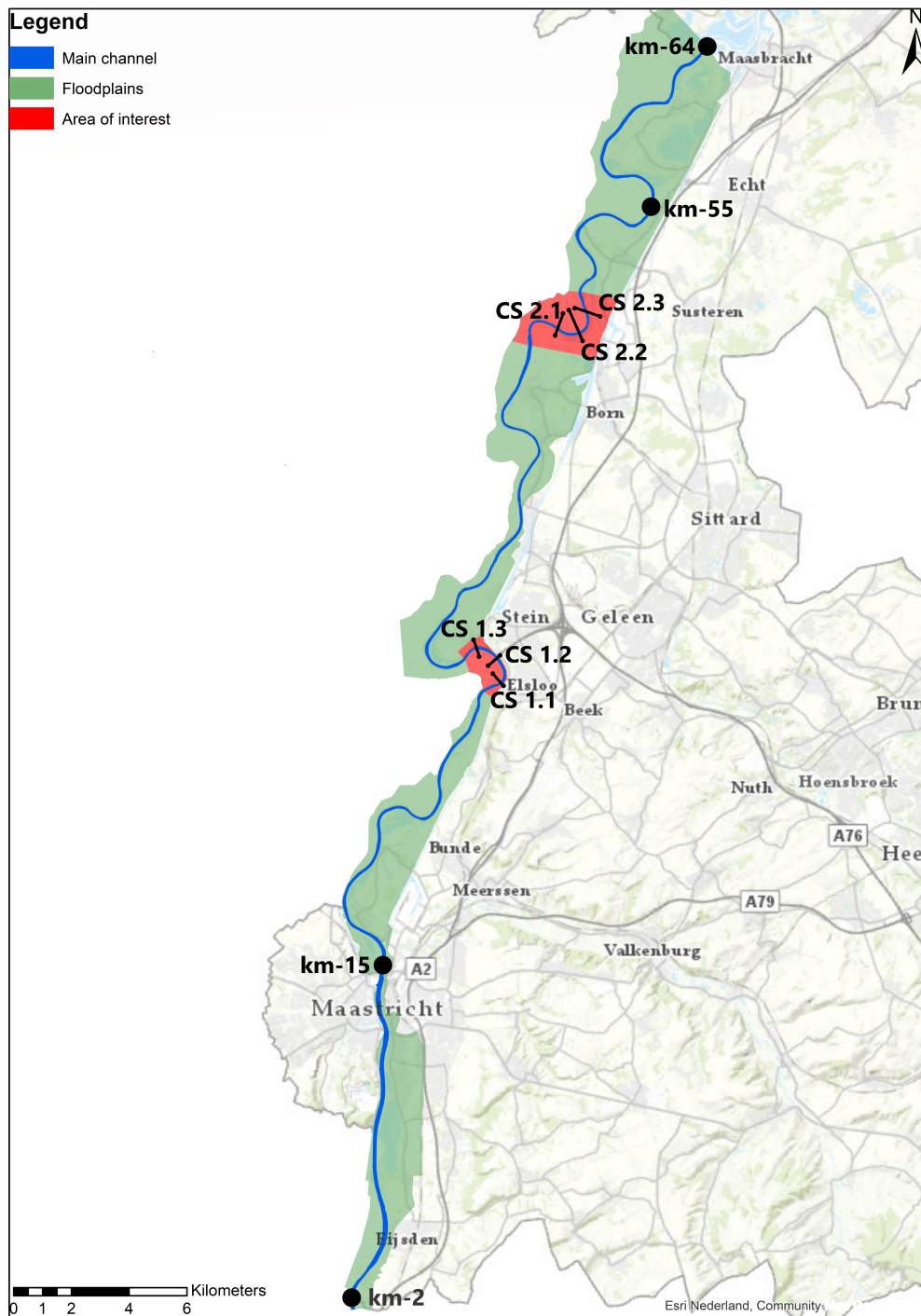


Figure 2.2: Shortened model-domain of the pre-release Meuse-model. The trajectory between km-15 and km-55 is the Grensmaas river. The model-domain ranges from km-2 Eijsden till km-64 (Maasbracht). The blue and green colour represent respectively the main channel and floodplains. The computed hydrodynamics in the red regions are considered for the evaluation of the grids. The black lines illustrate the cross-sectional areas we focused on.

## 2.3 Hypothetical river meanders

This section touches upon the hypothetical river meanders. It starts with various model domains which are considered in Section 2.3.1. Afterwards, Section 2.3.2 gives insight in the implemented boundary and initial conditions.

### 2.3.1 Model domain

To isolate the effects/errors by grid generation choices on hydraulic modelling outcomes in river meanders, we setup hypothetical river meanders based on the intrinsic function by Langbein and Leopold (1966). The river characteristics of the hypothetical river meanders are chosen such that these are in line with those of the Grensmaas river. This helped to relate the outcomes of the hypothetical river meanders with those of the case study. The following river characteristics of the Grensmaas river are used in the development of the hypothetical river meanders:

- main channel width;
- floodplain width, which is half of the average total floodplains width;
- floodplain height with respect to the bed level of the main channel;
- river slope; and
- bottom friction in the main channel and floodplains.

Langbein and Leopold (1966) introduced the so-called sine-generated curves, which describes the rate of change in direction along its path by a sinusoidal function. The "direction angle" ( $\theta$ ) is defined as the angle between the meander curve and the horizontal. It is beneficial to use this theoretical approach as this curve was formulated to have the least average curvature per unit length. In other words, the sine-generated curve provides minimum changes in direction for a fluid particle traveling along the meander. This results in the least total work needed to accelerate a fluid particle (by changing its direction) through the river meander. Consequently, this leads to similar flow patterns as in a natural river meander (Langbein & Leopold, 1966). The curve is defined as follows:

$$\theta(l) = \omega \sin\left(\frac{2\pi l}{L}\right) \quad (2.14)$$

Here, the maximum angle which the curve makes with the horizontal is defined by  $\omega$  ( $^\circ$ ).  $L$  is the curve length from trough to trough, also known as the wavelength ( $m$ ).  $l$  is the position along the curve ( $m$ ). Since the direction angle of the curve at each distance is defined by  $\theta$ , the following is true:

$$\frac{\Delta x}{\Delta l} \approx \cos \theta \quad (2.15)$$

$$\frac{\Delta y}{\Delta l} \approx \sin \theta \quad (2.16)$$

Here,  $\Delta l$  is the covered distance along the curve. Taking  $\Delta l \rightarrow 0$  leads to the following:

$$\frac{dx}{dl} = \cos \theta \quad (2.17)$$

$$\frac{dy}{dl} = \sin \theta \quad (2.18)$$

Based on these equations, we can see that changes in  $l$ , lead to changes in  $x$ ,  $y$  and  $\theta$  in response. Consequently, we obtained functions for  $x$  and  $y$  by integrating the Equations 2.17 and 2.18 with respect to  $l$ . As a result, the sine-generated curve is then expressed parametrically by:

$$x(t) = \int_0^t \cos(\theta(l))dl = \int_0^t \cos \left[ \omega \sin \left( \frac{2\pi l}{L} \right) \right] dl \quad (2.19)$$

$$y(t) = \int_0^t \sin(\theta(l))dl = \int_0^t \sin \left[ \omega \sin \left( \frac{2\pi l}{L} \right) \right] dl \quad (2.20)$$

In these equations,  $t$  ranges from 0 to  $L$  along the meander curve. From Equations 2.19 and 2.20, we considered two meander curves: (i) a mild curve and (ii) a sharp curve. These two meander curves are reviewed since both are present in the Grensmaas river. Both curves consisted of a curve length  $L = 5km$  and a total length of  $L_{tot} = 30km$ . The mild and sharp meander curves are distinguished by the parameter  $\omega$ , which is  $0.2\pi$  and  $0.35\pi$  respectively as these parameter values correspond best with the mildest and sharpest river bends in the case study. This results in a greater sinuosity for the sharp meander eventually. The boundaries for both hypothetical mild and sharp river meander were obtained by making use of offset curves (also known as parallel curves) with a normal distance away from the acquired mild and sharp curves from Equations 2.19 and 2.20. The obtained mild and sharp curves from Equations 2.19 and 2.20 are considered as the thalweg of the hypothetical meanders since a flat bottom in cross-direction is implemented. The following parametric representation is applied to find the offset curve with a distance  $d$  in horizontal Cartesian coordinates ( $x$ - and  $y$ -direction):

$$x_d(t) = x(t) + \frac{d y'(t)}{\sqrt{x'(t)^2 + y'(t)^2}} \quad (2.21)$$

$$y_d(t) = y(t) + \frac{d x'(t)}{\sqrt{x'(t)^2 + y'(t)^2}} \quad (2.22)$$

From the above equations, we subdivided the mild and sharp curves into two cases: (i) in which only a main channel is composed (Figure 2.3); and (ii) in which floodplains are included as well (Figure 2.4). In other words, this research focused on four hypothetical meanders (Figure 2.5). It is worth noting that the horizontal distance which both mild and sharp meanders cover at the end is different since we considered different  $\omega$ -values for these cases. As a result, the horizontal distance which the sharper meanders cover is shorter, while the total meander length is equivalent for all hypothetical cases (Figure 2.5).

In all hypothetical meanders, a so-called "valley slope" of  $4.49e-4m/m$  is applied. In other words, the slope along a straight line through the meander bends. In this way, identical bed levels are obtained in both the mild and sharp meanders after a certain covered distance in the  $x$ -direction. The bed elevations along the hypothetical meanders are determined by first linearly interpolating between the bed levels along the thalweg at  $x_0$  and  $x_{end}$  of the mild and sharp curves. Next, we extended the resulting discrete values in cross-direction by applying offset curves such that identical or  $6m$  higher (floodplains) bed levels are obtained normal to the thalweg.

### 2.3.2 Boundary and initial conditions

The longitudinal upstream and downstream boundaries are located in the cross-direction of the hypothetical river meanders at respectively  $x = 0$  and  $l = L_{tot}$ . Throughout the entire spatial domain, a constant initial water level of  $0m$  with respect to the bed level

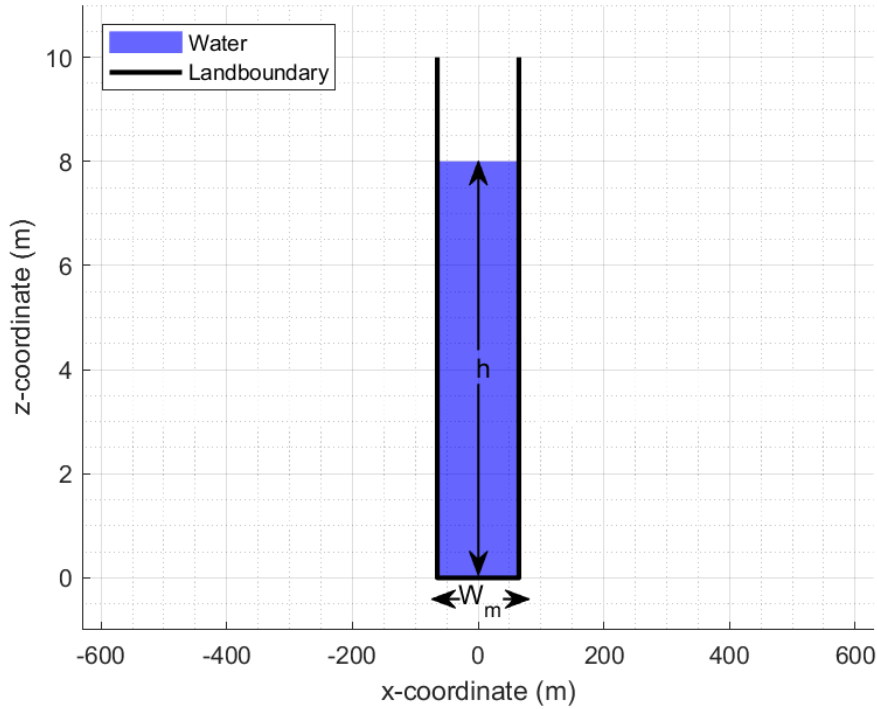


Figure 2.3: The applied cross-sections in the hypothetical river meander cases with only the main channel. Here,  $h$  stands for the water depth in the main channel and  $W_m$  for the main channel width.

of the main channel at  $x = 0$  is set. All four hypothetical river meanders are forced at  $x = 0$  with a semi-stationary discharge. The forcing is subdivided into three categories: (i) low-, (ii) mid- and (iii) high-range semi-stationary discharges. Each hypothetical case is initially forced with a low-range, which is eventually increased to a mid- and high range after each ten days (Table 2.2). The upstream boundary conditions for all hypothetical cases are unique since the river characteristics for each case is different, while similar flow patterns in the rivers are preferred. In other words, to create comparable water depths between the cases, different semi-stationary discharges are imposed.

The upstream boundary condition in each hypothetical meander is determined based on the imposed semi-stationary discharge in the case study. To acquire comparable flow conditions between the hypothetical meanders and case study, we considered the downstream boundary conditions of both the hypothetical meanders and the Grensmaas river (km-55). (It should be noted that the latter is the considered as the downstream boundary of the Grensmaas river). The downstream boundary conditions of the hypothetical meanders are set by predefined rating curves based on steady uniform flow considerations. (Figure B.1). The rating curve of the Grensmaas river at km-55 is determined based on measurements and WAQUA simulations for the river schematisations of the bathymetry and bottom friction of 2014-2015 (Rijkswaterstaat Zuid-Nederland, 2015). With the rating curve of the Grensmaas river at km-55, we related the water depths corresponding to the semi-stationary discharges of the Meuse-model to the water depths of each hypothetical meander. Consequently, we obtained identical water depths with different discharges for the hypothetical meanders.

The above mentioned principle is however not performed for the lowest semi-stationary discharge ( $250\text{m}^3/\text{s}$ ) of the Meuse-model, since it results in substantially lower water depths in the hypothetical river meanders. For that reason, the lowest range of the hypothetical

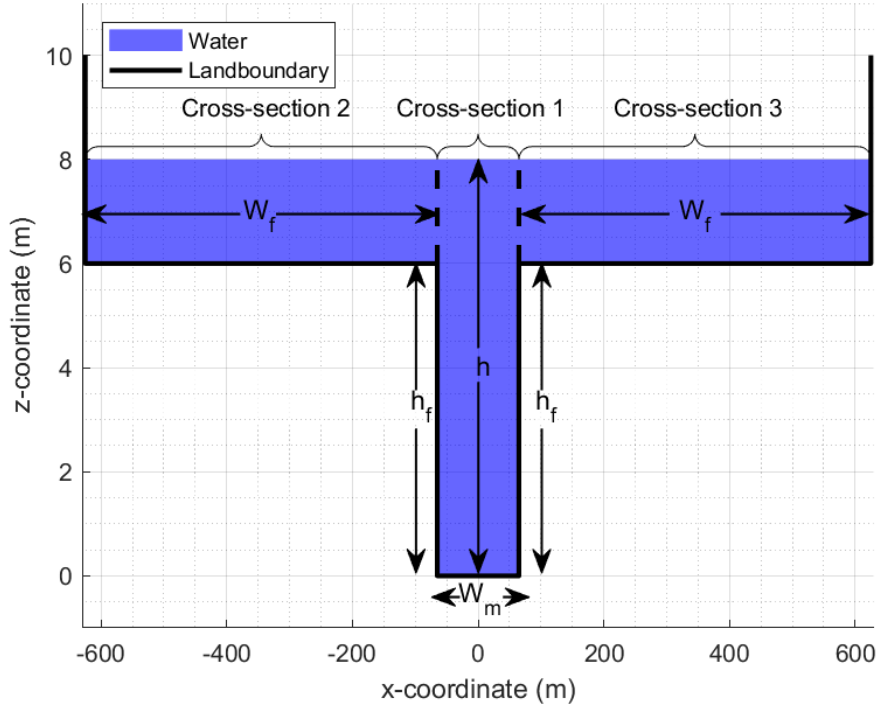


Figure 2.4: The applied cross-sections in the hypothetical river meander cases with the main channel and floodplains. Here,  $h$  stands for the water depth in the main channel,  $h_f$  for the water depth in the in the floodplains,  $W_m$  for the main channel width and  $W_f$  for the width of a single floodplain. The distinction in cross-sections is used for deriving the boundary conditions (see Section 2.3.2 and Appendix B).

river meanders is related to a semi-stationary discharge of  $1030\text{m}^3/\text{s}$  in the Grensmaas river at km-55. At this discharge level, floodplains, if present in the hypothetical cases, are not flooded but still contain a decent quantity of water in the main channel. The ratings curves for the hypothetical mild and sharp river meanders without floodplains are described by using the Chézy-formula:

$$Q = w_m 18 \log_{10} \left( \frac{12}{k_{s,m}} \left( \frac{w_m h}{w_m + 2h} \right) \right) h^{3/2} i^{1/2} \quad (2.23)$$

Here,  $h$  represents the equilibrium water depth in the main channel ( $m$ ),  $Q$  is the discharge ( $\text{m}^3/\text{s}$ ),  $w_m$  is the main channel width ( $m$ ),  $i$  is the slope ( $m/m$ ),  $k_{s,m}$  is the Nikuradse roughness coefficient in the main channel ( $m$ ). The equilibrium water depth is determined by carrying out an iterative process. The Qh-relationship changes if water propagates through the floodplains:

$$Q = w_m 18 \log_{10} \left( \frac{12}{k_{s,m}} \left( \frac{w_m h}{w_m + 2h} \right) \right) h^{3/2} i^{1/2} + w_f 36 \log_{10} \left( \frac{12}{k_{s,f}} \left( \frac{w_f (h - h_f)}{w_f + (h - h_f)} \right) \right) (h - h_f)^{3/2} i^{1/2} \quad (2.24)$$

In this expression,  $w_f$  represents the width of a single floodplain ( $m$ ),  $h_f$  is the floodplain height with respect to the main channel ( $m$ ) and  $k_{s,f}$  is the Nikuradse roughness coefficient of the floodplains ( $m$ ). (See Appendix B for a detailed procedure to derive Equation 2.23 and 2.24.)

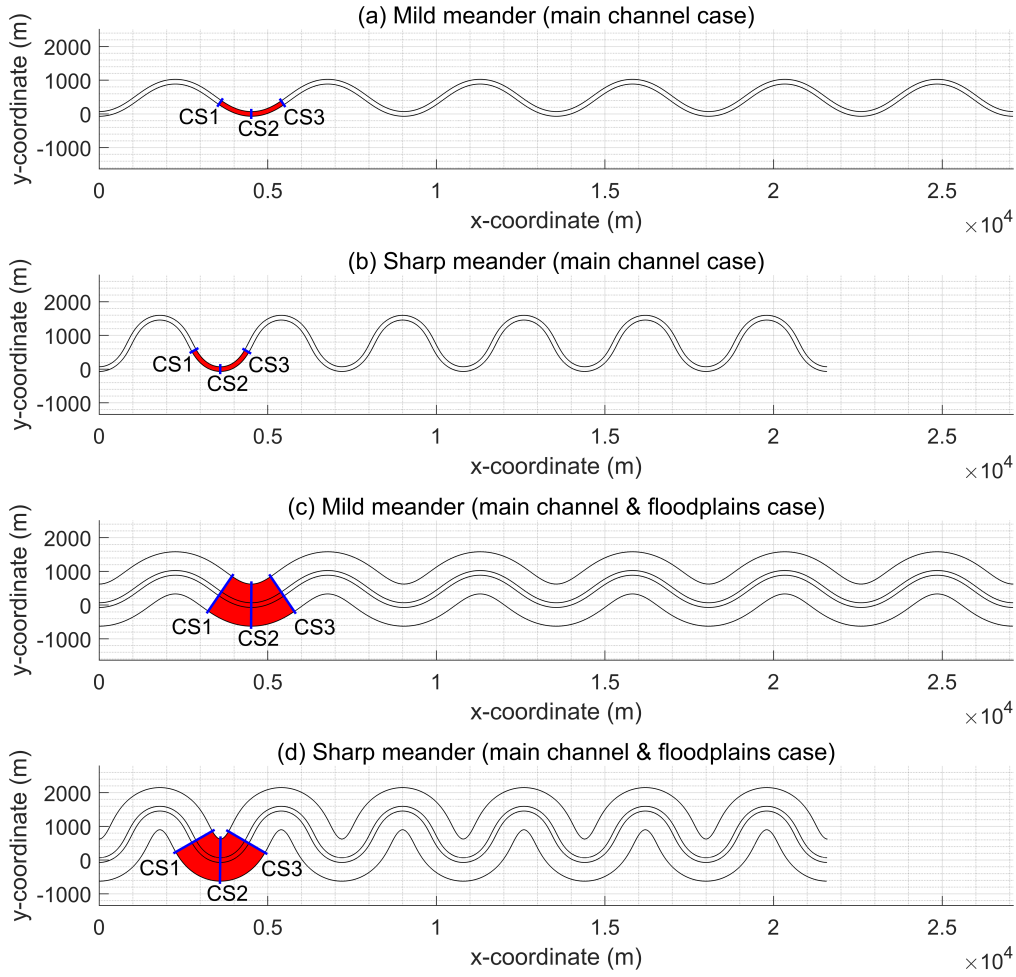


Figure 2.5: A top-view of the four hypothetical river meanders. The land boundaries are given in black. The computed hydrodynamics in the red regions are considered for the evaluation of the grids. The blue lines illustrate the cross-sectional areas.

For the hypothetical river meanders, we analysed the hydrodynamics in the second river bends (Figure 2.5: red regions). These regions are chosen since these are considerable far away from the downstream boundary condition. The latter showed to be highly influential throughout the spatial domain. To capture the hydrodynamics in longitudinal direction within river bends, we analysed the bend entrance (CS 1), bend apex (CS 2) and bend exit (CS 3). We examined the complete cross-sectional areas at the bend entrance, apex and exit, in order to gain insight in the hydrodynamics in the transverse flow direction.

Table 2.2: The imposed semi-stationary discharges in the hypothetical river meanders. Mild and sharp refer to respectively the mild and sharp hypothetical river meanders.

	low-range ( $m^3/s$ ) (0-10 days)	mid-range ( $m^3/s$ ) (10-20 days)	high-range ( $m^3/s$ ) (20-30 days)
Grensmaas river km-55	1030	2260	3430
Mild no floodplains	946	2247	3002
Sharp no floodplains	844	2005	2679
Mild floodplains	946	2359	4259
Sharp floodplains	844	2106	3801

## 2.4 Grids

This section provides a view on the various grids that are considered in this study. First, Section 2.4.1 discusses the various setups, which are of importance in the grid designs (Section 2.4.1). Afterwards, Section 2.4.2 presents the constructed grids and the underlying choices which are considered during the construction of those grids.

### 2.4.1 Aspects in grid generation choices

When generating grids, several guidelines are of importance. In this study, the following aspects are considered in the grid generation:

- Discretisation of the bathymetry;
- Orthogonality;
- Smoothness; and
- Aspect ratio.

With respect to the discretisation of the bathymetry, we discretised the bed levels on the corner nodes of the grid cells in the hypothetical cases without floodplains (Figure 2.6a). The bed level at the cell faces is then determined by the mean between the two corner nodes of a grid cell (Figure 2.6a). The bed level at the cell center of a grid cell is then eventually computed by the lowest mean-values between two corners nodes (Figure 2.6a) (Deltares, 2019b).

Another setup is required in the hypothetical cases with floodplains since a clear distinction between the main channel and floodplains is essential. Otherwise, we would have obtained large discretisation errors of the bathymetry, which might have influenced the hydrodynamics massively (Figure 2.7). Therefore, the bed levels are projected directly at the cell center (Figure 2.6b). As a result, the bed level at the cell faces is then determined by the maximum bed level considering the two cells next to a flow link (Figure 2.6b) (Deltares, 2019b).

For the case study, we discretised the bed levels on the corner nodes. This is in contrast to the hypothetical cases with the main channel and floodplains. The setup in the latter case, results in an overestimation of the bed levels at the cell faces and hence higher water levels by each grid (De Jong & Mohamed, 2016). Furthermore, the case study consists of a more gradual transitions between the main channel and the floodplains, which makes the discretisation on the cell nodes applicable. Nonetheless, the differences in bed level at the transition are briefly considered. For the grid generation, there are two options: (i) placing the grid lines at the transition between the main channel and floodplains at the lower lying grounds (Figure 2.7a); or (ii) placing the grid lines at the transition in the floodplains (Figure 2.7b). In the hydraulic model, the water storage in a grid cell is defined by the the bed levels at the cell center. The determined bed levels at the cell faces on the other hand, define the flow area to the neighbouring cell. Consequently, the setup in Figure 2.7a and Figure 2.7b leads to an overestimation and underestimation of the flow area respectively. It is essential to simulate the flow area properly, since the water level in the river largely depends on it. Therefore, for the case study, the grid lines are located in the main channel, while the transition is modelled by defining it as a fixed weir when the transition between the main channel and floodplains are steep (slope steeper than 1 : 7 (Hoefsloot & Van Doornik, 2020)). The fixed weirs are assigned a crest level, which corresponds to the height of the floodplain (De Jong, 2020). It should be noted that the derivation of the bed levels from baseline-maas-j14\_6-w14 database are done separately for each grid, since the discretising bed levels from Baseline is a grid dependent process.

This applies to other grid dependent input variables as well, such as the bed roughness and fixed weirs.

Having orthogonal grids is beneficial with respect to the computation time, since the pressure gradient only depends on two pressure points which are specified in the cell circumcentres (see Section 2.1.2). In this study, we strived for an orthogonality of  $\cos \alpha < 0.02$ , which is a maximum deviation of  $2^\circ$  from a perfectly orthogonal grid cells ( $90^\circ$ ) (Minns et al., 2019). It is worth noting that curvilinear grids are known to attain a higher orthogonality than triangular grids.

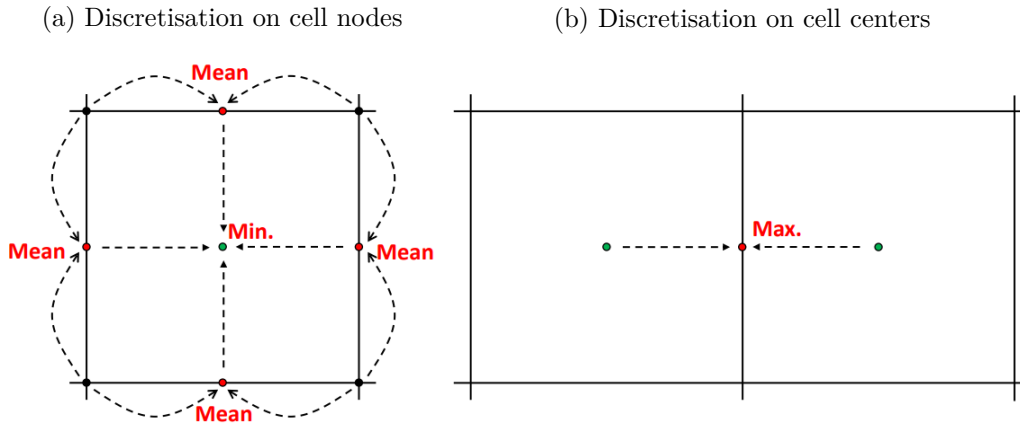


Figure 2.6: An illustration of how the bed level is discretised in (a) the cases with the main channel and (b) the cases with the main channel and floodplains. The solid black lines and filled black circles represent respectively the borders and nodes of the grid cells. The bed level at the cell faces are computed at the red filled circles. The green filled dots symbolise the bed level of a grid cell at the grid center.

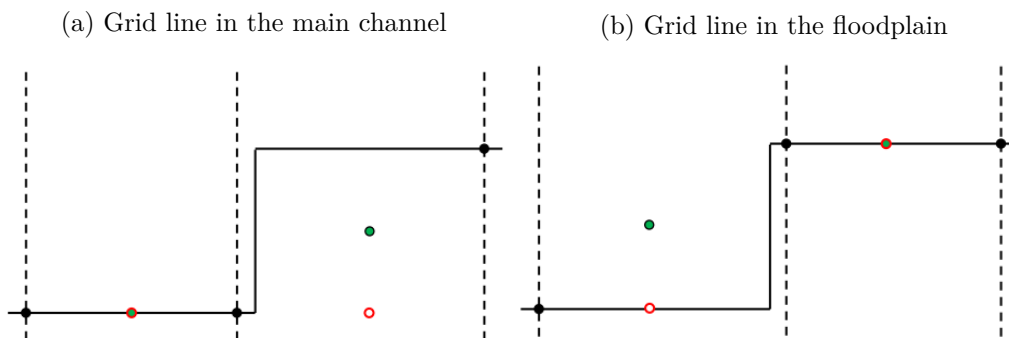


Figure 2.7: A cross-section view of the bed level in case of the hypothetical river meanders with floodplains. The solid black line is the original bed level. The dotted black line represent the grid lines. The black and green filled circles denote the bed level at the grid nodes and cell faces respectively. The bed level at the cell center positions are given with the red circle. (a) illustrates an increase in the discharge capacity of the main channel when the bed level is discretised on the grid nodes, whereas (b) results in a lower discharge capacity. (De Jong, 2020).

The smoothness is defined as the ratio of the areas of two adjacent grid cells. In order to minimise errors in the finite difference approximations, grids should be as smooth as possible (Deltares, 2020). A perfect smoothness is obtained when the area of the adjacent grid cells are equivalent. Nevertheless, criteria with respect to the smoothness are hard to

combine with those of the orthogonality in for instance a hybrid grid, while accurate model outcomes can be obtained with non-smooth grids as well (Minns et al., 2019). However, according to Minns et al. (2019) it is still important to construct grids with a smoothness as close to one as possible. We aimed to construct grids with maximum smoothness of 1.2, which is recommended by both Minns et al. (2019). This is in line with Luijendijk (2020) who suggested a smoothness less than 1.1 in areas of interest and a maximum smoothness of 1.4 at the outer ends of the model domain.

The aspect ratio for a curvilinear grid cell is defined as the ratio between the width and length of the grid cell (width-length ratio). The aspect ratio for a triangular grid cell on the other hand, is defined by the ratio between the longest two edges. For application in river models, it is possible to have a maximum aspect ratio of 5 for curvilinear grid cells because of the dominant flow direction. An aspect ratio equal to or greater than 5 may however result in curvilinear grid cells which are not capable of correctly modelling rapid flow changes in the flow direction, especially in cases with sharp bends. Therefore, we strived to construct curvilinear grid cells with maximum aspect ratio of 4. For triangular grid cells, we aimed for an aspect ratio of maximum 2, which is recommended by the Minns et al. (2019).

#### 2.4.2 Constructed grids

In order to analyse the effect of different grid shapes and grid resolutions, several grids are constructed with respect to the study areas. In the main channel of mild and sharp hypothetical river meanders, curvilinear and triangular grids are considered with both three different grid resolutions (high, medium and low) (Figure 2.8 and 2.9). Regarding the resolution in the main channel of the curvilinear grids, 20, 10 and 5 grid cells are placed in the transverse flow direction for respectively the high, medium and low resolution. Moreover, the curvilinear grid cells are aligned in the flow direction to make it capable of following the river course. To match the same degree of grid resolution with triangular grids, we focused on constructing triangular grids with approximately the same number of grid cells as the curvilinear grids. A major disadvantage of triangular grids is that, contrary to curvilinear grids, cells are less stretched in the flow direction leading to a smaller resolution in the transverse flow direction. Consequently, triangular grids with 8, 4 and 3 cells in the transverse flow direction were constructed for respectively the high, medium and low resolution. (See Table C.1 in Appendix C.1 for additional information about the grid properties for the hypothetical cases without floodplains.)

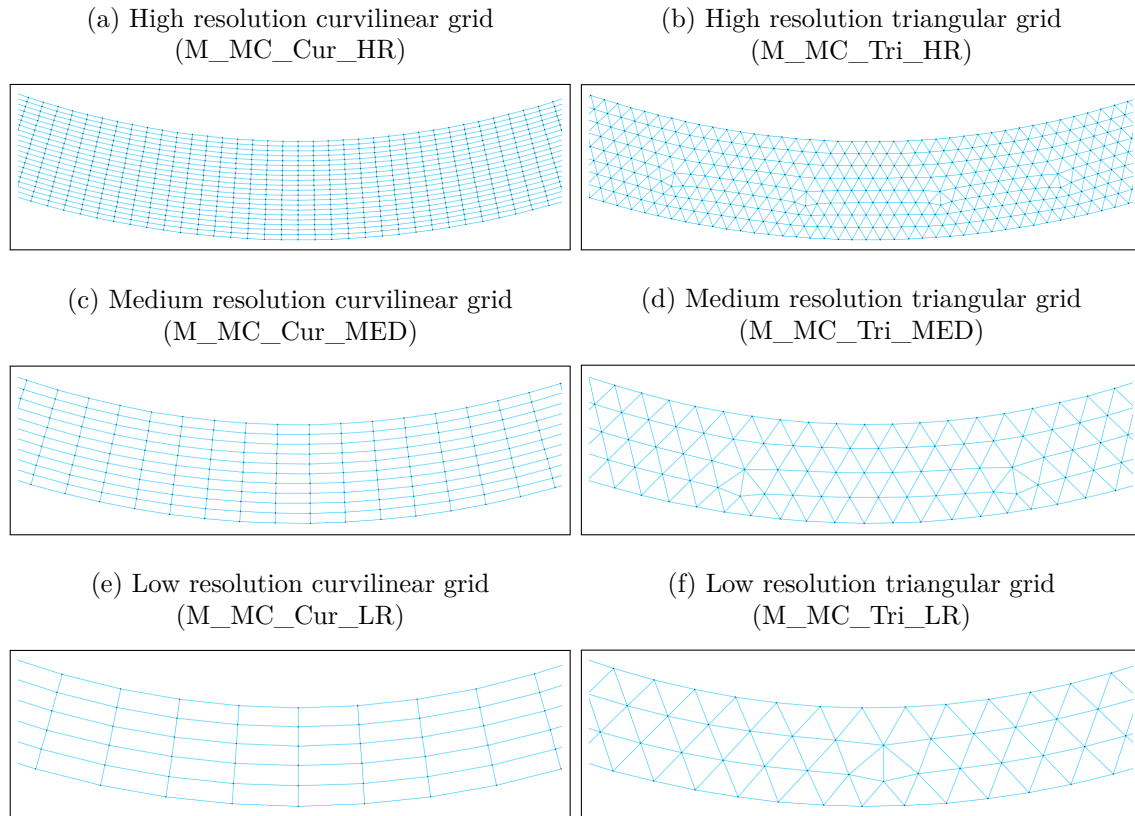


Figure 2.8: The six considered grids in the second bend of hypothetical mild river meander without floodplains. The names of the grids are given between brackets: M stands for mild; MC for main channel; Cur and Tri for respectively curvilinear and triangular; and HR, MED and LR for high, medium and low resolution respectively.

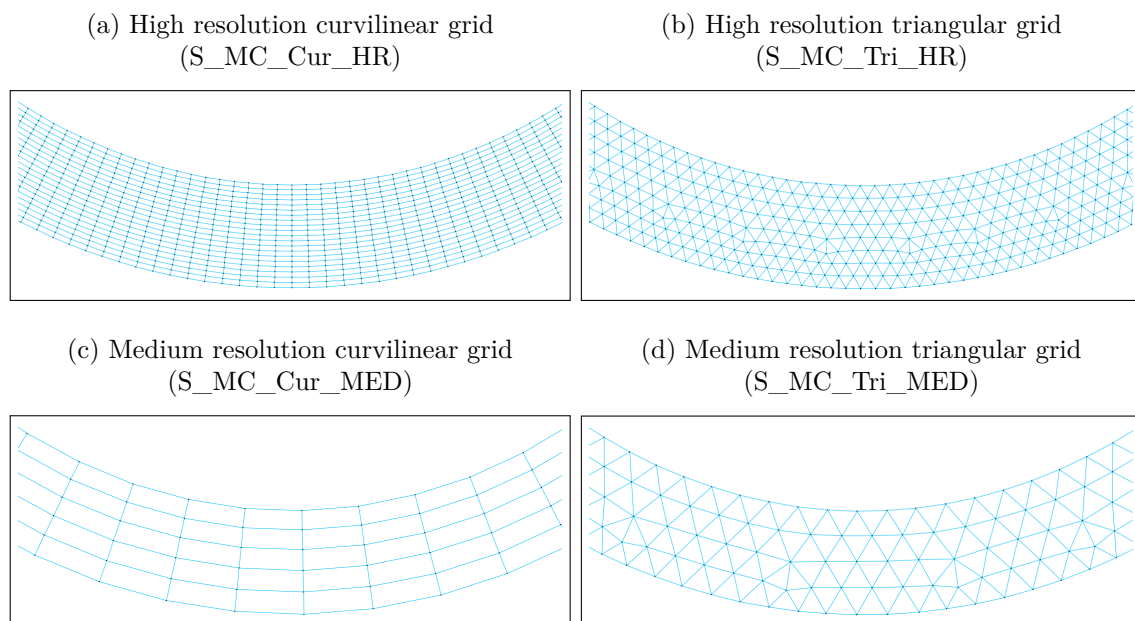


Figure 2.9: The six considered grids in the second bend of the hypothetical sharp river meander without floodplains. The names of the grids are given between brackets: S stands for sharp; MC for main channel, Cur and Tri for respectively curvilinear and triangular; and HR, MED and LR (see next page) for high, medium and low resolution respectively.

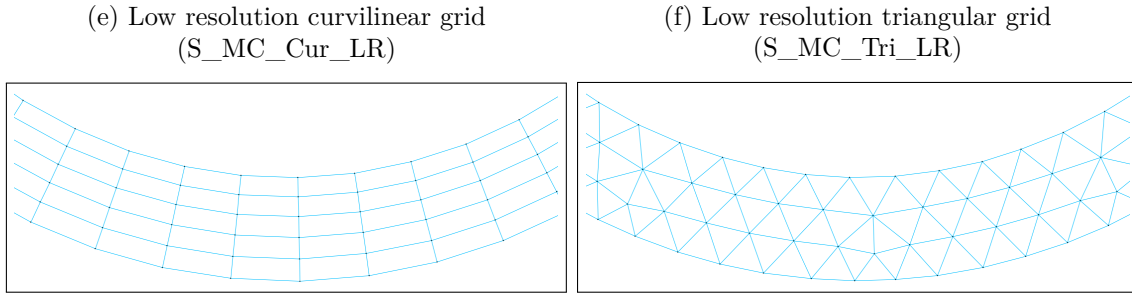


Figure 2.9: (continued)

Curvilinear and triangular grids, as well as hybrid grids, are used in the hypothetical cases when floodplains are incorporated (Figure 2.10 and Figure 2.11). The latter serves as a good alternative since the triangular grid cells prevent unnecessary small grid cells in floodplains of river bends, while the curvilinear grid cells in the main channel are stretched in the flow direction. Containing these two properties makes hybrid grids beneficial with respect to the computation time. In terms of the grid resolution, only two levels are examined: (i) a high and (ii) a medium grid resolution. Contrary to the main channel cases, low resolution grids are not considered since it is expected that grids with large cells induce greater numerical effects, such as false diffusion and numerical diffusion, which makes it not a responsible choice to apply in 2D depth-averaged river models. Regarding the curvilinear and triangular grids, both the high and medium resolution grids have the same resolution in transverse flow direction as the previously considered high and medium resolution grids in the main channels. In the case of the triangular grids, it is common to fill the model domain randomly with triangular grids cells. Nevertheless, to create a clear transition between the main channel and floodplains, we firstly discretised the main channel, whereafter we focused on the discretisation of the floodplains. To construct triangular grids in the floodplains, we used the net links positioned at the boundary of the triangular grid in the main channel (representing the grid boundary). In this way, a single triangular grid cell in the floodplains is connected with each triangular grid cell in the main channel. Constructing a grid in this way is referred to as “alignment with the flow direction” (Bomers et al., 2019). Consequently, we obtained triangular grids which are structurally well-oriented with the main channel course along the study areas. Furthermore, we acquired a well-captured bathymetry due to the positioning of the net links at the boundary of the main channel.

In regard to the curvilinear grids, no special treatment is required as the resolutions in transverse direction are automatically adjusted with the preferred number of grids in that direction. In contrast to the curvilinear grids for the cases without floodplains, smaller aspect ratios are considered in the main channel since this helps to have appropriate aspect ratios at the outer and bend of the floodplains. Otherwise, aspect ratios would have been greater than the prescriptive maximum of 5 at the outer bend of the floodplains. This is highly disadvantageous with respect to the computation time as the aspect ratio of the grid cells at the inner bend of the floodplains become smaller than one, which is especially the case in the sharper river meanders. The curvilinear grid cells are, similarly to the cases without floodplains, aligned in the flow direction. Constructing the curvilinear grids in this way, helps to create a clear transition between the main channel and floodplains as no curvilinear grid cell is located in between the two regions. By doing so, the bathymetry is captured correctly leading less over- or underestimations of the cross-sectional areas.

As for the hybrid grids, the high and medium resolution variants consisted again of respectively 20 and 10 curvilinear grid cells across the width of the main channel. The floodplains are subsequently discretised such that each curvilinear grid cell is connected

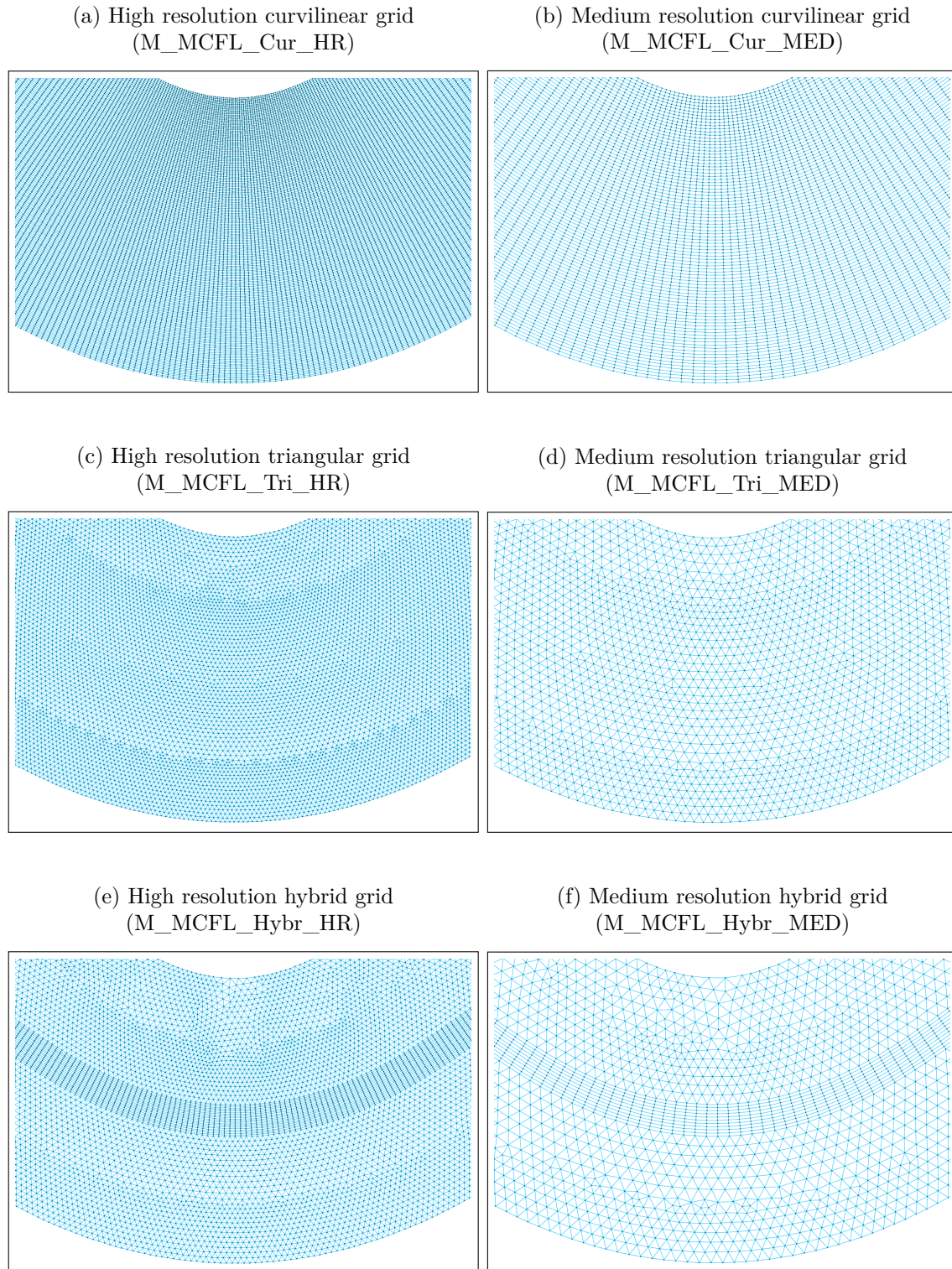
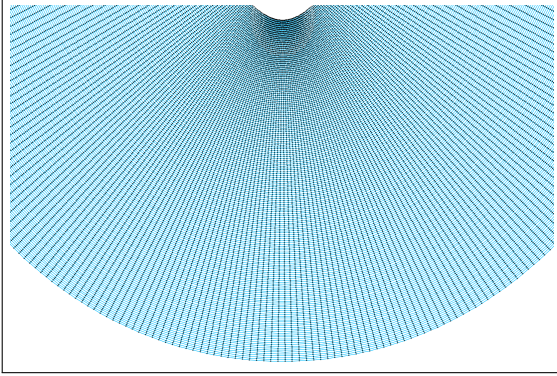


Figure 2.10: The six considered grids in the second bend of the hypothetical mild river meander with floodplains. The names of the grids are given between brackets: M stands for mild; MCFL for main channel & floodplains; Cur, Tri and Hybr for respectively curvilinear, triangular and hybrid; and HR and MED for high and medium resolution respectively.

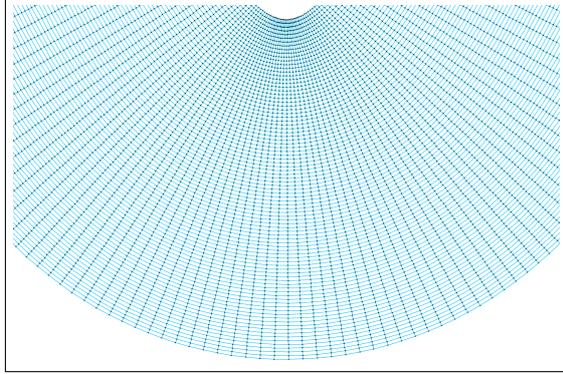
with one single triangular grid cell at the main channel-floodplain boundary. Therefore, we adjusted the size of the triangular grid cells to the length of net links located at the boundary of the curvilinear grid cells. (See Table C.2 in Appendix C.2 for additional

information about the grid properties for the hypothetical cases with floodplains.)

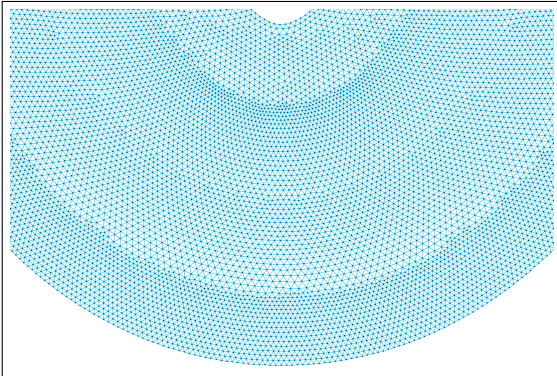
(a) High resolution curvilinear grid  
(S\_MCFL\_Cur\_HR)



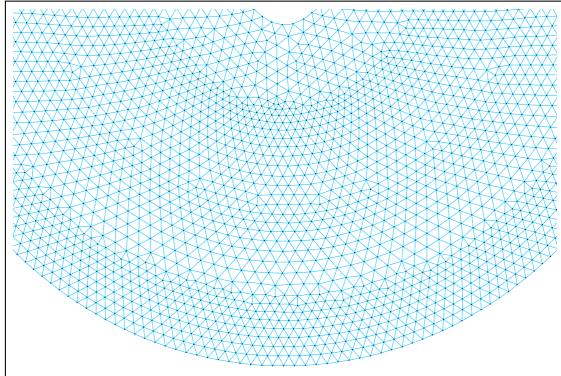
(b) Medium resolution curvilinear grid  
(S\_MCFL\_Cur\_MED)



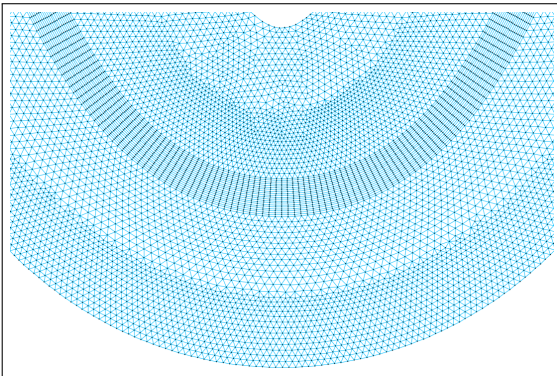
(c) High resolution triangular grid  
(S\_MCFL\_Tri\_HR)



(d) Medium resolution triangular grid  
(S\_MCFL\_Tri\_MED)



(e) High resolution hybrid grid  
(S\_MCFL\_Hybr\_HR)



(f) Medium resolution hybrid grid  
(S\_MCFL\_Hybr\_MED)

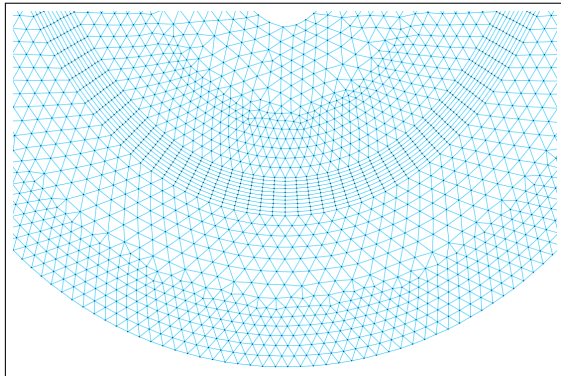


Figure 2.11: The six considered grids in the second bend of the hypothetical sharp river meander with floodplains. The names of the grids are given between brackets: S stands for sharp; MCFL for main channel & floodplains; Cur, Tri and Hybr for respectively curvilinear, triangular and hybrid; and HR and MED for high and medium resolution respectively.

For the Grensmaas river, similar grid shapes are constructed as for the hypothetical cases

with floodplains (Figure 2.12). However, the curvilinear grid is replaced by a grid which is developed by Deltares (an independent institute for applied research in the field of water and subsurface), since the Grensmaas river consists of large floodplains and sharp bends (see Figure 2.2). The latter grid discretises the model domain with as many curvilinear grid cells as possible. Quadrilateral (a polygon with four edges (or sides) and four vertices or corners) grid cells are located at sharp river bends (floodplains). Using quadrilateral grid cells results in a discretisation in which the curvilinear grid cells are orientated as much as possible in the flow direction, while no overlapping and/or infinitely small grid cells are obtained in the sharp and large floodplains of the Grensmaas river. Nevertheless, the former grid contains comparable grid properties as the curvilinear grid in the hypothetical cases: (i) similar aspect ratios in the main channel as the curvilinear grid for the hypothetical cases with only the main channel; (ii) curvilinear grid cells in large parts of the the floodplains and (iii) grid cells are placed such that it satisfies the orthogonal principle as much as possible. In contrast to the curvilinear grid in the hypothetical cases with floodplains, the transverse grid resolution in the floodplains decreases exponentially with a factor 1.05. In terms of the grid resolution, again two levels are examined for the different grids shapes: (i) a high and (ii) medium grid resolution. Regarding the resolution in the main channel of the developed grid by Deltares, a minimum of 16 and 8 grid cells are placed in the transverse flow direction. Considering a minimum number of grid cells across the main channel width allowed us to apply more grid cells at areas where the main channel is wider.

The triangular grids are constructed such that approximately the same number of grid cells are applied in the main channel as the high and medium resolution grids of Deltares (Figure 2.12). Consequently, a minimum of 6 and 3 triangular grid cells were placed across the width of the main channel for respectively the high and medium resolution. The main channel and floodplains are discretised separately for the same reasons as we mentioned for the hypothetical cases. Furthermore, discretising the main channel and floodplains separately allowed us to implement a lower grid resolution at the outer ends of the floodplains. This is implemented since significantly less water flowed through the higher grounds at the outer ends of the floodplains, while a lower grid resolution was beneficial with respect to the computation time.

Regarding the hybrid grids, 20 and 10 curvilinear grid cells were placed across the width of the main channel for respectively the high and medium resolution variants. In contrast to the developed grid by Deltares and triangular grids, a constant grid resolution in the main channel is applied since increasing/decreasing the number of curvilinear grid cells across the main channel width is not possible for a hybrid grid due to the adjacent triangular grid cells at the main channel boundaries. The curvilinear grid cells in the main channel do have the same dimensions as the high and medium resolution grid developed by Deltares. It should be noted that at locations where the main channel is small only 8 or 16 curvilinear grid cells are required based on the developed grid by Deltares. This led to 2 and 4 curvilinear grid cells that are placed outside the borders of the main channel for respectively the high and medium resolution hybrid grids. With respect to the discretisation of the floodplains, each curvilinear grid cell in the main channel is connected with one single triangular grid cell in the floodplain areas.

It is worth noting that the outer ends of the constructed grids for the case study are considered some distance away from the actual floodplain boundaries. In this way, grid cells at the actual floodplain boundaries are less influenced by the boundaries at the outer ends of the grid. In other words, we obtained the same grid cell dimensions at the actual floodplain boundaries as for most of the floodplains. To decrease the computation time, we indicated areas that are permanently dry during the simulation period. As a result, no computations are performed in grid cells that are located in those areas. This applies

to, for instance, the outer ends of the constructed extensive grids for the case study. (See Table C.3 in Appendix C.4 for additional information about the grid properties for the case study.)

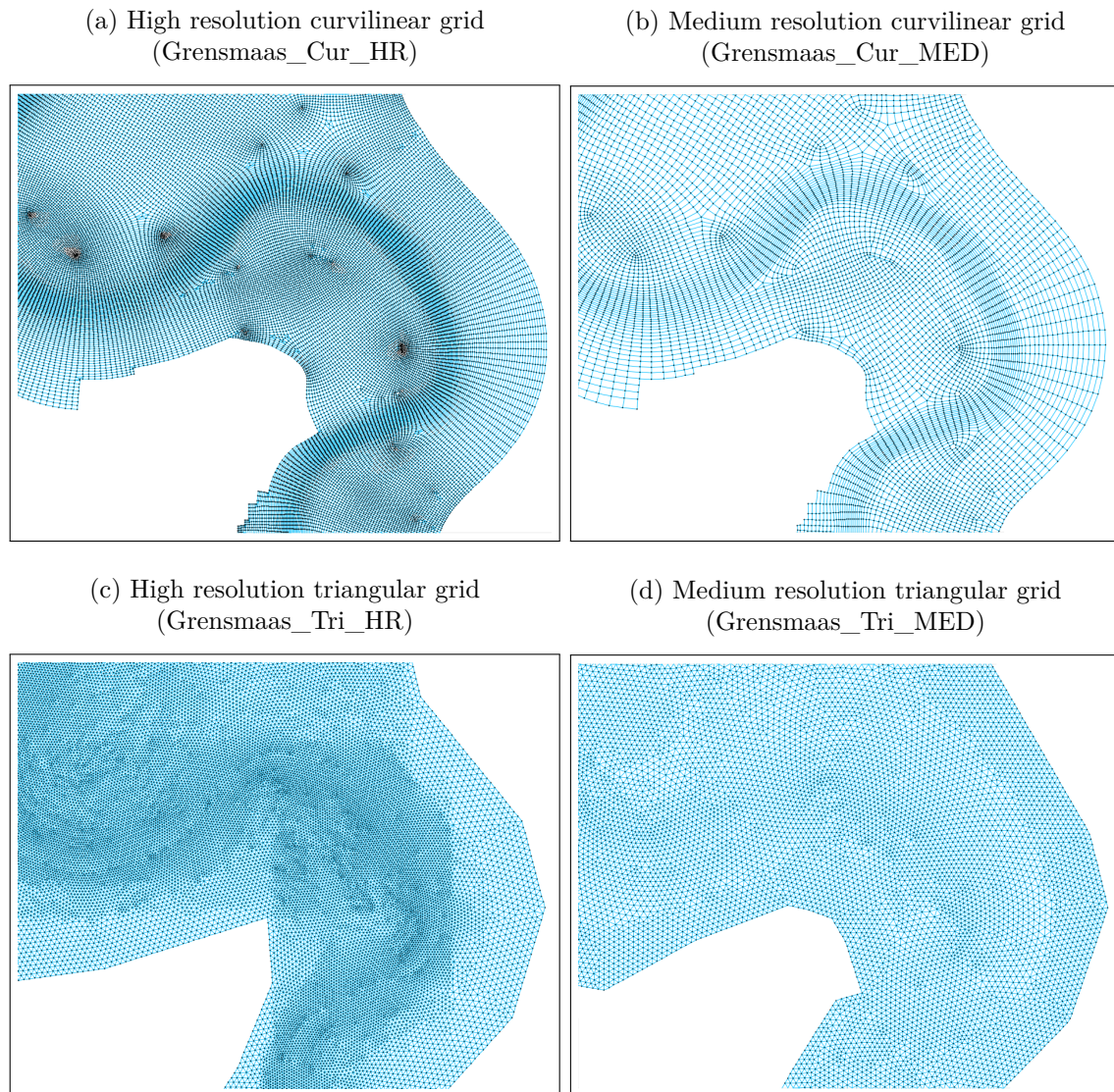


Figure 2.12: The six considered grids for the case study in the river bend (area of interest) with almost no floodplains (see Figure 2.2). The names of the grids are given between brackets: Grensmaas stands for the Grensmaas river; Cur, Tri and Hybr for respectively curvilinear (as much as possible), triangular and hybrid (see next page); and HR and MED for high and medium resolution respectively.

In order to gain an insight in how a local increase in grid resolution affects the hydraulic river modelling outcomes in the case study, we considered two local grid refinements for each constructed medium resolution grid shape (Figure 2.13). The first local grid refinement is the upstream area of interest in the Grensmaas river, where almost no floodplain areas are present (see Figure 2.2). The second grid refinement is located in the river bend downstream where wide floodplain regions are located (see Figure 2.2). The local refinements for each grid shape do have the same resolution as the higher resolution variants. This means that, for instance, the medium resolution hybrid grid contains 20 curvilinear grid cell across the width of the main channel at the two locally refined areas. A minor exception is made for the locally refined triangular grid, which in contrast to the non-refined

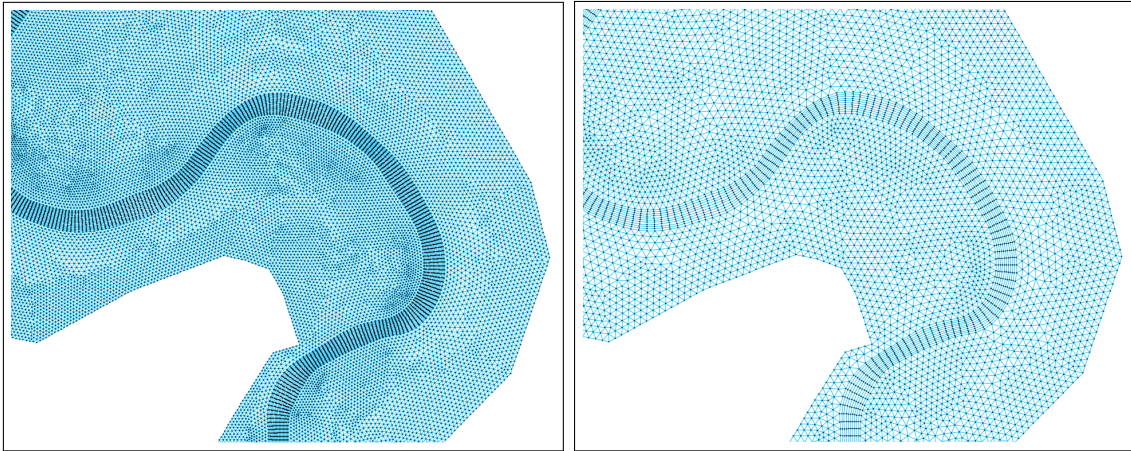
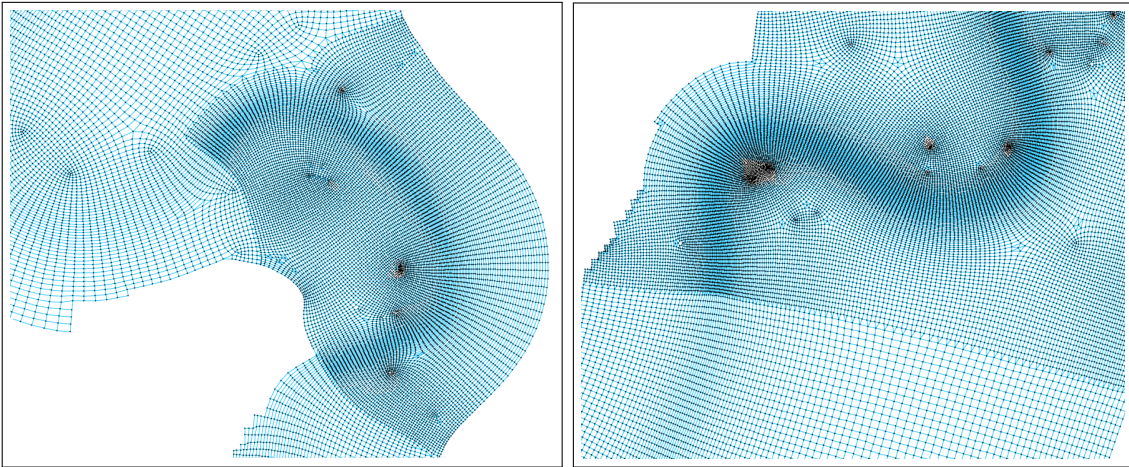
(e) High resolution hybrid grid  
(Grensmaas\_Hybr\_HR)(f) Medium resolution hybrid grid  
(Grensmaas\_Hybr\_MED)

Figure 2.12: (Continued)

triangular grids contains a similar resolution at the outer ends of the floodplains as at the main channel. Since this only applies to small areas within the study area, it is expected not to be at the expense of the computation time.

The medium resolution variants of each grid shape are locally refined by first focusing on the regions which should be refined. Therefore, we excluded the rest of the grids. Once the regions were refined, we merged the locally refined areas with the medium resolution grid variants. Nevertheless, special treatments were necessary to prevent grid cells to be connected to more grid cells than the number of its net links. Therefore, we made use of triangular grid cells at the transition between the medium resolution and the locally refined regions. Nonetheless, the developed grid by Deltares is constructed with exponentially increasing grid cell dimensions towards the outer ends of the floodplains. Consequently, applying only triangular grid cells was at the expense of the orthogonality and smoothness. Therefore, for the locally refined medium resolution grid developed by Deltares, quadrilateral grid cells in the form of trapeziums are also considered. The quadrilateral grid cells are located in between triangular grid cells to cope with the increasing grid cell dimensions towards the outer ends of the floodplains for the both the medium and locally refined regions (see Figure C.1 in Appendix C.3 for a close-up of the locally refined grids). (See Table C.3 in Appendix C.4 for additional information about the grid properties for the case study.)

- (a) Locally refined curvilinear grid at the bend  
with almost no floodplains  
(Grensmaas\_Cur\_MED\_Loc\_Ref)
- (b) Locally refined curvilinear grid at the bend  
with wide floodplains  
(Grensmaas\_Cur\_MED\_Loc\_Ref)



- (c) Locally refined triangular grid at the bend  
with almost no floodplains  
(Grensmaas\_Tri\_MED\_Loc\_Ref)
- (d) Locally refined triangular grid at the bend  
with wide floodplains  
(Grensmaas\_Tri\_MED\_Loc\_Ref)

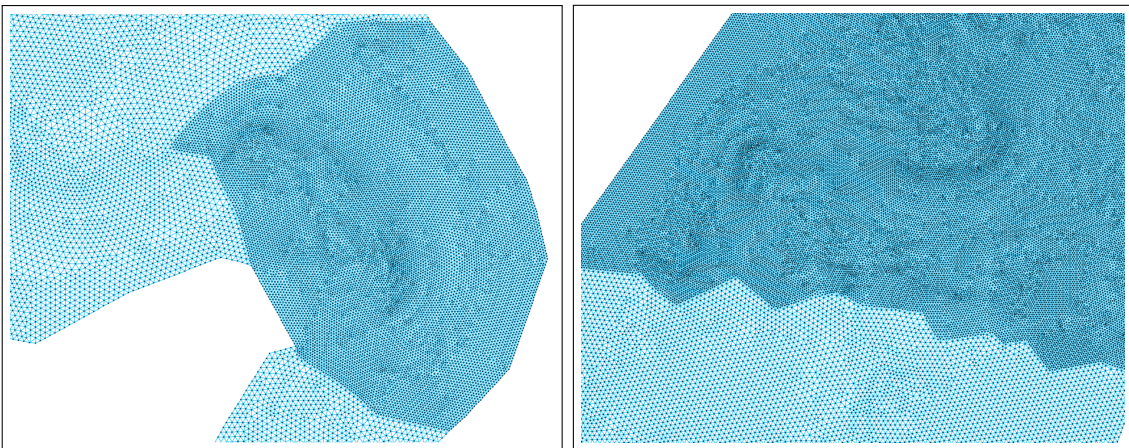


Figure 2.13: The three locally refined grids for the case study in the river bends (areas of interest) with almost no and wide floodplains (see Figure 2.2). The names of the grids are given between brackets: Grensmaas stands for the Grensmaas river; Cur, Tri and Hybr for respectively curvilinear (as much as possible), triangular and hybrid (see next page); HR and MED for high and medium resolution respectively; and Loc and Ref for locally and refined respectively.

- (e) Locally refined hybrid grid at the bend with almost no floodplains  
(Grensmaas\_Hybr\_MED\_Loc\_Ref)
- (f) Locally refined hybrid grid at the bend with wide floodplains  
(Grensmaas\_Hybr\_MED\_Loc\_Ref)

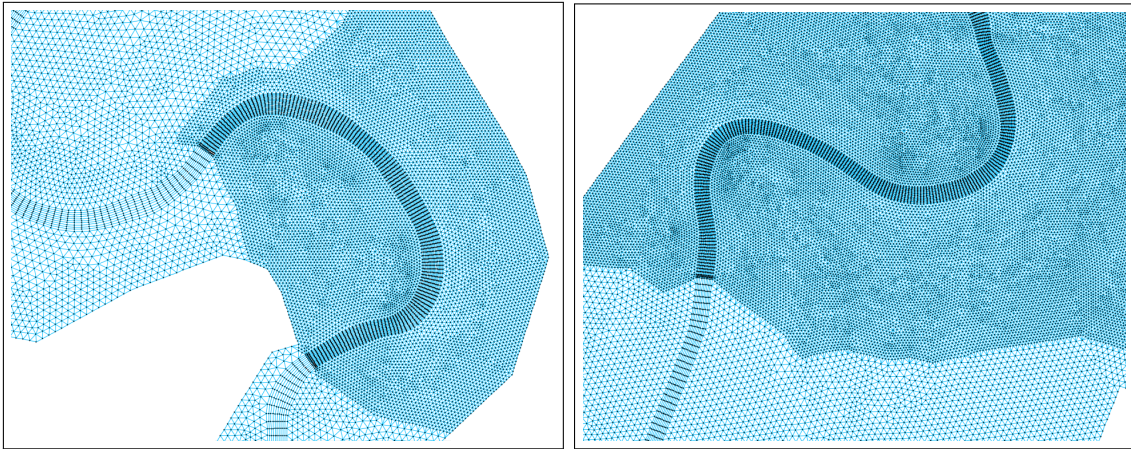


Figure 2.13: (Continued)

### 3 Results

This section provides the results of the hypothetical river meanders (Section 3.1) followed by those of the case study (Section 3.2).

#### 3.1 Hypothetical river meanders

The evaluation of the hypothetical river meanders starts with the main channel case of the mild river meander (Section 3.1.1). This is followed by the main channel case of the sharper river meander (Section 3.1.2) and floodplain variants (Section 3.1.3) respectively. Discussing the results of the hypothetical river meanders in this order helps to consider the effects by grid generation choices in the relatively simplest case first. The gained insights are then used in the analysis of the cases in which more geometric features such as a sharper river meander and floodplains are included.

##### 3.1.1 Mild river meander (main channel case)

To explore the differences between the six model simulations, we first assessed the general flood patterns. It was found that the six grids simulated more or less the same general flood patterns: (i) an elevated water surface near the outer bank at CS 1, CS 2 and CS 3 (Figure 3.1); and (ii) higher depth-averaged flow velocities close to the inner bank at the bend entrance and apex (Figure 3.2). The former is in line with Robert (2003), who described the build-up of water adjacent to the outer bank as a result of the outward directed centrifugal forces. The observed elevated depth-averaged velocity profile at the bend entrance and apex is similar to those observed by Lai (2010). As a consequence of the sudden transverse tilting of the water surface in the river bend, a flow acceleration is induced by the streamwise pressure gradients at the inner bank of the bend entrance and apex (Zeng et al., 2008). The disappearance of the elevated water surface at the bend exit causes the flow to decelerate in the inner half of the cross-sections (Zeng et al., 2008). The opposite occurs at the outer bank where the flow decelerates at the bend entrance and accelerates at the bend exit.

With the lowest discharge range, similar flood pattern profiles are obtained for the water depths and flow velocities for all grids (see Figure D.1 and Figure D.2 in Appendix D.1). Nonetheless, water depth and depth-averaged flow velocity differences between the inner and outer bank are larger when higher discharges are considered, since higher discharges correspond to greater flow velocities in a river bend and hence greater centrifugal forces. Despite obtaining the similar general flood patterns, both the simulated water depth and depth-averaged flow velocity values by each grid differ considerably. Comparing the water depths generated by the six grids, we obtained higher water depth predictions by the lower resolutions variants of both the curvilinear and triangular grids in the highest discharge range (Figure 3.1). As for the depth-averaged flow velocities, we observed lower values at the inner bank with coarser grids through almost the entire river bend (Figure 3.2). The opposite occurred at the outer bank, where greater depth-averaged flow velocities are obtained with the coarser grids (Figure 3.2). Furthermore, the differences at the inner bank are greater than those at the outer bank, indicating lower depth-averaged flow velocities by the coarser grids overall. Considering the depth-averaged flow velocity in transverse flow direction, a steeper profile is obtained with the high resolution variants of both grid types (Figure 3.2). With coarser grids, on the other hand, a more diffused depth-averaged flow velocity profile is predicted, which shows the influence of the false diffusion and numerical diffusion.

The acquired differences between the six grids are in agreement with the findings of Caviedes-Voullième et al. (2012) and Bomers et al. (2019), which proved that grid coars-

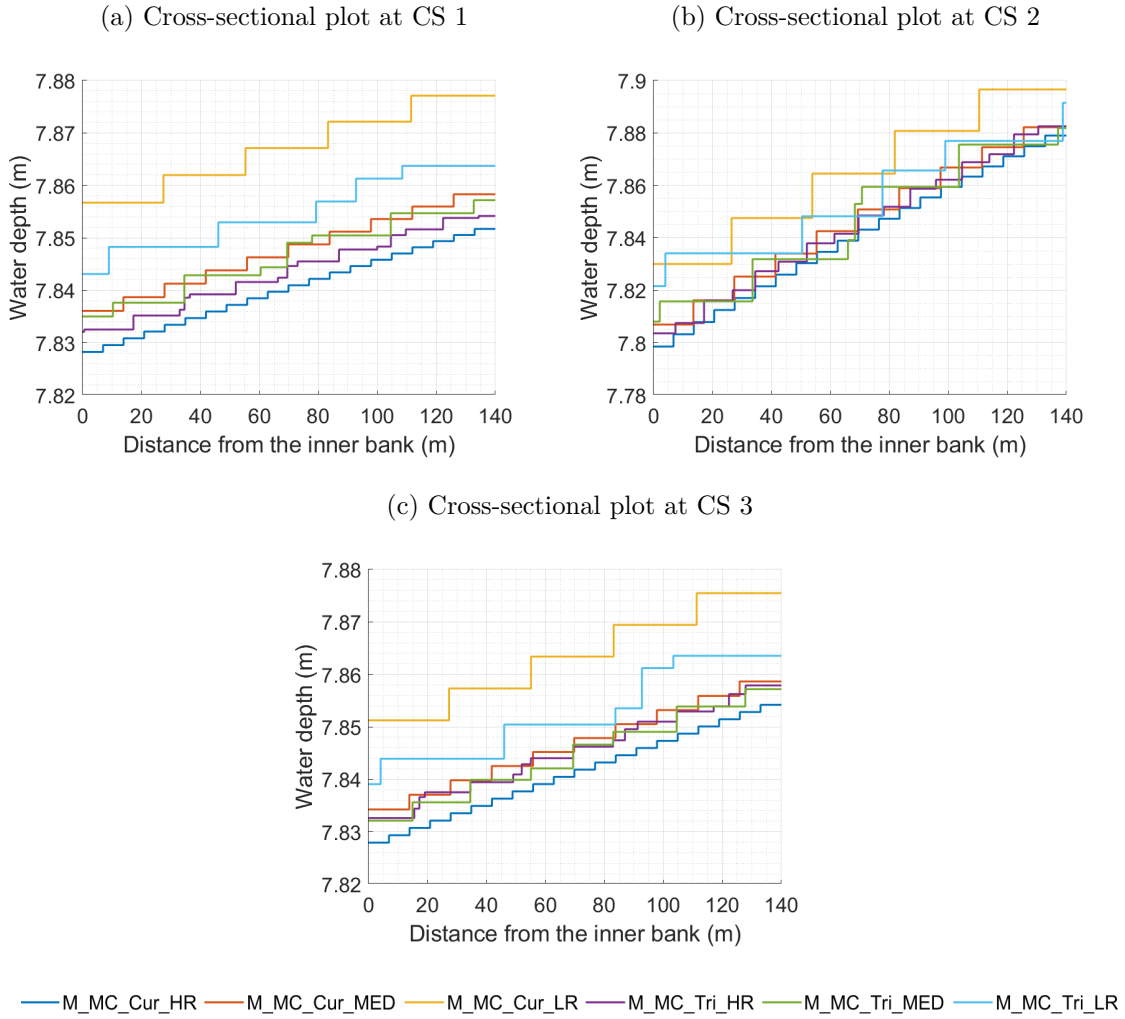


Figure 3.1: Cross-sectional view of the simulated water depth for the mild river meander (main channel case) with the highest discharge range at CS 1, CS 2 and CS 3 by the six considered grids. Regarding the names: M stands for mild; MC for main channel; Cur and Tri for respectively curvilinear and triangular; and HR, MED and LR for high, medium and low resolution respectively.

ening in rivers lead to lower depth-averaged flow velocities and hence higher water depths. The same differences between the grids, but in a smaller extent, are found in the lowest discharge range (see Figure D.1 and Figure D.2 in Appendix D.1). This shows that the false diffusion and numerical diffusion are indeed proportional to the depth-averaged flow velocity (see Equation 2.12). Respectively larger and smaller water depth and depth-averaged flow velocity differences are obtained in the medium discharge range relative to the lowest and highest discharge range.

Regarding the differences between grid shapes, we found somewhat lower water depths and higher depth-averaged flow velocities with the highest resolution curvilinear grid than with the same resolution variant for the triangular grid (Figure 3.1 and Figure 3.2). This suggests a slightly higher false diffusion for the latter grid, which is in contrast to the findings of Bomers et al. (2019). The differences with Bomers et al. (2019) are caused by the imposed geometry of the mild river meander, which allowed the curvilinear grid cells in this study to be aligned in the flow direction. Aligning curvilinear grid cells is more difficult in case studies in which large floodplain areas and sharp bends are included. Nonetheless, almost no differences in water depth are observed between the medium reso-

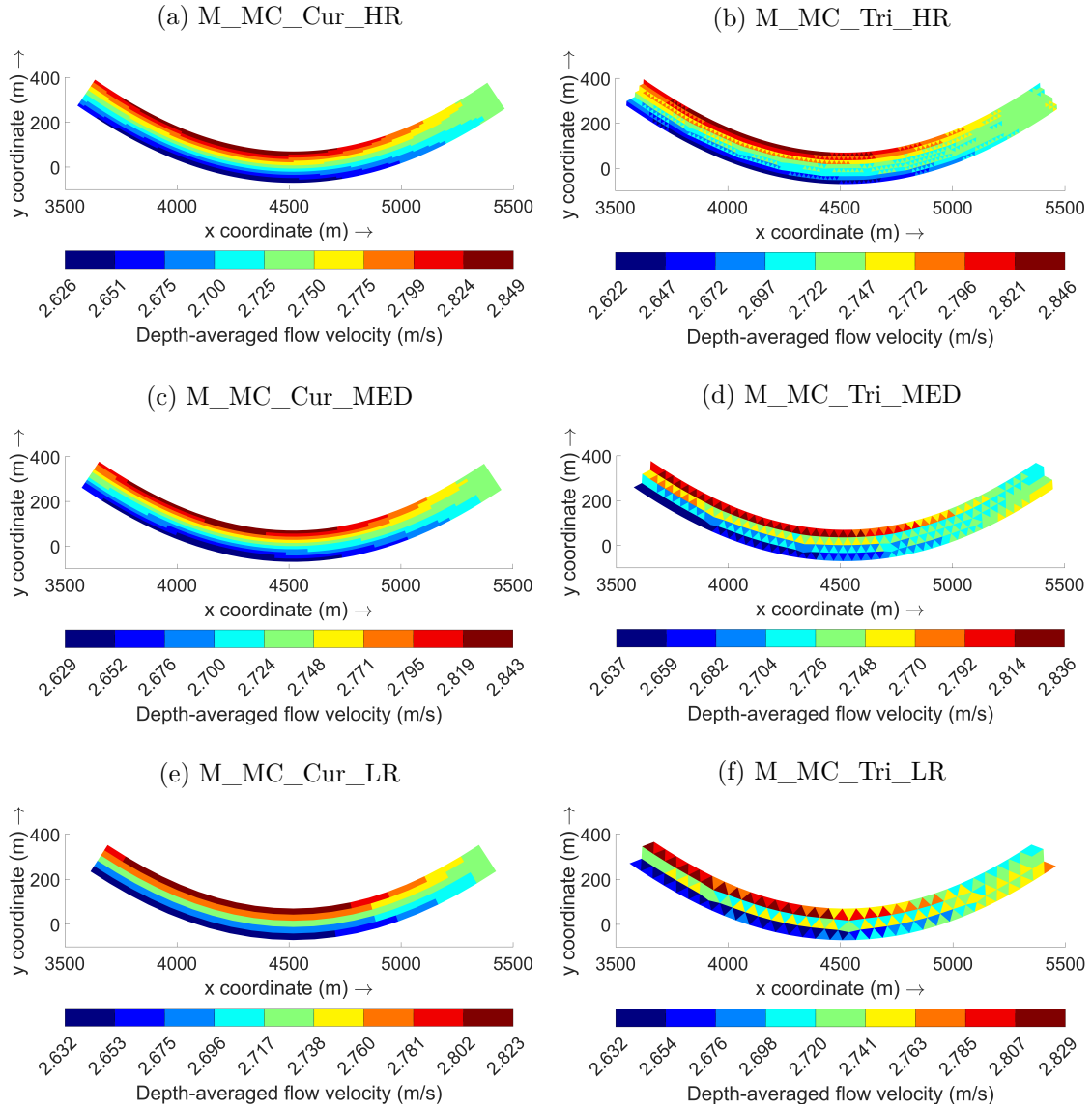


Figure 3.2: Map-plots of the simulated depth-averaged flow velocities for the mild river meander (main channel case) with the highest discharge range by the six considered grids. Regarding the names: M stands for mild; MC for main channel; Cur and Tri for respectively curvilinear and triangular; and HR, MED and LR for high, medium and low resolution respectively.

lution variants of the both the curvilinear and triangular grids (Figure 3.1 and Figure 3.2). In regards to the lowest resolution variants, the opposite occurred as the lowest resolution curvilinear grid simulated higher water depths and lower maximum depth-averaged flow velocities (Figure 3.1 and Figure 3.2). A greater false diffusion is obtained by the lowest resolution curvilinear grid since its cells are stretched by more than 100 meters, whereas the cells of the triangular grid are much more capable of capturing flow changes in the direction of the flow. This indicates that grid resolution is more influential for curvilinear grids than triangular grids, if curvilinear grid cells contain high aspect ratios.

In terms of the influence by the grid resolution as well as the grid shape, it is observed that the former seem to be more dominant. Larger water depth and depth-averaged flow velocity differences are obtained when applying coarser grids than using a different grid shape. This can be explained by considering the expression for the false coefficient (Equation 2.7) and the modified equation for the one-dimensional advection problem (Equation

2.12). Both false diffusion and numerical diffusion do depend largely on the grid size, while the orientation of the grid lines with respect to the flow direction only affects the false diffusion.

In regards to the computation time, differences are obtained which differ in the order of hours to minutes (Table 3.1). As one might expect, the higher resolution grids required more computation time than the coarser grids. Furthermore, having curvilinear grid cells instead of triangular grid cells, in case of the same resolution, resulted in lower computation times since the former are stretched in the flow direction. This eventually leads to a greater time step  $\Delta t$  (see Section 2.4.1).

Table 3.1: The computation time of all six grids for the mild river meander (main channel case). Here T stands for the computation time,  $\Delta t$  for the average time step and  $T_{ref}$  for the reference computation time, which is chosen to be the computation time of M\_MC\_Cur\_HR. Regarding the names: M stands for mild; MC for main channel; Cur and Tri for respectively curvilinear and triangular; and HR, MED and LR for high, medium and low resolution respectively.

Grid	T(h:min:s)	$\Delta t$ (s)	$T_{ref}/T$
M_MC_Cur_HR	03:02:00	3.5	1.0
M_MC_Cur_MED	00:15:15	8.8	11.9
M_MC_Cur_LR	00:01:09	22.4	138.2
M_MC_Tri_HR	03:55:06	1.9	0.8
M_MC_Tri_MED	00:18:54	3.8	9.6
M_MC_Tri_LR	00:06:45	5.2	27.0

### 3.1.2 Sharp river meander (main channel case)

In comparison to the milder variant, lower semi-stationary discharges are imposed at the upstream boundary of the sharp river meander. Consequently, we obtained water depths in the same order of magnitude between the two cases (Figure 3.3). Nonetheless, lower discharges led to smaller depth-averaged flow velocities values through the river bend in the sharper variant (Figure 3.4).

Regarding the general flood patterns in the sharp river meander, all six grids simulated an elevated water surface near the outer bank at CS 1, CS 2 and CS 3 (Figure 3.3). These observations correspond with those in the milder bend. Additionally, the water depth differences between the inner and outer bank (steepness of the water surface in the transverse flow direction) by each grid in the latter variant are in the same order of magnitude as those computed in the sharper bend. With the lowest and medium discharge range, similar flood pattern profiles are obtained for the water depth but only with lower water depth values. (See Figure D.3 in Appendix D.1 for the cross-section views of the simulated water depth for the sharp river meander (main channel case) with the lowest discharge range).

In terms of the depth-averaged velocity profiles, most grids tend to simulate higher depth-averaged flow velocities close to the inner bank at the bend entrance and apex, which is also seen in the main channel case of the mild river meander (Figure 3.4a, -b, -c and -e). Only the lowest and medium resolution triangular grids provide somewhat different results as the depth-averaged flow velocities decelerated at the inner bank of the bend apex and accelerated at the outer bank of the bend exit (Figure 3.4d and -f). Such patterns can even be seen in the highest resolution triangular grid, which has a tendency of decreasing the depth-averaged flow velocity earlier than the curvilinear grids at the inner bank after the bend apex. Comparable depth-averaged flow velocity profiles are obtained with the

lowest and medium discharge range. (See Figure D.4 in Appendix D.1 for the map-plots of the simulated depth-averaged flow velocity for the sharp river meander (main channel case) with the lowest discharge range). As the sinuosity of the meander increased, a higher resolution for triangular grids in transverse flow direction seems to be required to capture the rapid flow changes in the sharper river bend. The lowest resolution curvilinear grid simulated remarkably a similar depth-averaged flow velocity profile as the higher resolution curvilinear grids despite having only 5 cells in the transverse flow direction and largely stretched cells.

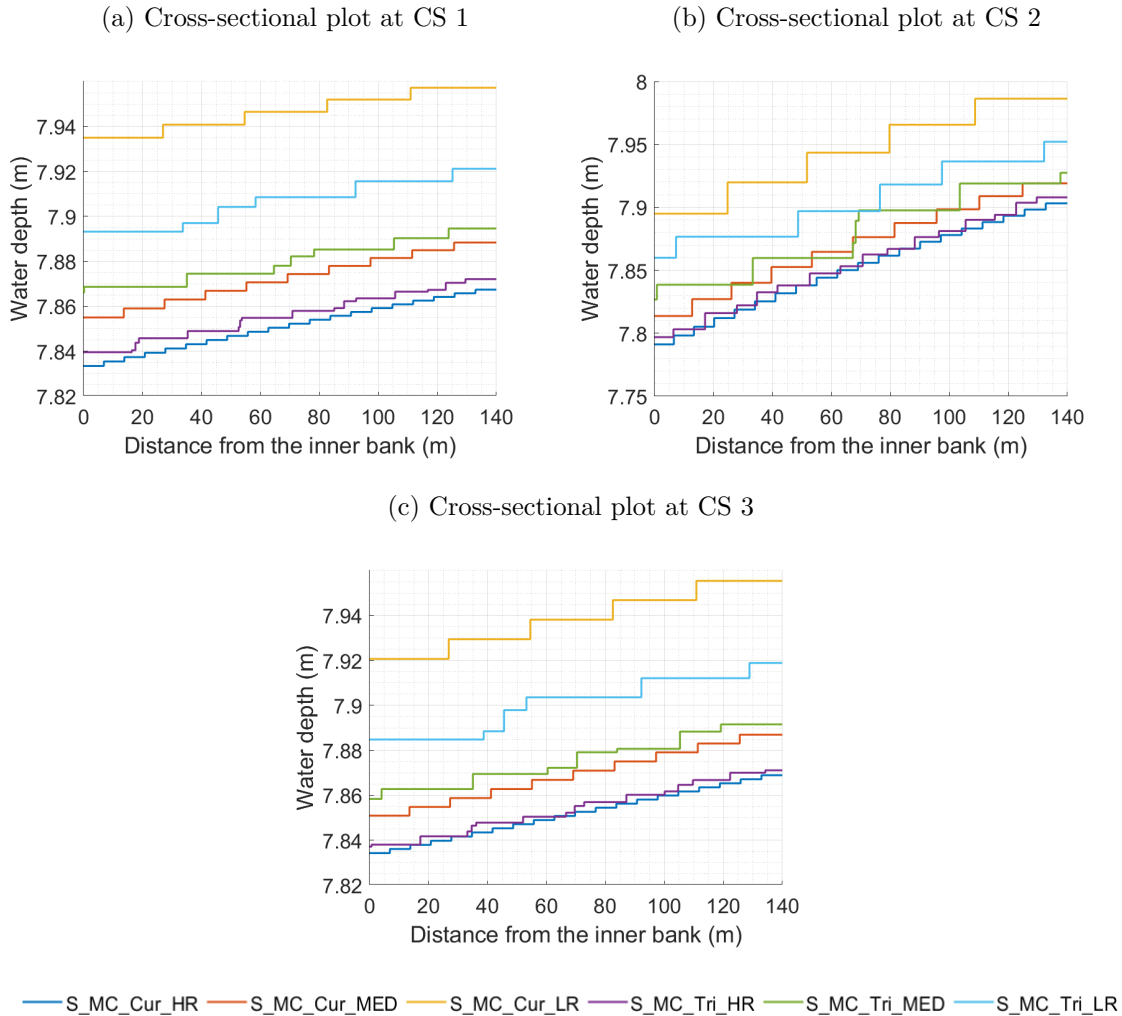


Figure 3.3: Cross-sectional view of the simulated water depth in the sharp river meander (main channel case) for the highest discharge range at CS 1, CS 2 and CS 3 by the six considered grids. Regarding the names: S stands for sharp; MC for main channel; Cur and Tri for respectively curvilinear and triangular; and HR, MED and LR for high, medium and low resolution respectively.

Apart from the general flood patterns for the depth-averaged flow velocity, large deviations in terms of the depth-averaged flow velocity values are obtained between the grids as well. Through the entire river bend lower depth-averaged flow velocities are simulated with the coarser grids (Figure 3.4), which eventually led to higher water depths (Figure 3.3). In the lowest and medium discharge range, smaller depth-averaged flow velocity differences are obtained, which resulted in to smaller differences in the simulated water depth between the grids.

Furthermore, considering the the depth-averaged flow velocity in transverse flow direction,

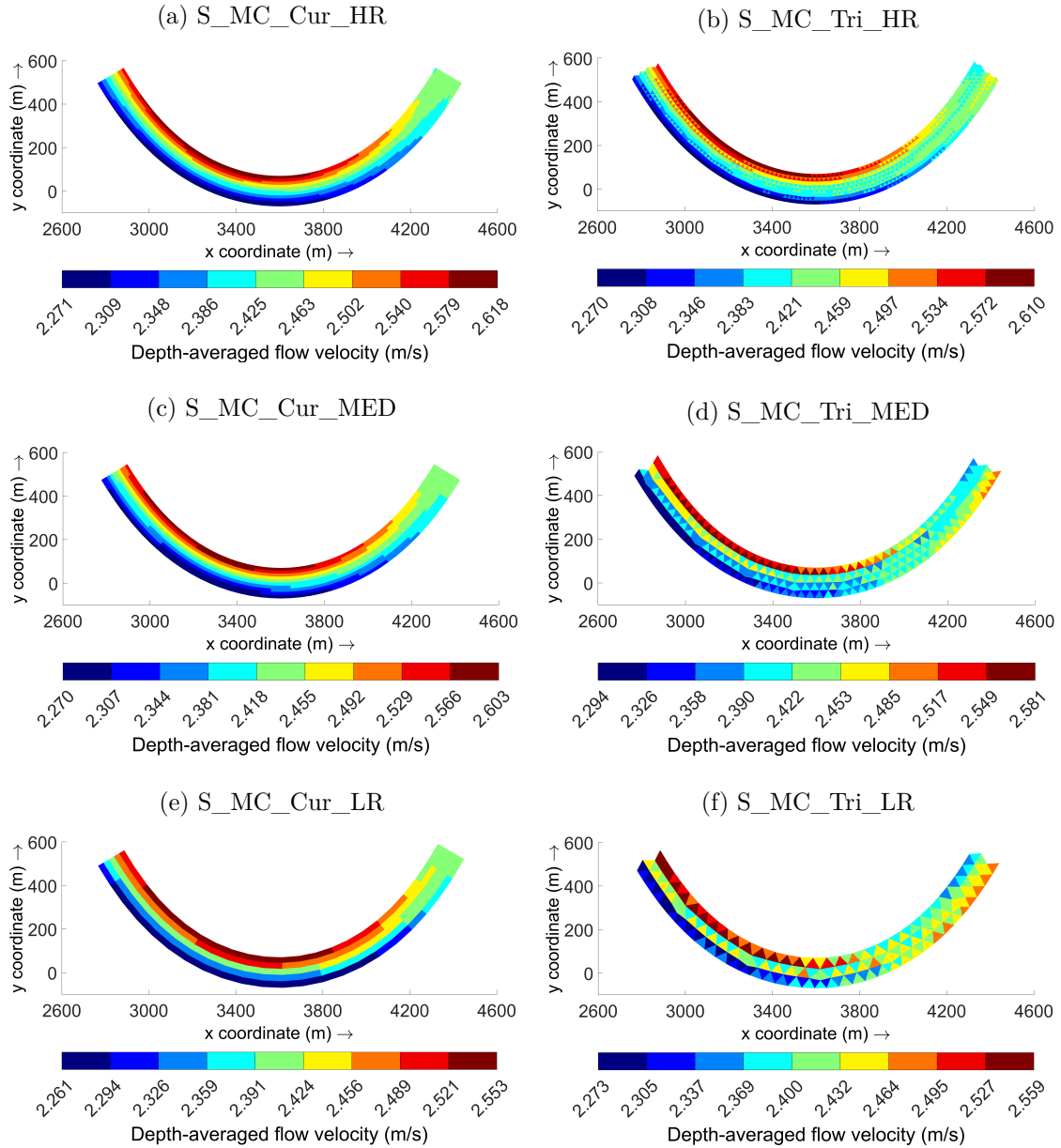


Figure 3.4: Map-plots of the simulated depth-averaged flow velocities for the sharp river meander (main channel case) with the highest discharge range by the six considered grids. Regarding the names: S stands for sharp; MC for main channel; Cur and Tri for respectively curvilinear and triangular; and HR, MED and LR for high, medium and low resolution respectively.

a more skewed profile is acquired by all six grids in the sharper bend than in the milder bend discussed earlier. A more skewed depth-averaged flow velocity profile induces a greater numerical diffusion as rapid flow changes in transverse and flow direction in sharp meandering bends do occur. Consequently, larger depth-averaged flow velocity and water depth differences are obtained in the sharper meander than in the milder case.

In regard to the differences between grid shapes, more or less similar results with respect to the main channel case of the mild river meander are obtained: (i) slightly lower water depths and depth-averaged flow velocities with the highest resolution curvilinear grid than with the same resolution variant for the triangular grid (Figure 3.3 and Figure 3.4); and (ii) higher water depths and somewhat smaller depth-averaged flow velocities with the

lowest curvilinear grid compared to the lowest resolution triangular grid (Figure 3.3 and Figure 3.4). In contrast to the results in the milder variant, slightly larger differences are observed between the medium resolution curvilinear and triangular grids. The former grid simulated lower water depths and higher maximum depth-averaged flow velocities. This once again shows that curvilinear grids with high aspect ratios are more sensitive to changes in grid resolutions than triangular grids.

Regarding the computation time, similar differences are obtained between the grids as in the milder meander (Table 3.2). In comparison to the computation times of the curvilinear grids in the mild river meander, shorter computation times are needed for the curvilinear grids in the sharp river meander (Table 3.1 and Table 3.2). The curvilinear grids in the sharper variant are slightly more stretched in the flow direction in case of the same grid resolution, which led to greater average time steps. For the triangular grids, shorter computation times are required in the sharp river meander as well.

Table 3.2: The computation time of all six grids for the sharp river meander (main channel case). Here T stands for the computation time,  $\Delta t$  for the average time step and  $T_{ref}$  for the reference computation time, which is chosen to be the computation time of S\_MC\_Cur\_HR. Regarding the names: S stands for sharp; MC for main channel; Cur and Tri for respectively curvilinear and triangular; and HR, MED and LR for high, medium and low resolution respectively.

Grid	T(h:min:s)	$\Delta t$ (s)	$T_{ref}/T$
S_MC_Cur_HR	02:34:51	4.0	1.0
S_MC_Cur_MED	00:14:19	10.2	10.8
S_MC_Cur_LR	00:00:59	23.8	157.5
S_MC_Tri_HR	02:40:14	2.2	1.0
S_MC_Tri_MED	00:28:14	4.7	5.5
S_MC_Tri_LR	00:04:29	7.3	34.5

### 3.1.3 Floodplain involvement

For the analysis of the hypothetical cases in which floodplains are present, we mainly focus on the water levels instead of water depths. As a consequence of the floodplain involvement, large water depth differences are obtained between the main channel and floodplains, which eventually is at the expense of a detailed display of the water surface. When considering water levels, a closer view of the water surface can be acquired as water levels between the main channel and floodplains do not differ as significantly as water depth values (Figure 3.5).

(In this subsection, the results of the sharp meander with floodplains are presented. For the results with respect to the hydrodynamics of the milder variant, which are comparable to the sharper case, we refer to the Appendix D.3).

In regards to the general flood patterns in the sharp river meander, all six grids simulated an elevated water surface near the outer bank of CS 1 and CS 2 (Figure 3.5). The elevation of the water surface is substantially larger in the main channel as higher depth-averaged flow velocities in bend correspond to greater centrifugal forces (Figure 3.6). At CS 3, the transverse tilting of the water surface is still present in the main channel, whereas the depth-averaged flow velocities in the floodplains are too small to induce outward directed centrifugal forces.

With respect to the depth-averaged flow velocities, differences are obtained in the main channel and at the transition between main channel and floodplain areas (Figure 3.6). With respect to the latter, a clear diffusion-like appearance is visible. It is presumed

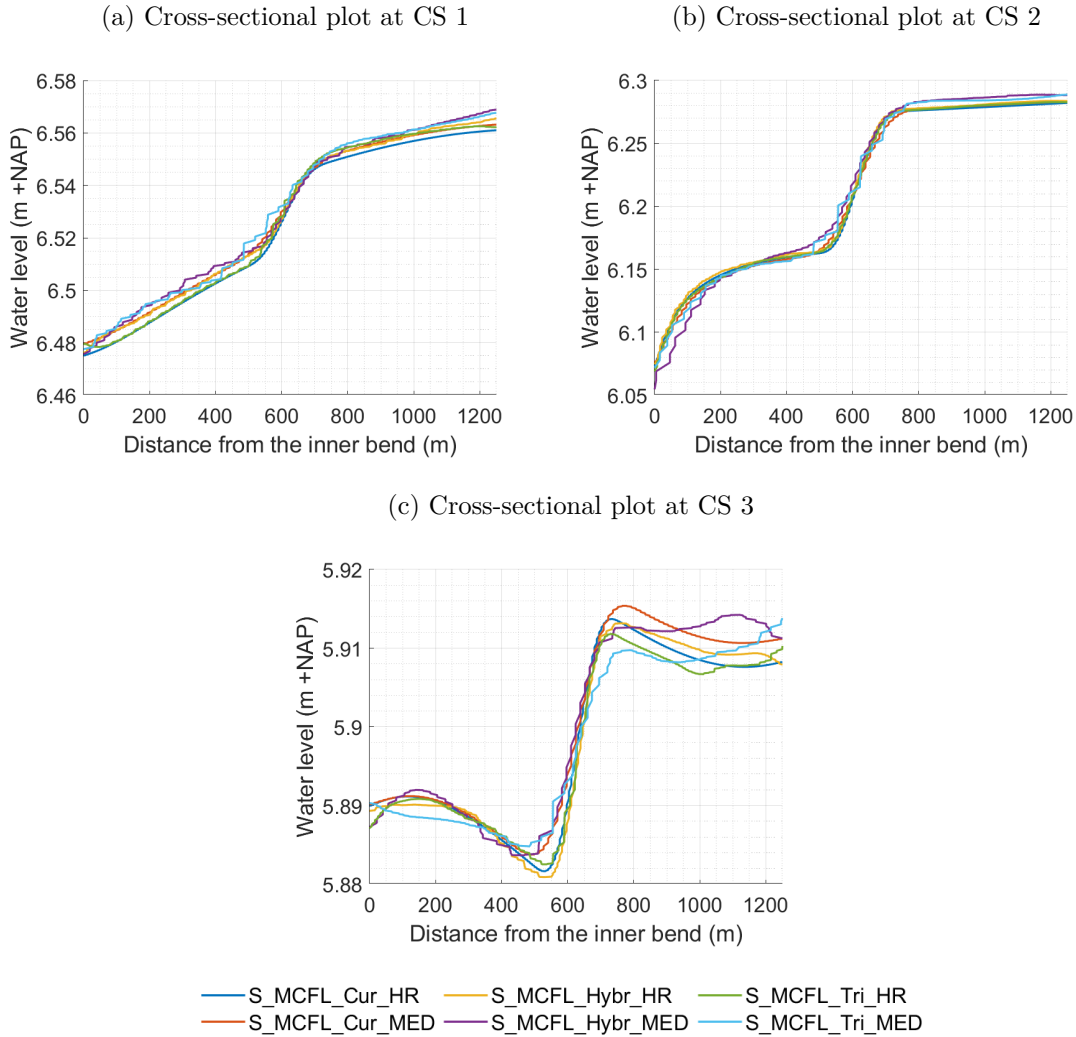


Figure 3.5: Cross-sectional view of the simulated water level in the sharp river meander (main channel and floodplain case) for the highest discharge range at CS 1, CS 2 and CS 3 by the six considered grids. Regarding the names: S stands for sharp; MCFL for main channel & floodplains; Cur, Tri and Hybr for respectively curvilinear, triangular and hybrid; and HR and MED for high and medium resolution respectively.

that due to large decrease in depth-averaged flow velocity from the main channel to the floodplain areas, a substantial increase in the diffusive term such as in Equation 2.12 is obtained and hence a greater numerical diffusion. At the transition between the main channel and floodplains, a more diffusion-like appearance is simulated by the coarser grids since the larger grid cells led to a greater false diffusion and numerical diffusion (Figure 3.6).

In terms of the grid shape, a more diffused depth-averaged flow velocity profiles are obtained at the transition between the main channel and floodplains by both the hybrid and triangular grids in comparison to the curvilinear grids. The grid cells of the former two seemed to generate a larger numerical diffusion and false diffusion than the latter one in the floodplain areas. A greater numerical diffusion is obtained by the triangular grid cells due to the smaller resolution in the transverse flow direction. A smaller false diffusion by the curvilinear grid cells is a result of a better alignment of these grid cells in the flow direction in the floodplain areas. The depth-averaged flow velocity differences between the hybrid and triangular grids can be explained by the fact that the size of the triangular cells of the hybrid grid are larger, which led to a higher numerical diffusion on top of the

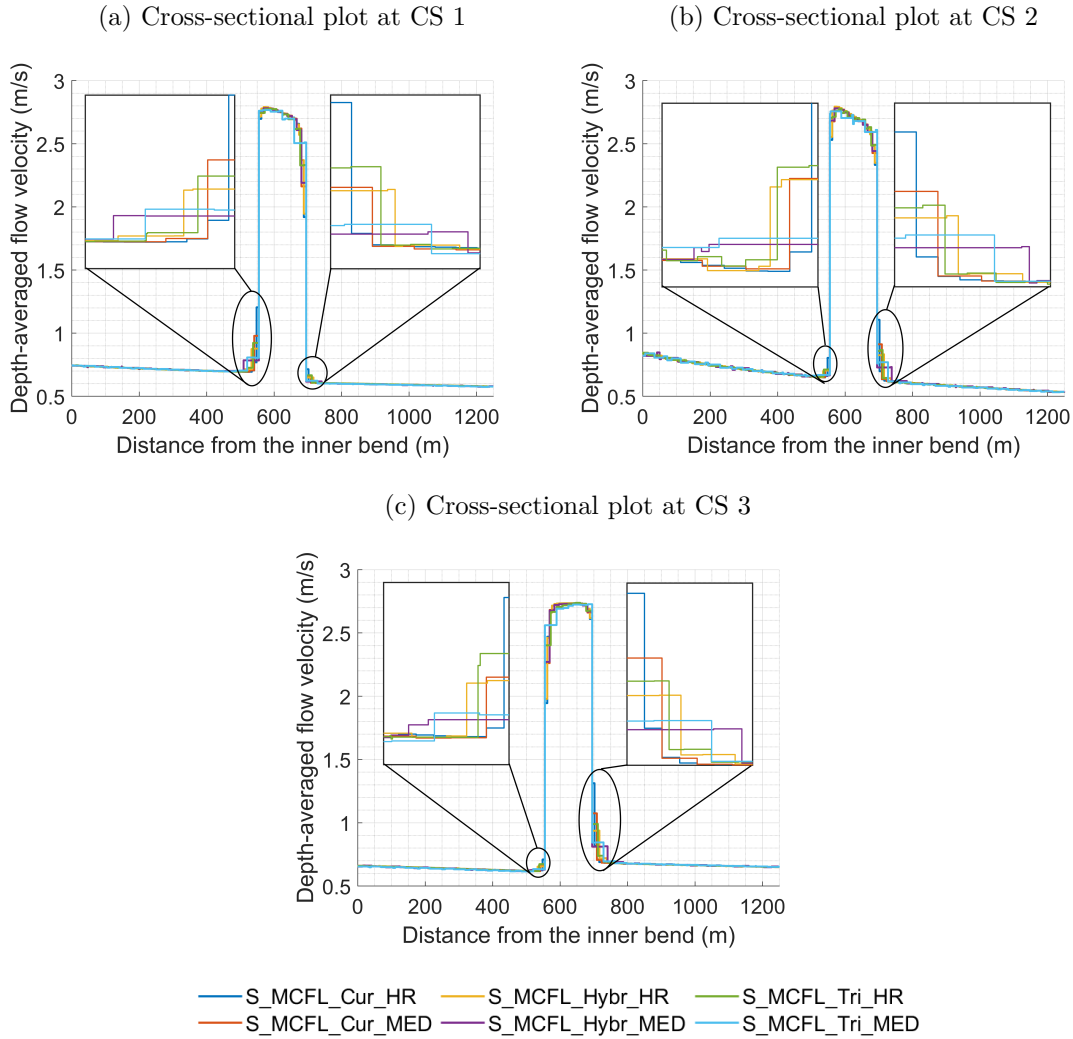


Figure 3.6: Cross-sectional view of the simulated depth-averaged flow velocity in the sharp river meander (main channel and floodplain case) for the highest discharge range at CS 1, CS 2 and CS 3 by the six considered grids. Regarding the names: S stands for sharp; MCFL for main channel & floodplains; Cur, Tri and Hybr for respectively curvilinear, triangular and hybrid; and HR and MED for high and medium resolution respectively.

generated false diffusion.

Despite the significant deviations in the depth-averaged flow velocity profiles, minor differences are obtained between the simulated water levels by the six grids. This is in contrast to the main channel cases. For the main channel cases, it has been addressed that relatively less differences in water depth and depth-averaged flow velocities are simulated by the grids when low discharges are imposed upstream. These findings also apply to the floodplains areas in which low depth-averaged flow velocities are present. In the cases in which floodplains are included, it can be seen that almost no depth-averaged flow velocity differences are visible in the floodplain areas. Consequently, relatively smaller differences in depth-averaged flow velocities are obtained between the grids over the entire spatial domain in comparison to the main channel cases. As a result of the floodplain involvement, the generated numerical effects in the main channel and at the transition between main channel and floodplain areas are smeared out through the model domain and hence dampened. This indicates that the induced numerical effects are proportional to the discharge per unit width. The latter is proportional to the mean depth-averaged flow velocity over a cross-section. The proportionality to the discharge per unit width also suggest that

the influence by generated numerical effects become less significant in hypothetical river meanders with a wide main channel and small floodplains.

Regarding the computation time of both the mild and sharp hypothetical river meanders in which floodplains are included, several differences can be observed. In the mild river meander with floodplains, having curvilinear grid cells instead of triangular grid cells, in case of the same resolution, results in lower computation times since the former is stretched in the flow direction (Table 3.3). However, in the sharp river meander with floodplains, the opposite occurred as the triangular grid cells have a lower computation time compared to the curvilinear grids. This is probably a consequence of the wide floodplains in combination with the sharp bends, which led to small curvilinear grid cells in the inner bends (Table 3.4). Additionally, comparing the computation time of the curvilinear grids in the mild river meander to the sharper variant, it can be seen that the curvilinear grids have higher computation time in the latter case due to the combination of wide floodplains and the sharper bends (Tables 3.3 and 3.4). This is however not the case in regards to the hybrid and triangular grids (Tables 3.3 and 3.4).

The hybrid grids on other hand, seemed to have a lower computation time in both the mild and sharp river meanders, which is probably due to the slightly larger triangular grid cell sizes in the floodplains compared to the curvilinear and triangular grids, as well as having stretched curvilinear grid cells in the main channel (Tables 3.3 and 3.4).

Table 3.3: The computation time of all six grids for the sharp river meander (main channel & floodplain case). Here T stands for the computation time,  $\Delta t$  for the average time step and  $T_{ref}$  for the reference computation time, which is chosen to be the computation time of M\_MCFL\_Cur\_HR. Regarding the names: M stands for mild; MCFL for main channel & floodplains; Cur, Tri and Hybr for respectively curvilinear, triangular and hybrid; and HR and MED for high and medium resolution respectively

Grid	T(h:min:s)	$\Delta t$ (s)	$T_{ref}/T$
M_MCFL_Cur_HR	31:30:56	3.6	1.0
M_MCFL_Cur_MED	02:55:32	8.2	10.8
M_MCFL_Hybr_HR	13:13:18	4.1	2.4
M_MCFL_Hybr_MED	01:02:45	11.2	30.1
M_MCFL_Tri_HR	41:16:45	1.9	0.7
M_MCFL_Tri_MED	04:20:20	3.8	7.3

Table 3.4: The computation time of all six grids for the sharp river meander (main channel & floodplain case). Here T stands for the computation time,  $\Delta t$  for the average time step and  $T_{ref}$  for the reference computation time, which is chosen to be the computation time of S\_MCFL\_Cur\_HR. Regarding the names: S stands for sharp; MCFL for main channel & floodplains; Cur, Tri and Hybr for respectively curvilinear, triangular and hybrid; and HR and MED for high and medium resolution respectively

Grid	T(h:min:s)	$\Delta t$ (s)	$T_{ref}/T$
S_MCFL_Cur_HR	56:02:55	2.2	1.0
S_MCFL_Cur_MED	05:47:37	4.7	9.7
S_MCFL_Hybr_HR	14:35:13	3.7	3.8
S_MCFL_Hybr_MED	01:15:07	9.4	44.8
S_MCFL_Tri_HR	43:40:49	1.9	1.3
S_MCFL_Tri_MED	04:43:50	3.7	11.8

## 3.2 Case study

The assessment of the case study begins with the river bend of the Grensmaas river where almost no floodplains are present (Section 3.2.1). Thereby, the main focus lies upon CS 1.1, CS 1.2 and CS 1.3 (See Figure 2.2). This is followed by the region where the floodplain areas are large (CS 2.1, CS 2.2, and CS 2.3) (Section 3.2.2). Afterwards, the impact of a local grid refinement is discussed (Section 3.2.3). At last, the computation time for each used grid in the case study is provided (Section 3.2.4).

### 3.2.1 River bend (small floodplain areas)

Similar to the hypothetical cases, we first assessed the general flood patterns to explore the differences between the six model simulations. The findings showed that all the six grids simulated more or less the same general flood patterns during the highest discharge range as in the hypothetical cases with floodplains: (i) an elevated water surface near the outer bank at CS 1.1, CS 1.2 and CS 1.3 (Figure 3.7a, -c and -e); and (ii) higher depth-averaged flow velocities in the main channel at CS 1.1, CS 1.2 and CS 1.3 (Figure 3.7b, -d and -f). Despite obtaining similar general flood patterns by each grid, both simulated water levels and depth-averaged flow velocities by each grid differ significantly (Figure 3.7). Comparing the water levels simulated by the six grids, we obtained higher water level predictions by the lower resolutions variants of the curvilinear, hybrid and triangular grids for the highest discharge range through the entire river bend (Figure 3.7a, -c and -e). In regards to the depth-averaged flow velocities, lower values are obtained in the main channel with the coarser grids throughout the river bend (Figure 3.7b, -d and -f). The opposite occurred at the floodplain area, where higher depth-averaged flow velocities are observed with the coarser grids (Figure 3.7b, -d and -f).

With respect to the grid shapes, curvilinear and hybrid grids produced similar water levels and depth-averaged flow velocities under the same level of grid resolution. The results of the triangular grids are less comparable, with the coarsest resolution triangular grid simulating the largest water levels relative to the other grids. These observations are in line with Lai (2010). This suggests that triangular grids require a higher resolution to achieve the same level of accuracy as the curvilinear and hybrid grids.

In comparison to the hypothetical river meanders, we obtained greater differences in water levels and depth-averaged flow velocities. This shows that the bathymetry discretisation plays an essential role in hydraulic river models. Moreover, the bathymetry discretisation can be more influential than numerical effects such as numerical diffusion and false diffusion, since significant differences in water levels and depth-averaged velocities are acquired between the fully curvilinear and fully triangular grids (Figure 3.7).

The same order of water level differences are also found in the lowest and medium discharge range in the main channel at the bend apex (Table 3.5). (Similar deviations in water levels are also observed at the bend entrance and exit.) This is in contrast to the hypothetical cases in which smaller differences are obtained at lower discharges and hence lower flow velocities. This indicates that the discretisation of the bathymetry is highly influential under low and high discharge conditions, whereas numerical effects, such false diffusion and numerical diffusion, become more noticeable at higher discharge conditions.

In terms of the discretised bathymetry, all grids overestimated the cross-sectional areas at the bend entrance (CS 1.1), apex (CS 1.2) and exit (CS 1.3) in comparison to the bathymetry data directly from the baseline-j14\_6-w14 database (Table 3.6). These significant differences in flow areas indicate that substantial bathymetry discretisation errors can be expected even with high resolution grids. Additionally, larger flow areas are obtained with the lower resolutions variants of the fully curvilinear, hybrid and fully triangular grids. As result, lower depth-averaged flow velocities are computed in the main channel

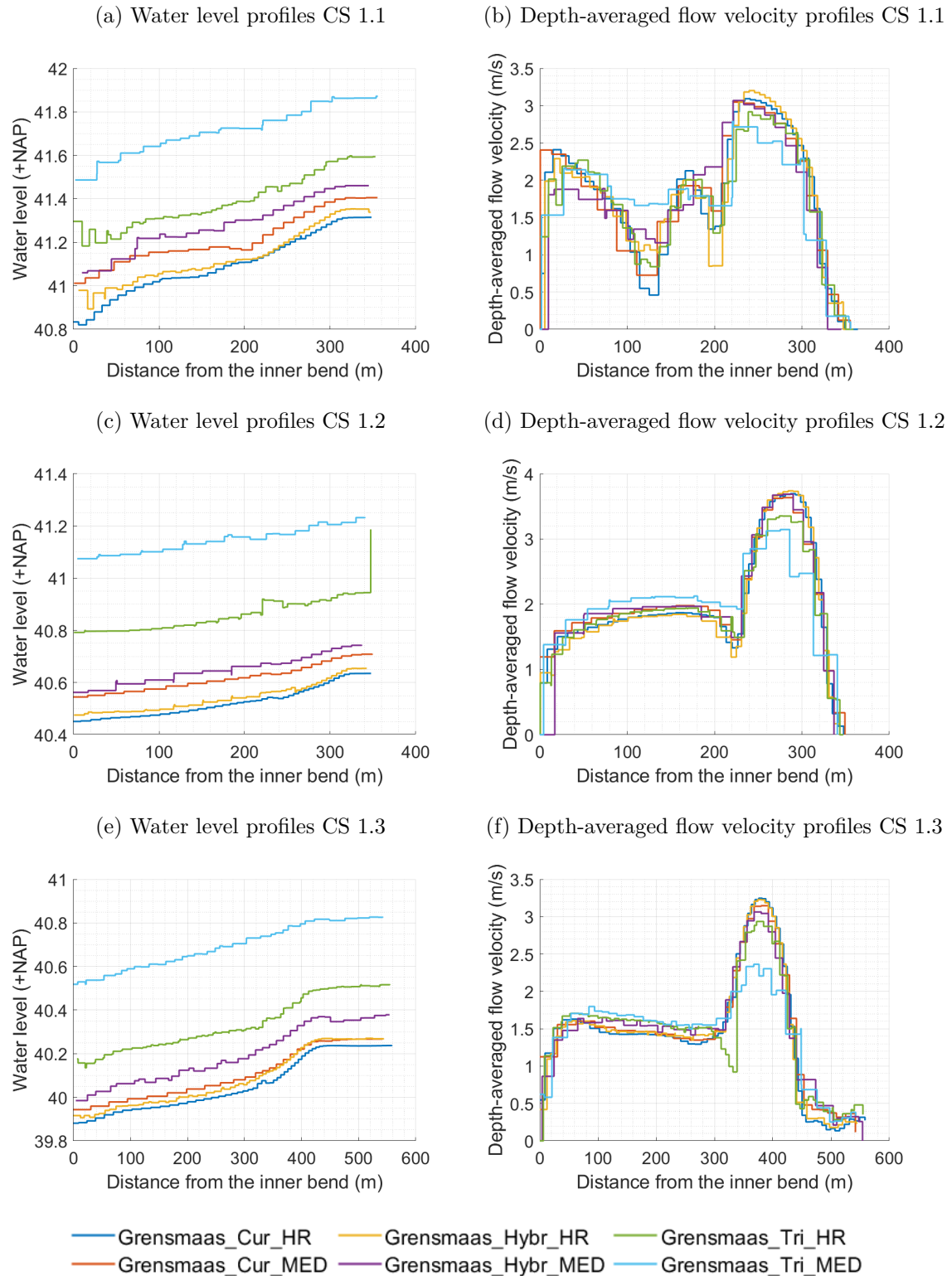


Figure 3.7: Cross-sectional view of the simulated water levels and depth-averaged flow velocities for the highest discharge range at CS 1.1, CS 1.2 and CS 1.3. Regarding the names: Grensmaas stands for the Grensmaas river; Cur, Tri and Hybr for respectively curvilinear (as much as possible), triangular and hybrid; and HR and MED for high and medium resolution respectively.

by the coarser grids. However, the reduction in depth-averaged flow velocity is not as significant as the increase in flow-area in the main channel, which led to higher water

levels through the cross-sectional areas CS 1.1, CS 1.2 and CS1.3 and hence higher depth averaged flow velocities in the floodplain areas. The largest differences in bed levels between the grids are observed in the main channel, whereas similar bed levels are obtained in the floodplain areas (Figure E.2 in Appendix E.1).

The flow areas between the grid shapes differ as well, with the triangular grids having higher flow areas through the main channel than curvilinear grids (Table 3.6). The flow areas for the hybrid grids vary more than the latter two grids, as the transition from curvilinear to triangular grid cells at the main channel boundary can lead to a smaller or larger flow area. An example of the former is the flow area at CS 1.2 with the Grensmaas\_Hybr\_HR, which is smaller than the rest of the flow areas at CS 1.2 (Table 3.6). A larger flow area by a hybrid grid is for instance obtained at CS 1.3 with the Grensmaas\_Hybr\_MED compared to the other flow areas.

Table 3.5: Predicted water levels in the main channel at the bend apex (CS 1.2) for the three discharges ranges by the six grids. Regarding the names: Grensmaas stands for the Grensmaas river; Cur, Tri and Hybr for respectively curvilinear (as much as possible), triangular and hybrid; and HR and MED for high and medium resolution respectively.

Grid	Water level low-range (m +NAP)	Water level mid-range (m +NAP)	Water level high-range (m +NAP)
Grensmaas_Cur_HR	34.51	39.46	40.57
Grensmaas_Cur_MED	34.61	39.55	40.67
Grensmaas_Hybr_HR	34.53	39.45	40.60
Grensmaas_Hybr_MED	34.62	39.57	40.71
Grensmaas_Tri_HR	34.61	39.73	40.88
Grensmaas_Tri_MED	35.08	40.06	41.15

Table 3.6: The flow area through the main channel at the bend entrance (CS 1.1), apex (CS 1.2) and exit (CS 1.3) for the six grids and the bathymetry data directly from the baseline-maas-j14\_6-w14 database. Regarding the names: Grensmaas stands for the Grensmaas river; Cur, Tri and Hybr for respectively curvilinear (as much as possible), triangular and hybrid; and HR and MED for high and medium resolution respectively.

Grid	Flow area CS 1.1 ( $m^2$ )	Flow area CS 1.2 ( $m^2$ )	Flow area CS 1.3 ( $m^2$ )
Grensmaas_Cur_HR	722.1	634.8	650.5
Grensmaas_Cur_MED	771.7	662.1	678.7
Grensmaas_Hybr_HR	736.1	620.4	665.1
Grensmaas_Hybr_MED	791.1	668.7	697.8
Grensmaas_Tri_HR	745.8	653.4	655.5
Grensmaas_Tri_MED	783.3	673.0	678.4
baseline-maas-j14_6-w14	665.7	584.8	602.9

### 3.2.2 River bend (wide floodplain areas)

Regarding the general flood patterns in the river bend with wide floodplains, all six grids simulated elevated water surface near the outer bank at CS 2.1, CS 2.2 and CS 2.3 (Figure 3.8a, -c and e). Apart from the higher depth-averaged flow velocities in the main channel, significantly larger depth-averaged flow velocities are obtained at the inner bend (Figure

2.2). This can be explained by the fact that at high discharges, water tends to take the shortest path through the bend, which is at the left floodplain at the inner bend.

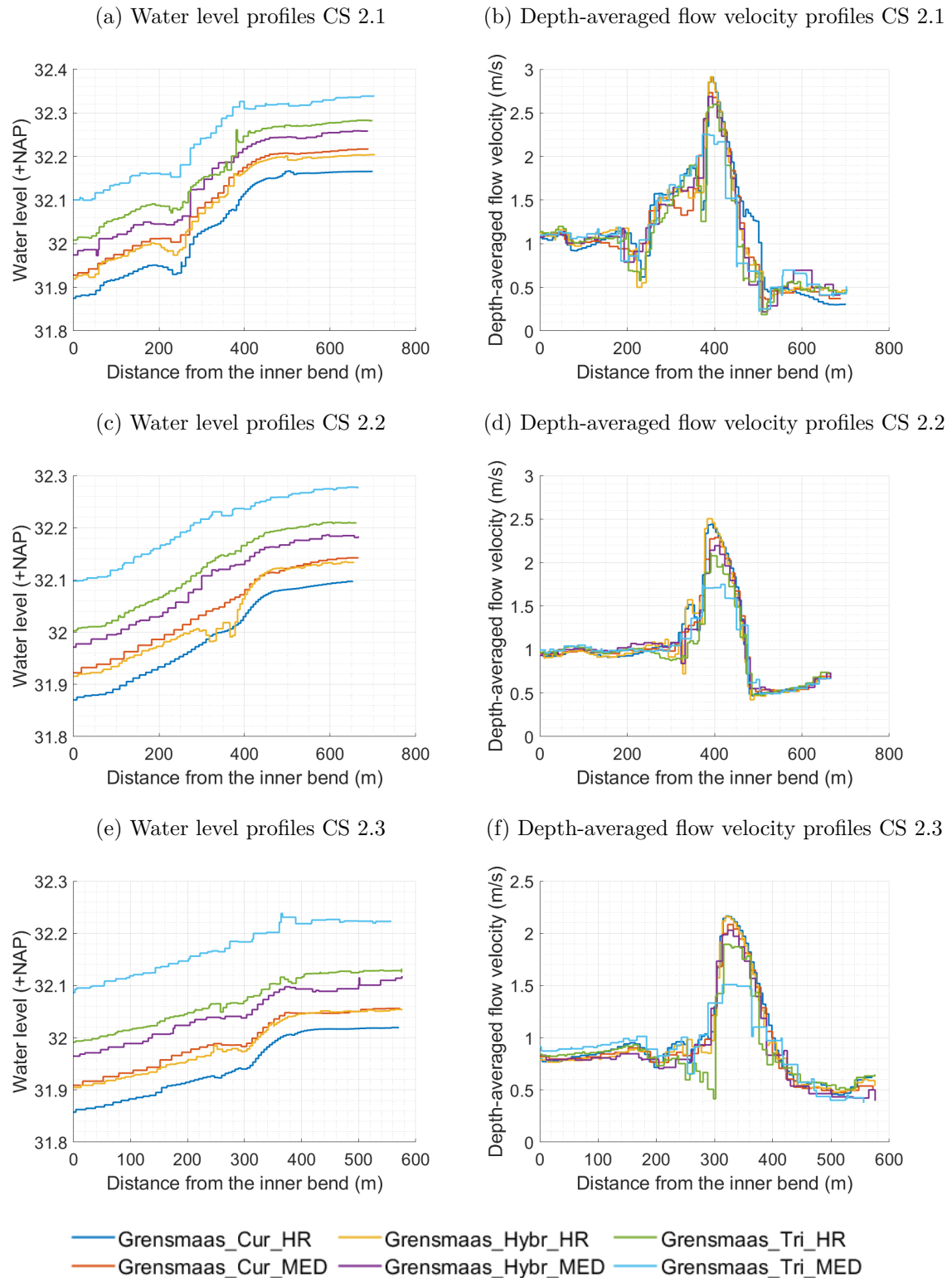


Figure 3.8: Cross-sectional view of the simulated water levels and depth-averaged flow velocities for the highest discharge range at CS 2.1, CS 2.2 and CS 2.3. Regarding the names: Grensmaas stands for the Grensmaas river; Cur, Tri and Hybr for respectively curvilinear (as much as possible), triangular and hybrid; and HR and MED for high and medium resolution respectively.

Similar as in the river bend with the small floodplain area, significant differences are obtained in water levels and depth-averaged flow velocities between the grids (Figure 3.8). Again, the lowest resolution grids simulated higher water levels and smaller depth-averaged flow velocities in the main channel for the highest discharge range. Regarding the grid shape, curvilinear and hybrid grids predicted once more lower water levels and higher depth-averaged flow velocities in the main channel for the highest discharge range in comparison to the triangular grids. Furthermore, considering the lower discharge ranges, we observed once again notable deviations in water levels in the main channel at the bend apex (CS 2.2) (Table 3.7). This suggests that the discretisation of the bathymetry is an important factor in hydraulic river models, since the numerical effects in the hypothetical river meanders led to minor differences in water levels and depth-averaged flow velocities in comparison to the case study.

Table 3.7: Predicted water levels in the main channel at the bend apex (CS 2.2) for the three discharges ranges by the six grids. Regarding the names: Grensmaas stands for the Grensmaas river; Cur, Tri and Hybr for respectively curvilinear (as much as possible), triangular and hybrid; and HR and MED for high and medium resolution respectively.

Grid	Water level low-range (m +NAP)	Water level mid-range (m +NAP)	Water level high-range (m +NAP)
Grensmaas_Cur_HR	25.19	30.94	32.07
Grensmaas_Cur_MED	25.33	31.06	32.11
Grensmaas_Hybr_HR	25.16	30.96	32.11
Grensmaas_Hybr_MED	25.33	31.11	32.16
Grensmaas_Tri_HR	25.37	31.24	32.19
Grensmaas_Tri_MED	26.20	31.54	32.25

Regarding the discretised bathymetry, the cross-sectional areas at the bend entrance (CS 2.1), apex (CS 2.2) and exit (CS 2.3) are once again overestimated by all the fully curvilinear, hybrid and fully triangular grids in comparison to the bathymetry data directly from the baseline-j14\_6-w14 database (Table 3.8). The largest flow areas are obtained with the coarser grids of each grid shape. Consequently, coarser grids simulated lower depth-averaged flow velocities. Nonetheless, higher water levels through the cross-sectional areas CS 2.1, CS 2.2 and CS 2.3 are obtained. Similar to the previously discussed river bend, the reduction in depth-averaged flow velocity is not as significant as the increase in flow-area in the main channel. The largest differences in bed levels between the grids are again observed in the main channel, whereas the bed levels in the floodplain areas are approximately the same (Figure E.4 in Appendix E.2).

It is noteworthy that in the river bend with wide floodplains greater water level differences between the grids are obtained at the lower discharges compared to the highest discharge range. This is in contrast to the first discussed river bend which had a small floodplain area. In the case of the river bend with wide floodplains, it can be seen that less depth-averaged flow velocity differences do occur in the floodplain areas between the grids since the bed levels in the floodplain areas for all grids are approximately the same (Figure 3.8). Consequently, relatively smaller differences in depth-averaged flow velocities are obtained between the grids over the entire spatial domain in comparison to the river bend with a small floodplain area. As a result of the large floodplain involvement, the influence of the bathymetry discretisation in the main channel is smeared out through the model domain and hence dampened. These observations are in line with those of the hypothetical river meanders in which floodplains are included.

Table 3.8: The flow area through the main channel at the bend entrance (CS 2.1), apex (CS 2.2) and exit (CS 2.3) for the six grids and the bathymetry data directly from the baseline-maas-j14\_6-w14 database. Regarding the names: Grensmaas stands for the Grensmaas river; Cur, Tri and Hybr for respectively curvilinear (as much as possible), triangular and hybrid; and HR and MED for high and medium resolution respectively.

Grid	Flow area CS 2.1 ( $m^2$ )	Flow area CS 2.2 ( $m^2$ )	Flow area CS 2.3 ( $m^2$ )
Grensmaas_Cur_HR	816.2	825.3	452.8
Grensmaas_Cur_MED	870.7	887.4	491.2
Grensmaas_Hybr_HR	816.8	824.0	456.8
Grensmaas_Hybr_MED	896.1	841.8	489.6
Grensmaas_Tri_HR	834.7	829.0	477.4
Grensmaas_Tri_MED	887.5	860.5	477.8
baseline-maas-j14_6-w14	756.3	737.6	414.9

### 3.2.3 Local grid refinement

Section 3.2.1 and 3.2.2 showed that significant changes in bed levels occur between the grids, which have major effects on the hydrodynamics through the river. In order to gain insight in how a local resolution change in grids influences the model outcomes, we firstly analysed the flow area through the main channel at CS 1.1, CS 1.2, CS 1.3, CS 2.1, CS 2.2 and CS 2.3.

The findings showed that a smaller flow area through the main channel is obtained at all cross-sectional areas with the locally refined grids in comparison to the medium resolution grids (Table 3.9 and Table 3.10). For the Grensmaas\_Tri\_MED\_Loc\_Ref, even smaller flow areas are acquired than the Grensmaas\_Tri\_HR, which is likely a result of the higher resolution of the locally refined grid at the outer ends of the floodplains. However, differences in flow area between the locally refined grids and the bathymetry data directly from the baseline-j14\_6-w14 database are still present.

Table 3.9: The flow area through the main channel at the bend entrance (CS 1.1), apex (CS 1.2) and exit (CS 1.3) for the three locally refined grids. Regarding the names: Grensmaas stands for the Grensmaas river; Cur, Tri and Hybr for respectively curvilinear (as much as possible), triangular and hybrid; HR and MED for high and medium resolution respectively; and Loc and Ref for locally and refined respectively.

Grid	Flow area CS 1.1 ( $m^2$ )	Flow area CS 1.2 ( $m^2$ )	Flow area CS 1.3 ( $m^2$ )
Grensmaas_Cur_MED_Loc_Ref	719.9	633.7	646.7
Grensmaas_Hybr_MED_Loc_Ref	742.2	620.5	664.5
Grensmaas_Tri_MED_Loc_Ref	733.1	640.8	651.5

In the river bend with the small floodplain area, a local grid refined led to a reduction in water level at the bend apex CS 1.2 compared to the coarsest grids of each grid shape (Table 3.11). (Similar deviations in water level are also observed at the bend entrance and exit.) Especially the Grensmaas\_Cur\_MED\_Loc\_Ref and Grensmaas\_Hybr\_MED\_Loc\_Ref simulated water level values close to those of the higher resolution grids of these grid shapes. The water levels computed by the Grensmaas\_Tri\_MED\_Loc\_Ref converges as well to water level values generated by the higher resolution variant. However, the simulated water levels by the former still differ substantially with respect to the higher

Table 3.10: The flow area through the main channel at the bend entrance (CS 2.1), apex (CS 2.2) and exit (CS 2.3) for the three locally refined grids. Regarding the names: Grensmaas stands for the Grensmaas river; Cur, Tri and Hybr for respectively curvilinear (as much as possible), triangular and hybrid; HR and MED for high and medium resolution respectively; and Loc and Ref for locally and refined respectively.

Grid	Flow area CS 2.1 ( $m^2$ )	Flow area CS 2.2 ( $m^2$ )	Flow area CS 2.3 ( $m^2$ )
Grensmaas_Cur_MED_Loc_Ref	813.0	821.2	450.3
Grensmaas_Hybr_MED_Loc_Ref	823.6	820.4	456.7
Grensmaas_Tri_MED_Loc_Ref	835.9	811.5	468.8

resolution variant, which is less the case for locally refined curvilinear and hybrid grids. This suggests that triangular grids are less responsive to local grid refinements as curvilinear and hybrid grids.

Regarding the river bend with the wide floodplain areas, similar results are obtained (Table 3.12). The water levels simulated during the high discharge range by the Grensmaas\_Tri\_MED\_Loc\_Ref are in this river bend closer to water level values generated by the higher resolution variant as in the river bend with a small floodplain area. This can be explained by the fact that the simulated water levels differences during the highest discharge range by the medium and high resolution triangular grids are deviate less in contrast to the river bend with small floodplains.

Table 3.11: Predicted water levels in the main channel at the bend apex (CS 1.2) for the three discharges ranges by the three locally refined grids. Regarding the names: Grensmaas stands for the Grensmaas river; Cur, Tri and Hybr for respectively curvilinear (as much as possible), triangular and hybrid; HR and MED for high and medium resolution respectively; and Loc and Ref for locally and refined respectively.

Grid	Water level low-range (m +NAP)	Water level mid-range (m +NAP)	Water level high-range (m +NAP)
Grensmaas_Cur_MED_Loc_Ref	34.57	39.44	40.58
Grensmaas_Hybr_MED_Loc_Ref	34.56	39.45	40.61
Grensmaas_Tri_MED_Loc_Ref	34.77	39.87	41.04

Table 3.12: Predicted water levels in the main channel at the bend apex (CS 2.2) for the three discharges ranges by the three locally refined grids. Regarding the names: Grensmaas stands for the Grensmaas river; Cur, Tri and Hybr for respectively curvilinear (as much as possible), triangular and hybrid; HR and MED for high and medium resolution respectively; and Loc and Ref for locally and refined respectively.

Grid	Water level low-range (m +NAP)	Water level mid-range (m +NAP)	Water level high-range (m +NAP)
Grensmaas_Cur_MED_Loc_Ref	25.22	31.00	32.11
Grensmaas_Hybr_MED_Loc_Ref	25.20	31.03	32.13
Grensmaas_Tri_MED_Loc_Ref	25.70	31.41	32.20

### 3.2.4 Computation time

For the case study, the computation time of the nine considered grids differ in order of days to hours, which is similar to the applied grids in hypothetical river meanders where floodplains are included (Table 3.13). As one might expect, the higher resolution grids of each grid shape required more computation time than the coarser grids. Moreover, in case of the same resolution, having curvilinear grid cells instead of triangular grid cells led to higher computation times since the former are stretched in the flow direction. Consequently, smaller time steps are obtained with triangular grid cells (see Section 2.4.1). The hybrid grids, on the other hand, have computation times which are in between those of the curvilinear and triangular grids. This can be explained by the fact that the hybrid grids contain both curvilinear and triangular grid cells.

Despite having two locally refined river bends, significantly longer computation times were required for the locally refined grids with respect to the medium resolution grids for each grid shape. The local refinements in the curvilinear grid led to approximately 4.5 times longer computation times relative to the Grensmaas\_Cur\_MED. The local refinements in the triangular grid, however, resulted in an increase of approximately 2 times the computation time of the medium variant (Table 3.13). When it comes to the time steps, the locally refined triangular grid has on average a greater time step than the locally refined curvilinear and hybrid grids. This indicates that curvilinear and hybrid grids are more sensitive for local grid refinements in river bends in regards to the computation time as curvilinear grid cells may become significantly smaller in size. Larger average time steps for the curvilinear and triangular grids are obtained at the medium resolutions compared to the triangular grids, which explains why the locally refined curvilinear and hybrid grids are more computationally efficient than the locally refined triangular grid.

Table 3.13: The computation time of all nine grids for the case study. Here T stands for the computation time,  $\Delta t$  for the average time step and  $T_{ref}$  for the reference computation time, which is chosen to be the computation time of Grensmaas\_Cur\_HR. Regarding the names: Grensmaas stands for the Grensmaas river; Cur, Tri and Hybr for respectively curvilinear (as much as possible), triangular and hybrid; HR and MED for high and medium resolution respectively; and Loc and Ref for locally and refined respectively.

Grid	T(h:min:s)	$\Delta t$ (s)	$T_{ref}/T$
Grensmaas_Cur_HR	43:31:11	1.0	1.0
Grensmaas_Cur_MED	02:34:06	4.8	16.9
Grensmaas_Cur_MED_Loc_Ref	11:04:27	1.4	3.9
Grensmaas_Hybr_HR	65:31:09	0.9	0.7
Grensmaas_Hybr_MED	06:01:13	3.6	7.2
Grensmaas_Hybr_MED_Loc_Ref	20:17:05	1.1	2.1
Grensmaas_Tri_HR	68:43:00	0.9	0.6
Grensmaas_Tri_MED	12:12:15	2.1	3.6
Grensmaas_Tri_MED_Loc_Ref	23:10:33	1.5	1.9

## 4 Discussion

In this research, the influence of grid generation choices on hydraulic river modelling outcomes in river meander bends was analysed. This section starts with discussion on the grid generation choices in hydraulic river models (Section 4.1). Next, the limitations of this study are discussed (Section 4.2). Finally, the implications of this study are addressed (Section 4.3).

### 4.1 Influences of the grid generation choices

In this study, we simulated the hydrodynamics with different grid shapes and grid resolutions through hypothetical river meanders, which are idealised rivers, and the Grensmaas river. Hypothetical river meanders are considered to first gain an insight in how influential and under which conditions effects by grid generation choices affect hydraulic river modelling outcomes if model errors by bathymetry accuracy are excluded. Afterwards, we verified whether these numerical effects by grid generation choices are found in a natural river as well. In this subsection, we touch upon both the numerical and bed level discretisation effects, and the computation time. We start with the former and discuss whether the theoretical framework presented in Section 2.1.2 corresponds to our findings. In regards to the bed level discretisation effects, we compare the results to the literature. Afterwards, we compare the required computation time for each grid in the hypothetical river meanders and case study to the literature.

#### 4.1.1 Numerical effects

In this study, we addressed two types of numerical effects: (i) false diffusion; and (ii) numerical diffusion. According to Patankar (1980), the former is a numerical effect with a diffusion-like appearance, which can be reduced by increasing the grid resolution and/or projecting the grid cells such that grid lines are better aligned with the direction of the flow. The findings in our study for the hypothetical river meanders are in line with Patankar (1980), since a more diffused depth-averaged flow velocity cross-sectional profiles are obtained by the coarser grids. Despite having larger grid cells, the coarser grids also tend to have grid lines which are less parallel to the flow direction in river bends in order to capture the flow changes. This is especially the case for curvilinear grid cells, which in our study contain on average aspect ratios of four. Furthermore, Patankar (1980) showed that false diffusion becomes smaller at lower depth-averaged flow velocities. This contribution to the false diffusion corresponds to the findings of the hypothetical river meanders, since we obtained lower water level differences between grid shapes with approximately the same resolution at lower depth-averaged flow velocities.

Considering Equation 2.12 in Section 2.1.2, the extent of the numerical diffusion increases with (i) larger grid cells; (ii) greater depth-averaged flow velocities; and (iii) rapid flow changes. The contribution of these three factors to the numerical diffusion correspond to the findings in the hypothetical river meanders. So, did we find a more diffused depth-averaged flow velocity cross-sectional profiles with the coarser grids and/or at higher discharge ranges and hence higher depth-averaged flow velocities. Furthermore, in sharper river bends and at the transition between main channel and floodplain, greater diffusion effects are noticed as a result of the rapid flow changes at those regions. For the hypothetical river meanders, grid resolution seemed to generate more numerical diffusion and false diffusion as the differences in depth-averaged flow velocities and water levels between grid resolutions are substantially larger than between grid shapes.

### 4.1.2 Bed level discretisation effects

According to De Jong and Mohamed (2016) there are several ways to discretise model domains in D-Flow FM. In this study, we discretised the bed levels in two ways: (i) on the corner nodes of the grid cells; and (ii) directly at the cell center of the grid cells. The latter is applied to the hypothetical river meanders where floodplains are included in order to avoid discretisation errors of the bathymetry at the transition between the main channel and floodplains. This setup was not required for the hypothetical river meanders with only the main channel. For the case study, we discretised the bed levels on the corner nodes in order to avoid overestimation of the bed levels at the cell faces and hence higher water levels by each grid.

In the hypothetical river meanders, the combined effects of both the false diffusion and numerical diffusion on simulated water level differed in the order of millimeters to centimeters. The maximum deviation observed in the hypothetical river meanders is approximately  $11\text{cm}$ , which is contrast to Bomers et al. (2019) who found significantly greater water level differences between several grid resolutions and grid shapes in a case study. This indicates that the presence of a variable bathymetry is highly influential in hydraulic river models.

In De Jong and Mohamed (2016) several discretisation methods are applied to the same grids, which led to substantial deviations in water levels as well. These deviations were in the same order of magnitude as the differences of Bomers et al. (2019). The findings of this study showed significant water level differences between the grids at the two considered river bends in the case study. These water level differences were in the same order of magnitude as those in De Jong and Mohamed (2016) and Bomers et al. (2019). Additionally, we obtained significant differences in depth-averaged flow velocity profiles.

Furthermore, according to Bomers et al. (2019), bed level discretisation and numerical effects are more influential in river sections where floodplain areas are wide. This is in contrast to the findings of this study, as in both the hypothetical river meanders with floodplains and the Grensmaas river with the wide floodplain areas, smaller deviations in depth-averaged flow velocity and water level profiles are obtained. The analysis of the study showed that as a result of large floodplain involvement, the influence of the numerical effects and bathymetry discretisation in the main channel is smeared out trough the model domain and hence dampened.

### 4.1.3 Computation time

In this study, the required computation time between grids differed in the order of days to minutes. The shortest computation times were found in the hypothetical river meanders in which we only considered the main channel. In both the mild and sharp hypothetical river meanders with only the main channel, the computation times of the curvilinear grids were lower than those of the triangular grids, since the former were stretched in the flow direction without having infinitely small grid cells at the inner bank of the river bend.

In the hypothetical river meanders with floodplains and the Grensmaas river, the computation times varied in the order of days to hours. In both cases, computation times of days were found for the highest resolution grids. Computation times of hours were observed for the medium resolution grids. In Bomers et al. (2019), curvilinear, hybrid and triangular grids with respectively 12, 8 and 10 grid cells across the width of the main channel are in terms of the grid resolution comparable with the medium resolution grids in the hypothetical river meanders with floodplains and the Grensmaas river. Even though the model domains of respectively the hypothetical river meanders with floodplains and the Grensmaas river were a factor 1.3 and 1.7 larger than the considered model domain by Bomers et al. (2019), significantly longer computation times were required in this study.

An explanation of the differences in computation time between the studies could be due several factors such as the width of the model domains and performance of the processor of the applied computer.

Despite the overall shorter computation times in Bomers et al. (2019), hybrid grids have shown to be computationally efficient in the hypothetical river meanders with floodplains and the Grensmaas river as well as in Bomers et al. (2019). Curvilinear grids on the other hand, become less efficient when large floodplains are included since curvilinear grid cells tend to become sufficiently small. This is especially true for higher resolution grids. Similar findings were also observed by Bomers et al. (2019) as a curvilinear grid with 16 grid cells across the main channel width resulted in the longest computation time in Bomers et al. (2019).

For the Grensmaas river, applying curvilinear grid cells instead of hybrid and triangular grids was more efficient. The grid cells of the former were stretched in the flow direction, without having small grid cells in sharp and wide floodplain areas due to the inclusion of quadrilateral grid cells. Quadrilateral grid cells prevented no overlapping and/or infinitely small grid cells.

## 4.2 Limitations

To create comparable water depths between the hypothetical river meanders and the case study, different semi-stationary discharges are imposed since the river characteristics of each hypothetical case and the case study are unique. To acquire comparable flow conditions between the hypothetical river meanders and the case study, we imposed semi-stationary discharges such that similar flow conditions at the end of the Grensmaas river (km-55) and the hypothetical river meanders are obtained. Despite having similar flow conditions at the end of the Grensmaas river and the hypothetical river meanders, substantial depth-averaged flow velocity differences are observed between the analysed river bends in the case study and the hypothetical river meanders. In both river bends in the case study, higher depth-averaged flow velocities are simulated during the high discharge conditions in the main channel than those in the hypothetical river meanders during the highest discharge range. As we have noticed in the hypothetical river meanders, numerical effects such as false diffusion and numerical diffusion become more influential at higher depth-averaged flow velocities. Consequently, greater numerical effects are expected to take place in the case study during high discharge conditions than in the hypothetical river meander. However, for the medium discharge range, depth-averaged flow velocity values in the river bends in the case study (Figure E.1 and Figure E.3) correspond much more to those in the hypothetical river meanders during high discharge conditions. Comparing the better matched flow conditions at the medium discharge range for the case study and the high discharge condition for the hypothetical river meanders indicates once again that the effect by the bed level discretisation is a more dominant factor in hydraulic river models due to the large differences in water level and depth-averaged flow velocities between the grids in the case study for medium discharge conditions.

In this study, the influence of the numerical and bed level discretisation effects in the hypothetical river meanders and case study are analysed for three constant flow scenarios: (i) low; (ii) mid; and (iii) high discharge range. In practical cases, variable discharges are much more common instead of a constant discharge at the upstream boundary. Consequently, this study does not consider the numerical and discretisation effects in the case of, for instance, a discharge wave, in which depth-averaged flow velocity accelerate and decelerate later on. For a discharge wave, it is presumed that more numerical errors are generated during rise of the discharge wave than when it descends. Furthermore, it is expected that less numerical errors are generated further downstream in a river, since the height of a discharge wave weakens along a (meandering) river channel. The effects by the

bathymetry discretisation remains probably the same as during a constant flow scenario. Nonetheless, even for a discharge wave, it is presumed that the bathymetry discretisation is significantly more influential than numerical effects.

In regards to the physical horizontal turbulence, D-Flow FM offers two options: (i) applying a constant horizontal eddy viscosity coefficient; and (ii) a simple horizontal model, the so called "Smagorinsky model". In this study, a uniform horizontal eddy viscosity of  $0.1m^2/s$  was used in the hypothetical river meanders. In the case study, a combination of a uniform horizontal eddy viscosity of  $0.1m^2/s$  and the Smagorinsky model was used, in which the former is added on top of the horizontal eddy viscosity coefficient determined by the Smagorinsky model (Deltares, 2019a). Consequently, higher horizontal eddy viscosities are present in the case study in comparison to the hypothetical river meanders. In De Jong and Mohamed (2016), it was found that higher horizontal eddy viscosity coefficients lead to respectively lower and higher depth-averaged flow velocities in the main channel and floodplains. Moreover, De Jong and Mohamed (2016) showed that as a result of lower depth-averaged flow velocities in the main channel, higher water levels are simulated. With respect to this study, the findings of De Jong and Mohamed (2016) suggest that higher depth-averaged flow velocities could have been acquired in the floodplains for the hypothetical river meanders if the physical horizontal turbulence was modelled with the same model set up as in the case study. Whether relatively larger differences in depth-averaged flow velocities would have been obtained in the hypothetical river meanders with floodplains and hence greater numerical effects remains unknown. Nonetheless, it is presumed that bathymetry discretisation is significantly more influential than numerical effects, since the differences in water level and depth-averaged flow velocities in the hypothetical river meander without floodplains (in which throughout the entire spatial domain high depth-averaged flow velocities were simulated) were significantly smaller than those in the case study.

Furthermore, during the analysis of the hypothetical river meanders, the downstream boundary condition seemed to be influential in river bends upstream. Therefore, we evaluated the second bend in the hypothetical river meanders in order to exclude the effects of the downstream boundary condition. However, the second bend in the hypothetical river meanders is close to the upstream boundary conditions. This makes this study unable to give insight in whether numerical effects in the hypothetical river meander propagate or stay constant throughout the model domain.

In the case study, apart from the bed level variations, roughness characteristics did differ between the grids as well. This means that the numerical and bed level discretisation effects were not fully isolated, since roughness discretisation may influence model outcomes as well. According to Caviedes-Voullième et al. (2012), influences by the roughness discretisation can be considered as insignificant if small differences are observed between the average roughness and the distributed roughness through the spatial domain. Additionally, Caviedes-Voullième et al. (2012) noted that if important variations in roughness are present, special treatment with respect to the roughness discretisation may be required.

### 4.3 Implications

In previous research, grid shape and grid resolution effects have already been studied. Caviedes-Voullième et al. (2012) highlighted that in river models, grid coarsening and poor alignment between grid and the direction of the flow led to diffused discharge waves and hence lower depth-averaged flow velocities. These findings have been confirmed by De Jong and Mohamed (2016) and Bomers et al. (2019) who showed both that coarser grids simulate higher water levels, which is likely a result of the reduction in depth-averaged flow velocities by coarser grids. This study has gained insight in the effects of grid generation choices on hydraulic modelling outcomes in both hypothetical and natural river meanders.

In both cases, simulated water levels became higher with coarser grids, whereas depth-averaged flow velocities are diffused.

Caviedes-Voullième et al. (2012) and Bomers et al. (2019) addressed that numerical effects can be as influential as physical friction. De Jong and Mohamed (2016) on the other hand, showed that bed level discretisation plays a major role in hydraulic river models. In this study, the contribution of the numerical effect to water level and depth-averaged flow velocity deviations in the hypothetical river meander are notable. Additionally, grid resolution is more influential than grid shape. Nonetheless, the findings of this study also indicated that significant bed level differences are obtained between the grids in the case study, which led to major water level differences during both low and higher discharge conditions. Numerical effects on the other hand, became greater at higher depth-averaged flow velocities.

In Bomers et al. (2019) half of the applied grid structures led to unrealistic depth-averaged flow velocity profiles in river bends. According to Bomers et al. (2019) this could be due to aspect ratios up to 9 at some locations and/or a too low grid resolution. Bomers et al. (2019) found for instance unrealistic depth-averaged flow velocity profiles in river bends with a curvilinear grid and triangular grid consisting of respectively 6 curvilinear and 5 triangular grid cells across the width of the main channel. In this study, all constructed grids for the hypothetical river meanders were capable of representing more or less realistic flow patterns. This shows that coarse curvilinear and triangular grids with respectively 5 and 3 cells across the main channel of the hypothetical river meanders are capable of simulating the general flood patterns. In the Grensmaas river, maximum aspect ratios of 4 were applied to the grids. This did not lead to unrealistic depth-averaged flow velocity profiles. The coarse curvilinear and triangular grids with respectively 5 and 3 cells across the main channel were not considered in the case study. Nonetheless, a triangular grid with 4 grid cells across the main channel was included in the case study and showed realistic depth-averaged flow velocity profiles in both analysed river bends. Overall, this study has shown that the suggestions by Bomers et al. (2019) about grids with aspect ratios above 5 in river bends may be true, since all considered grids in this study, which all had aspect ratios lower than 5, led to more or less realistic depth-averaged flow velocity profiles in river bends. In contrast to Bomers et al. (2019), the applied grids in the case study were not calibrated.

In this study, hydraulic river modelling simulations were performed in D-Flow FM. Even though D-Flow FM is a widely used hydrodynamic simulation program, various alternative programs do exist as well, such as MIKE 21 FM and SRH-2D. The latter two programs are, similar to D-FLOW FM, based on a flexible grid clustering approach. In Lai (2010), SRH-2D was used to simulate a 90° meandering flume. Similar to this study (with the exception of the lowest resolution curvilinear in the hypothetical river meanders cases), it was found that more triangular cells are required to acquire the same level of accuracy as curvilinear grids. In Parsapour-Moghaddam et al. (2018), simulated water levels and depth-averaged flow velocities by a curvilinear grid in D-Flow FM were compared to those of a triangular grid in MIKE 21 FM. Similar to this study, higher water levels and lower depth-averaged flow velocities were obtained by the triangular grid. Therefore, it is presumed that the findings of this study also hold for alternative hydrodynamic simulation programs, such as MIKE 21 FM and SRH-2D.

In Caviedes-Voullième et al. (2012) and Bomers et al. (2019), it has been highlighted that grid coarsening and grid shape can have effects on the water level, which are in the same order of magnitude as physical friction. Therefore, both Caviedes-Voullième et al. (2012) and Bomers et al. (2019) recommended that roughness coefficients must be calibrated for every particular grid. This implies to our study as well, since significant differences in water levels and depth-averaged flow velocities are simulated by the grids due to the

numerical and especially bathymetry discretisation effects. According to Bomers et al. (2019), grids which are more sensitive to numerical and bathymetry discretisation effects, require a greater adjustment of the roughness coefficients in order to minimise the error between prediction and observation for a specific location. Therefore, it is presumed that, in terms of the grid resolution, the medium resolution grids in the Grensmaas river case are more affected by a calibration, since significant differences in flow areas are obtained in comparison to the bathymetry data directly from the baseline-j14\_6-w14 database. In regards to the grid shape, triangular grids are likely to be more affected by a calibration procedure due to larger deviations in flow areas compared to the bathymetry data directly from the baseline-j14\_6-w14 database. Additionally, Bomers et al. (2019) recommended a calibration at different discharges stages in order to accurately predict water levels during low flow conditions in meandering rivers as well. Our findings showed that this implies to Grensmaas river as well, since we have shown for instance that water level differences at low discharges can be larger at wide floodplains than at higher discharges stages.

This study has showed that performing a local grid refinement is an effect approach in order to decrease the bathymetry discretisation errors locally of a numerical solution. However, despite having obtained water levels and depth-averaged flow velocities which converges towards those of a higher grid resolution, performing a calibration procedure for locally refined grids is necessary as well. It is preferable to first carry out a local grid refinement before executing a calibration procedure, since generated discretised bathymetry errors were different in this study for the locally refined grids, and the fine and coarser grids. In terms of the calibration procedure, the bed roughness along the river course can be expressed by applying multiple roughness trajectories. If locally refined regions are considered as one of those roughness trajectory, different calibrated roughness coefficients can be obtained. For the Grensmaas river in this study, the latter would be more the case for the medium resolution triangular grid than for the curvilinear and hybrids grids, since triangular grids are probably more sensitive to calibration. In practise, however, calibrating various grids after each local refinement can be time expensive and unnecessary if the locally refined region is small in comparison to the roughness trajectory.

## 5 Conclusion

The objective of this study was to understand under which conditions grid generation choices affect hydraulic modelling outcomes in river bends. To reach this objective, we have set up hypothetical river meanders to isolate the effects by grid generation choices. The river characteristics of the hypothetical river meanders correspond with those of the Grensmaas river. Afterwards, we verified the model outcomes with those in the Grensmaas river. This section answers the research questions formulated in Section 1.4.

- (i) *How do by grid generation choices affect hydraulic river modelling outcomes in the main channel of hypothetical river meanders?*

In the hypothetical river meanders in which we only included the main channel, both curvilinear and triangular grids with three different resolutions were capable of simulating realistic flow patterns: (i) an elevated water surface near the outer bank at the bend entrance, apex and exit; and (ii) higher depth-averaged flow velocities close to the inner bank at the bend entrance and apex.

Numerical effects such as false diffusion and numerical diffusion are proportional to grid cell sizes, depth-averaged flow velocities, rapid flow changes and the orientation of the grid lines with respect to the flow direction. The latter two factors are more present at sharper bends.

Regarding the influence by both grid resolution and grid shape, it can be concluded that the former is more dominant as greater differences are obtained between different resolutions than with different grid shapes.

- (ii) *How do by grid generation choices affect hydraulic river modelling outcomes if floodplains are included in hypothetical river meanders?*

In the hypothetical river meanders in which floodplains are included, curvilinear, hybrid and triangular grids with two different resolutions were capable of simulating realistic flow patterns: (i) an elevated water surface near the outer bank at the bend entrance, apex and exit; and (ii) higher depth-averaged flow velocities close to the inner bank at the bend entrance and apex.

In terms of the depth-averaged flow velocities, a more diffusive-like appearance is present at the transition between the main channel and floodplain areas due to a large decrease in depth-averaged flow velocity from the main channel to the floodplain areas. This diffusive-like appearance is kept more under control with higher resolution grids than with coarser grids. Furthermore, greater numerical effects are present with hybrid and triangular grids, since using triangular grid cells are the expense of the grid resolution in transverse flow direction.

Despite the significant deviations in the depth-averaged flow velocity profiles, minor differences are obtained between the simulated water levels by the grids. In the cases in which floodplains are included, almost no depth-averaged flow velocity differences are observed in the floodplain areas. Consequently, relatively smaller differences in depth-averaged flow velocities are obtained between the grids over the entire spatial domain in comparison to the main channel cases. As a result of the floodplain involvement, the generated numerical effects in the main channel and at the transition between main channel and floodplain areas are smeared out through the model domain and hence dampened. This indicates that the induced numerical effects are proportional to the discharge per unit width. Thus numerical effects are more influential in small river sections.

- (iii) *Too what extent do the findings for the hypothetical cases also hold for a case study/natural river meander?*

Similar grids as the hypothetical river meanders were also implemented in the case study, the Grensmaas river. In the case study significant differences in simulated water levels and depth-averaged flow velocities between the grids are obtained. Higher water levels and lower depth-averaged flow velocities in the main channel were predicted by the coarser grids. This shows that the bathymetry discretisation plays an essential role in hydraulic river models. Since the differences between the grids are substantially larger in the case study at both low and higher discharge stages, we conclude that bathymetry discretisation is significantly more influential than numerical effects such as numerical diffusion and false diffusion.

In terms of the grid shape, curvilinear and hybrid grids produced similar results under the same level of grid resolution. This is not the case for the triangular grids, which shows that triangular grids require a higher resolution to achieve the same level of accuracy as the curvilinear and hybrid grids.

- (iv) *How does a local increase in grid resolution affect hydraulic river modelling outcomes in a case study/natural river meander?*

The use of a locally refined grid contributes to have water levels and depth-averaged flow velocities which converges towards those of a higher grid resolution. This is mostly a result of better representation of the bathymetry. Nonetheless, a local grid refinement is less responsive for triangular grids, since water levels still differ substantially with respect to the higher resolution variant. Despite these positive effects of local grid refinements, it is at the expense of the computation time. Furthermore, even though it is preferable to executing a calibration procedure after performing a local grid refinement, calibrating various grids after each local refinement can be time expensive and unnecessary if the locally refined region is small in comparison to the roughness trajectory for which the roughness coefficient is calibrated. However, executing a calibration procedure after performing a local grid refinement is advised if the considered grid without local refinements is sensitive for calibration and/or the local refined area covers a large part of a roughness trajectory in which it is included.

## 6 Recommendations

This section starts with given recommendations for future research (Section 6.1). Finally, we discuss some recommendations for practical usage when it comes to grid generation choices (Section 6.2).

### 6.1 Future research

First of all, the goal of the research was to obtain a better understanding of the influence of the grid generation choices on the hydraulic river modelling outcomes in river meanders. Hereby, we considered geometric features such as main channels and floodplains. Nevertheless, there are more geometric features present in natural rivers such as river bifurcations. Several geometric features may play a role in the hydrodynamics as well, which can result in different water level and depth-averaged flow velocity differences between grids. Furthermore, river bifurcations do need special treatment when it comes to the grid generation, since a modeller probably prefers to have similar grid resolutions in the downstream branches as in the upstream channel. An option is to increase the grid resolution with a factor two just upstream the river bifurcations. To connect the locally refined upstream section, a modeller can use triangular grid cells at the transition between the medium resolution and the locally refined region, which should be done manually. So far, a decent amount of scientific research has been performed in order to gain insight in the morphodynamics, while little is known about grid influences at river bifurcations. An important feature in terms of the morphodynamics, is the discharge partitioning between the downstream branches. However, influences by grid generation choices on the discharge partitioning is still unknown. Thus, we recommend to study the influence of grid generation choices on hydraulic river modelling outcomes at river bifurcations.

Secondly, hypothetical river meanders were set up to isolate the effects by grid generation choices on hydraulic modelling outcomes in river meanders. These effects were only analysed at the upstream end of the model domain. Whether the numerical effects by a grid grow along the river is yet unknown. Therefore, it is recommended to perform a study, in which the downstream boundary condition of a hypothetical river meander is not as influential upstream as in our hypothetical river models. In order to do this, we recommend a model domain with a straight channel at the downstream end instead of the meandering bends in this study.

Thirdly, in this study influences of numerical and bed level discretisation effects in hydraulic river modelling outcomes of river meanders are analysed for three constant flow scenarios. However, this study does not include insights in how grid generation choices affect hydraulic river modelling outcomes in the case of a discharge wave, in which depth-averaged flow velocity accelerate and decelerate later on. Even though it is presumed that the bathymetry discretisation is significantly more influential than numerical effects for a discharge wave as well, a clear view of the influence of the numerical and bathymetry discretisation effects for a discharge wave is still valuable.

Lastly, in the case study, it was found that coarser grids led to an overestimation of the cross-section areas. Ultimately, this led to a reduction in depth-averaged flow velocity in the main channel. However, the reduction in depth-averaged flow velocity was not as significant as the increase in flow-area in the main channel, which as result led to higher water levels through the cross-sectional areas. Why this pattern is obtained instead of a larger decrease in depth-averaged flow velocity is unknown and should be investigated in a new study.

## 6.2 Practical usage

From the conducted research, several practical recommendations can be considered for hydraulic river modellers. First of all, the case study showed that each constructed grid simulated significant different hydrodynamics due to the errors in the discretised bathymetry. In order to simulate water levels and depth-averaged flow velocities accurately, a calibration procedure is required. Thereby, it is important to state that coarse grids contain larger bed level discretisation errors and hence are more sensitive to calibration. In cases in which the bed roughness of the main channel is calibrated in order to compensate for the bathymetry discretisation errors, a substantial (unrealistic) discharge partitioning between the main channel and floodplains might be obtained, as well as unrealistic depth-averaged flow velocity profiles. Therefore, it is recommended to use calibrated roughness coefficients which are physically realistic.

For a locally refined grid, it is preferable to first carry out a local grid refinement before executing a calibration procedure. However, in reality, calibrating various grids after each local refinement can be time expensive and unnecessary if the locally refined region is small in comparison to the calibrated roughness trajectory. Furthermore, if small hydrodynamic differences are expected between a coarse and a fine grid, with each having the same grid shape, performing a calibration procedure after a local grid refinement might not be detrimental with respect to the model accuracy. Nonetheless, it is recommended that model results from a grid, which is locally refined after calibration, are analysed cautiously. The modeller can also consider a calibration for low and high discharge separately, since we obtained larger differences in water level between grids at low discharge stages than at high discharge stages in the Grensmaas river at the river bend with large floodplains. These results were mainly due to the bathymetry accuracy. In order to gain insights in, for example, impacts of river engineering projects regarding flood protection, it is recommended to calibrate grids for high discharge ranges.

For the case study, we considered for the curvilinear grid the pre-constructed grid by Deltares. This grid showed to be robust as a higher grid resolution did not result in large differences in the simulated hydrodynamics, such as for the triangular grid. In terms of the computation time, the pre-constructed grid by Deltares is considered as the best. Nonetheless, designing such grid is a labour-intensive procedure and can cost a substantial amount of time. For a case study, a good alternative is the hybrid grid, which results in similar water level and depth-averaged flow velocity profiles as the curvilinear grid by Deltares. Furthermore, despite having a larger computation time, a hybrid grid which is aligned in the flow direction, is easier generated than a curvilinear grid which grid lines are parallel to the flow direction. A modeller should bear in mind that it is also possible to discretise only the outer ends of the floodplain areas with triangular cells and the rest with curvilinear grid cells. This may decrease the computation time, while the triangular grid cells prevent small curvilinear grid cells in sharp and wide floodplains.

In regards to the triangular grids, this study has showed that a higher resolution is required for triangular grids to acquire the same level of accuracy as curvilinear grids in both the hypothetical river meanders without floodplains and the case study. In addition to this, since large flow area deviations are obtained with triangular grids in comparison to the bathymetry data directly from the baseline-j14\_6-w14 database, it is expected that triangular grids are highly sensitive for calibration and hence may obtain unrealistic calibrated roughness coefficients. Therefore, it is essential to verify and validate the numerical model in which triangular grids are applied. Thereby, a modeller should not only assess water levels, but also depth-averaged flow velocities.

This study showed that the effects of the bed level discretisation on hydraulic model outcomes are more dominant than the numerical effects. Therefore, it is recommended that a modeller first attempts to reduce the bed level errors before taking numerical

effects into consideration. Thereby, most attention should be placed on the bed level discretisation of the main channel, since most bed level errors are obtained in the main channel. Furthermore, this study revealed that the influence by both bed level errors as well as numerical effects become smaller at high discharges with wide floodplains. This means that a curvilinear or hybrid grid with more than 10 curvilinear grid cells in the main channel for high discharge conditions might not be required.

## References

- Altaie, H., & Dreyfuss, P. (2018). Numerical solutions for 2d depth-averaged shallow water equations. *International Mathematical Forum*, *13*, 79–90. <https://doi.org/10.12988/imf.2018.712102>
- Bailey, R. T. (2017). Managing false diffusion during second-order upwind simulations of liquid micromixing. *International Journal for Numerical Methods in Fluids*, *83*(12), 940–959. <https://doi.org/10.1002/flid.4335>
- Bilgili, E. (2020). *Evaluating the effect of grid shape and grid resolution on hydraulic river modelling of a straight channel* (Advanced Research Skills). University of Twente.
- Bomers, A., Schielen, R., & Hulscher, S. (2019). The influence of grid shape and grid size on hydraulic river modelling performance [Springer]. *Environmental fluid mechanics*, *19*(5), 1273–1294. <https://doi.org/10.1007/s10652-019-09670-4>
- Casulli, V., & Walters, R. A. (2000). An unstructured grid, three-dimensional model based on the shallow water equations. *International Journal for Numerical Methods in Fluids*, *32*(3), 331–348. [https://doi.org/10.1002/\(SICI\)1097-0363\(20000215\)32:3<331::AID-FLD941>3.0.CO;2-C](https://doi.org/10.1002/(SICI)1097-0363(20000215)32:3<331::AID-FLD941>3.0.CO;2-C)
- Caviedes-Voullième, D., Garcia-Navarro, P., & Murillo, J. (2012). Influence of mesh structure on 2d full shallow water equations and scs curve number simulation of rainfall/runoff events. *Journal of Hydrology*, *s 448–449*, 39–59. <https://doi.org/10.1016/j.jhydrol.2012.04.006>
- Colebrook, C. F. (1939). Turbulent flow in pipes, with particular reference to the transition region between the smooth and rough pipe laws. *Journal of the Institution of Civil Engineers*, *11*(4), 133–156. <https://doi.org/10.1680/ijoti.1939.13150>
- Courant, R., Friedrichs, K., & Lewy, H. (1928). Über die partiellen Differenzengleichungen der mathematischen Physik. *Mathematische Annalen*, *100*, 32–74. <https://doi.org/10.1007/BF01448839>
- De Jong, J. S. (2019). *Beknopte beschrijving van de modelopzet maas*. Deltares. Boussinesqweg 1.
- De Jong, J. S. (2020). *Ontwikkeling zesde-generatie maas-model. modelbouw, kalibratie en validatie (concept)*. Deltares. Boussinesqweg 1.
- De Jong, J. S., & Mohamed, Y. (2016). *Riviermodellen in d-hydro - pilot-applicatie rijntakken*. Deltares. Boussinesqweg 1.
- Deltares. (2019a). *Technical reference manual*. Version 1.1.0. Deltares. Boussinesqweg 1.
- Deltares. (2019b). *Technical user manual*. Version 1.5.0. Deltares. Boussinesqweg 1.
- Deltares. (2020). *Rgfgrid*. Version 5.00. Deltares. Boussinesqweg 1.
- Hardy, R., Bates, P., & Anderson, M. (1999). The importance of spatial resolution in hydraulic models for floodplain environments. *Journal of Hydrology*, *216*(1), 124–136. [https://doi.org/https://doi.org/10.1016/S0022-1694\(99\)00002-5](https://doi.org/https://doi.org/10.1016/S0022-1694(99)00002-5)
- Harlow, F. H., & Welch, J. E. (1965). Numerical calculation of time-dependent viscous incompressible flow of fluid with free surface. *The Physics of Fluids*, *8*(12), 2182–2189. <https://doi.org/10.1063/1.1761178>
- Hoefsloot, F., & Van Doornik, W. (2020). *Dataprotocol baseline 6.1.2*. Version 6.12. Rijkswaterstaat WVL and Deltares.
- Huthoff, F., Ouwerkerk, S., Daggenvoorde, R., Snoek, Y., & Voortman, B. (2020). *Irm quickscan afvoercapaciteit* (tech. rep.). HKV lijn in water.
- Kernkamp, H., Dam, A., Stelling, G., & Goede, E. (2011). Efficient scheme for the shallow water equations on unstructured grids with application to the continental shelf. *Ocean Dynamics*, *61*, 1175–1188. <https://doi.org/10.1007/s10236-011-0423-6>
- Kleptsova, O., Pietrzak, J., & Stelling, G. (2009). On the accurate and stable reconstruction of tangential velocities in c-grid ocean models [The Sixth International Work-

- shop on Unstructured Mesh Numerical Modelling of Coastal, Shelf and Ocean Flows]. *Ocean Modelling*, 28(1), 118–126. <https://doi.org/https://doi.org/10.1016/j.ocemod.2008.12.007>
- Lai, Y. (2010). Two-dimensional depth-averaged flow modeling with an unstructured hybrid mesh. *Journal of Hydraulic Engineering*, 136(1), 12–23. [https://doi.org/10.1061/\(ASCE\)HY.1943-7900.0000134](https://doi.org/10.1061/(ASCE)HY.1943-7900.0000134)
- Langbein, W. B., & Leopold, L. B. (1966). River meanders and the theory of minimum variance. In G. H. Dury (Ed.), *Rivers and river terraces* (pp. 238–263). London, Palgrave Macmillan UK. [https://doi.org/10.1007/978-1-349-15382-4\\_9](https://doi.org/10.1007/978-1-349-15382-4_9)
- Luijendijk, A. (2020). *Grid quality*. <https://publicwiki.deltares.nl/x/PABq> (accessed: 14.10.2020)
- Meier, H., Alves, J., & Mori, M. (1999). Comparison between staggered and collocated grids in the finite-volume method performance for single and multi-phase flows. *Computers & Chemical Engineering*, 23(3), 247–262. [https://doi.org/https://doi.org/10.1016/S0098-1354\(98\)00270-1](https://doi.org/https://doi.org/10.1016/S0098-1354(98)00270-1)
- Minns, T., Spruyt, A., & Kerkhoven, D. (2019). *Specificaties zesde-generatie modellen met d-hydro*. Deltares. Boussinesqweg 1.
- Mungkasi, S., Magdalena, I., Pudjaprasetya, S., Wiryanto, L., & Roberts, S. (2018). A staggered method for the shallow water equations involving varying channel width and topography. *International Journal for Multiscale Computational Engineering*, 16. <https://doi.org/10.1615/IntJMCompEng.2018027042>
- Nabi, M., Ottevanger, W., & Giri, S. (2017). Computational modelling of secondary flow on unstructured grids. <https://www.scopus.com/inward/record.uri?eid=2-s2.0-85016632408&partnerID=40&md5=7a5013653a4a18e521c33c67b1c81acd>
- Parsapour-Moghaddam, P., Rennie, C., & Slaney, J. (2018). Hydrodynamic simulation of an irregularly meandering gravel-bed river: Comparison of mike 21 fm and delft3d flow models. <https://doi.org/10.1051/e3sconf/20184002004>
- Patankar, S. V. (1980). *Numerical heat transfer and fluid flow*. Hemisphere Publishing Corporation (CRC Press, Taylor & Francis Group). <http://www.crcpress.com/product/isbn/9780891165224>
- Patel, M. K. (1987). *On the false-diffusion problem in the numerical modelling of convection-diffusion processes* (Doctoral dissertation). University of Greenwich.
- Perot, B. (2000). Conservation properties of unstructured staggered mesh schemes. *Journal of Computational Physics*, 159(1), 58–89. <https://doi.org/https://doi.org/10.1006/jcph.2000.6424>
- Pinho, J., Ferreira, R., Vieira, L., & Schwanenberg, D. (2015). Comparison between two hydrodynamic models for flooding simulations at river lima basin [cited By 16]. *Water Resources Management*, 29(2), 431–444. <https://doi.org/10.1007/s11269-014-0878-6>
- Rijkswaterstaat Zuid-Nederland. (2015). *Bijsluiter betrekkingslijnen 2014 2015*. Rijkswaterstaat. Avenue Ceramique 125.
- Robert, A. (2003). River processes - an introduction to fluvial dynamics.
- Roos, P. C. (2019). *Mathematical physics of water systems*. Drienerlolaan 5, University of Twente.
- Smith, S. D., & Banke, E. G. (1975). Variation of the sea surface drag coefficient with wind speed. *Quarterly Journal of the Royal Meteorological Society*, 101(429), 665–673. <https://doi.org/10.1002/qj.49710142920>
- Starikovičius, V., Čiegis, R., & Jakušev, A. (2006). Analysis of upwind and high-resolution schemes for solving convection dominated problems in porous media. *Mathematical Modelling and Analysis*, 11(4), 451–474. <https://doi.org/10.1080/13926292.2006.9637330>

- Stelling, G. (1983). On the construction of computational methods for shallow water flow problems. *Ph.D. thesis, Technical University of Delft*. <https://doi.org/http://resolver.tudelft.nl/uuid:d3b818cb-9f91-4369-a03e-d90c8c175a96>
- Tu, J., Yeoh, G.-H., & Liu, C. (2013a). Chapter 4 - cfd techniques—the basics (J. Tu, G.-H. Yeoh, & C. Liu, Eds.; Second Edition). In J. Tu, G.-H. Yeoh, & C. Liu (Eds.), *Computational fluid dynamics (second edition)* (Second Edition). Butterworth-Heinemann. <https://doi.org/https://doi.org/10.1016/B978-0-08-098243-4.00004-4>
- Tu, J., Yeoh, G.-H., & Liu, C. (2013b). Chapter 5 - cfd solution analysis—essentials (J. Tu, G.-H. Yeoh, & C. Liu, Eds.; Second Edition). In J. Tu, G.-H. Yeoh, & C. Liu (Eds.), *Computational fluid dynamics (second edition)* (Second Edition). Butterworth-Heinemann. <https://doi.org/https://doi.org/10.1016/B978-0-08-098243-4.00005-6>
- Vermeulen, B., Ribberink, J. S., de Vriend, H. J., Hulscher, S. J. M. H., & Souren, A. W. M. G. (2018). *River flow and sediment transport*. Drienerlolaan 5, University of Twente.
- Zeng, J., Constantinescu, G., Blanckaert, K., & Weber, L. (2008). Flow and bathymetry in sharp open-channel bends: Experiments and predictions. *Water Resources Research*, 44(9). <https://doi.org/10.1029/2007WR006303>

# Appendices

## A Modified equation one-dimensional advection problem

The one-dimensional advection equation is given by:

$$\frac{\partial u}{\partial t} + u \frac{\partial u}{\partial x} = 0 \quad (\text{A.1})$$

Using finite-differences and a first-order upwind scheme, the following discretisation is obtained:

$$u_{j,k+1} = u_{j,k} - \frac{u\Delta t}{\Delta x} \left[ u_{j,k} - u_{j-1,k} \right] \quad (\text{A.2})$$

To derive the modified equation for the one-dimensional advection problem, Taylor series expansions to the terms  $u_{j,k+1}$  and  $u_{j-1,k}$  are applied:

$$u_{j,k+1} = u_{j,k} + \Delta t \frac{\partial u}{\partial t} + \frac{(\Delta t)^2}{2!} \frac{\partial^2 u}{\partial t^2} + O\left[(\Delta t)^3\right] \quad (\text{A.3})$$

$$u_{j-1,k} = u_{j,k} - \Delta x \frac{\partial u}{\partial x} + \frac{(\Delta x)^2}{2!} \frac{\partial^2 u}{\partial x^2} + O\left[(\Delta x)^3\right] \quad (\text{A.4})$$

Substituting Equations A.3 and A.4 into Equation A.2 gives:

$$u_{j,k} + \Delta t \frac{\partial u}{\partial t} + \frac{(\Delta t)^2}{2} \frac{\partial^2 u}{\partial t^2} + O\left[(\Delta t)^3\right] = u_{j,k} - \frac{u\Delta t}{\Delta x} \left[ u_{j,k} - \left[ u_{j,k} - \Delta x \frac{\partial u}{\partial x} + \frac{(\Delta x)^2}{2} \frac{\partial^2 u}{\partial x^2} + O\left[(\Delta x)^3\right] \right] \right] \quad (\text{A.5})$$

which can be rearranged to:

$$\frac{\partial u}{\partial t} = -u \frac{\partial u}{\partial x} - \frac{\Delta t}{2} \frac{\partial^2 u}{\partial t^2} + u \frac{\Delta x}{2} \frac{\partial^2 u}{\partial x^2} + O\left[(\Delta t)^2, (\Delta x)^2\right] \quad (\text{A.6})$$

With Equation A.1, the second order time derivative  $\frac{\partial^2 u}{\partial t^2}$  can be rewritten as a second order spatial derivative. Therefore, we take the time derivative of the Equation A.1:

$$\frac{\partial^2 u}{\partial t^2} = -u \frac{\partial^2 u}{\partial x \partial t} = -u \frac{\partial}{\partial x} \left( \frac{\partial}{\partial t} \right) \quad (\text{A.7})$$

Substituting the one-dimensional advection into Equation A.7, results in the second order spatial derivative:

$$\frac{\partial^2 u}{\partial t^2} = u^2 \frac{\partial^2 u}{\partial x^2} \quad (\text{A.8})$$

Substituting Equation A.8 into Equation A.6 leads to:

$$\frac{\partial u}{\partial t} = -u \frac{\partial u}{\partial x} - u^2 \frac{\Delta t}{2} \frac{\partial^2 u}{\partial x^2} + u \frac{\Delta x}{2} \frac{\partial^2 u}{\partial x^2} + O\left[(\Delta t)^2, (\Delta x)^2\right] \quad (\text{A.9})$$

This can be rewritten to the modified equation for the one-dimensional advection problem:

$$\frac{\partial u}{\partial t} + u \frac{\partial u}{\partial x} = \frac{u\Delta x}{2} \left[ 1 - \frac{u\Delta t}{\Delta x} \right] \frac{\partial^2 u}{\partial x^2} + O\left[(\Delta t)^2, (\Delta x)^2\right] \quad (\text{A.10})$$

where  $C = \frac{u\Delta t}{\Delta x}$  represents the Courant number. The effect of the diffusive term, which is introduced due to the truncation error of the first-order upwind scheme, is illustrated in Figure A.1.

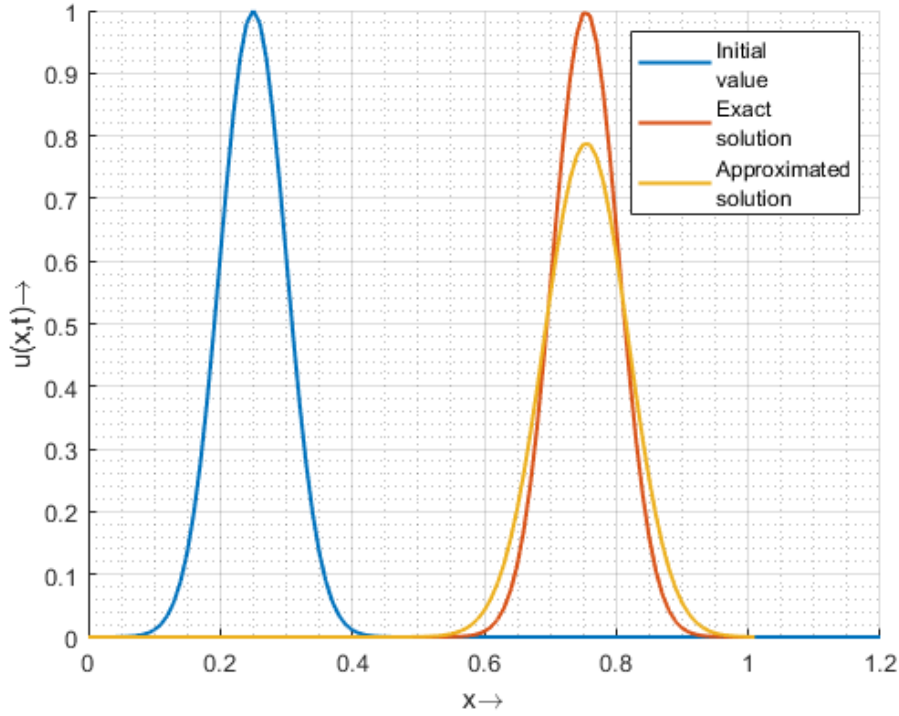


Figure A.1: An illustration of the induced numerical diffusion in an explicit first-order upwind scheme for the one-dimensional advection problem. The initial value is given by Gaussian function ( $u_0 = \exp(-200(x - 0.25)^2)$ ). The exact and approximated solutions are the velocities profiles after a certain time.

## B Derivation of the pre-defined rating curves

The pre-defined rating curves of each hypothetical river meander is determined with Chézy's law, which is an empirical formula that describes the mean flow velocity of turbulent open channel flow (Vermeulen et al., 2018):

$$\bar{u} = C(Ri)^{1/2} \quad (\text{B.1})$$

Here,  $\bar{u}$  represents the depth-averaged flow velocity ( $m/s$ ). It is assumed that the hydraulic radius is equal to the water depth, since the channel width is much larger than the water depth ( $w \gg h$ ):

$$\bar{u} = C(hi)^{1/2} \quad (\text{B.2})$$

Including the cross-sectional area ( $m^2$ ) results in:

$$Q = wCh^{3/2}i^{1/2} \quad (\text{B.3})$$

With the White-Colebrook relationship (Colebrook, 1939), Equation B.3 can be expressed as:

$$Q = 18w \log_{10} \left( \frac{12R}{k_s} \right) h^{3/2}i^{1/2} \quad (\text{B.4})$$

In the cases with only the main channel (Figure 2.3), hydraulic radius is written as:

$$R_m = \frac{w_m h}{w + 2h} \quad (\text{B.5})$$

Substituting Equation B.5 in Equation B.4 leads to:

$$Q = 18w_m \log_{10} \left( \frac{12}{k_s} \left( \frac{w_m h}{w_m + 2h} \right) \right) h^{3/2}i^{1/2} \quad (\text{B.6})$$

Special treatment is required in the hypothetical cases in which floodplains are included (Figure 2.4). As a consequence, Equation B.6 is only applicable if  $h \leq h_f$ . If  $h > h_f$ , the following procedure should be considered:

$$Q_{tot} = Q_1 + Q_2 + Q_3 \quad (\text{B.7})$$

Here,  $Q_{tot}$  refers to the total discharge through the cross-sectional area ( $m^3/s$ ).  $Q_1$ ,  $Q_2$  and  $Q_3$  are the discharges through respectively the cross-sectional areas 1, 2 and 3 (Figure 2.4). Combining Equation B.3 and Equation B.7 gives:

$$Q_{tot} = w_m C_m h^{3/2} i^{1/2} + 2w_f C_f (h - h_f)^{3/2} i^{1/2} \quad (\text{B.8})$$

Here,  $C_m$  and  $C_f$  correspond to the Chézy-roughness coefficient in respectively the main channel and floodplains. Applying the White-Colebrook relationship leads to:

$$Q_{tot} = 18w_m \log_{10} \left( \frac{12R_m}{k_{s,m}} \right) h^{3/2} i^{1/2} + 36w_f \log_{10} \left( \frac{12R_f}{k_{s,f}} \right) (h - h_f)^{3/2} i^{1/2} \quad (\text{B.9})$$

The hydraulic radius  $R_f$  in Equation B.9 applies to one single floodplain, which is given by:

$$R_f = \frac{w_f (h - h_f)}{w_f + h - h_f} \quad (\text{B.10})$$

Substituting the expressions for the hydraulic radius' (Equation B.5 and B.10) in Equation B.9 results in the used formula to determine the water depth in cases where floodplains are considered if  $h > h_f$ :

$$Q = w_m 18 \log_{10} \left( \frac{12}{k_{s,m}} \left( \frac{w_m h}{w_m + 2h} \right) \right) h^{3/2} i^{1/2} + w_f 36 \log_{10} \left( \frac{12}{k_{s,f}} \left( \frac{w_f (h - h_f)}{w_f + (h - h_f)} \right) \right) (h - h_f)^{3/2} i^{1/2} \quad (\text{B.11})$$

With Equation B.11, a clear distinction is obtained compared to the cases with only the main channel (Figure B.1) as the latter results in higher water depths with increasing discharges. The pre-defined rating curves of the Grensmaas river are, in contrast to the hypothetical river meanders, given as a relationship between the water level and discharge. To compare the pre-defined rating curves of the hypothetical river meanders with those of the Grensmaas river, the relationships of the latter should be expressed in water depths. Therefore, we considered the difference between water level and the bed level as the water depth (Figure B.1).

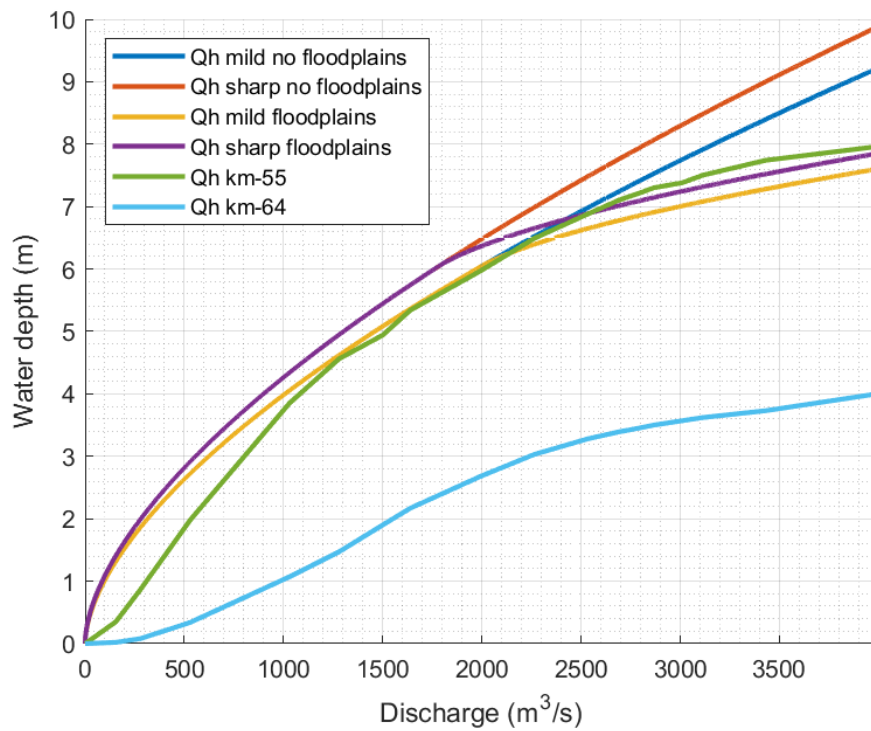


Figure B.1: The pre-defined rating curves (Qh-relationships) for the hypothetical river meanders and Grensmaas river at km-55 and km-64. In the legend, mild and sharp refer to respectively the mild and sharp hypothetical river meanders.

## C Grid properties

### C.1 Hypothetical cases: grids (main channel case)

Table C.1: Properties of the constructed grids for the hypothetical river meanders with only the main channel. Regarding the names: M and S stands respectively for mild and sharp; MC for main channel; Cur and Tri for respectively curvilinear and triangular; and HR, MED and LR for high, medium and low resolution respectively. Furthermore, min/max stands for minimum and maximum respectively.

<b>Mild river meander (main channel case)</b>				
Name	Grid shape	Number of grid cells across MC	Number of elements/nodes	Min./max. cell edge length
M_MC_Cur_HR	Curvilinear	20	24000/25221	6.838/26.855
M_MC_Cur_MED	Curvilinear	10	6000/6611	13.726/56.319
M_MC_Cur_LR	Curvilinear	5	1525/1836	26.685/105.070
M_MC_Tri_HR	Triangular	8	23926/13466	15.571/28.248
M_MC_Tri_MED	Triangular	4	5968/3734	26.232/53.676
M_MC_Tri_LR	Triangular	3	2994/2000	34.809/75.393
<b>Sharp river meander (main channel case)</b>				
Name	Grid shape	Number of grid cells across MC	Number of elements/nodes	Min./max. cell edge length
S_MC_Cur_HR	Curvilinear	20	24000/25221	6.719/28.269
S_MC_Cur_MED	Curvilinear	10	5740/6325	13.081/56.328
S_MC_Cur_LR	Curvilinear	5	1530/1842	25.687/110.500
S_MC_Tri_HR	Triangular	8	23926/13466	15.540/27.806
S_MC_Tri_MED	Triangular	4	5970/3735	28.265/53.462
S_MC_Tri_LR	Triangular	3	2996/2001	41.779/78.933

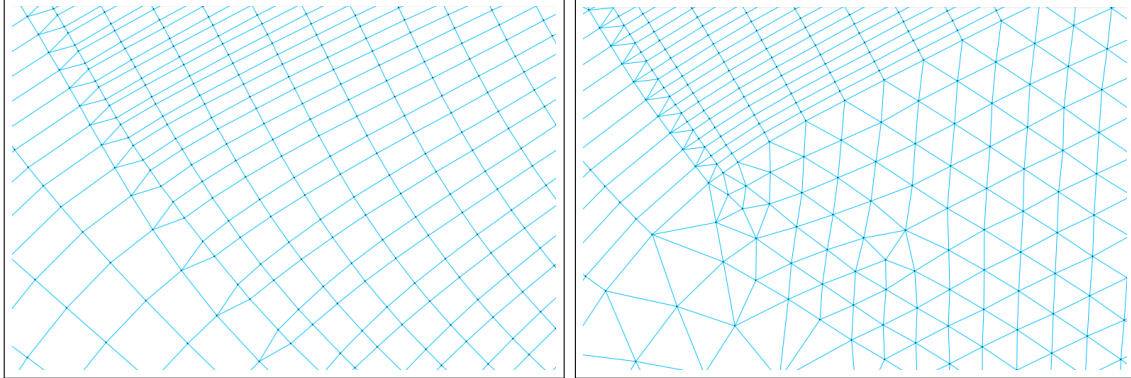
## C.2 Hypothetical cases: grids (main channel & floodplains case)

Table C.2: Properties of the constructed grids for the hypothetical river meanders with the main channel and floodplains. Regarding the names: S stands for sharp; MCFL for main channel & floodplains; Cur, Tri and Hybr for respectively curvilinear, triangular and hybrid; and HR and MED for high and medium resolution respectively. Furthermore, min/max stands for minimum and maximum respectively.

<b>Mild river meander (main channel &amp; floodplains case)</b>				
Name	Grid shape	Number of grid cells across MC	Number of elements/nodes	Min./max. cell edge length
M_MCFL_Cur_HR	Curvilinear	20	270000/271681	6.778/27.366
M_MCFL_Cur_MED	Curvilinear	10	67500/68341	13.750/54.727
M_MCFL_Tri_HR	Triangular	8	219346/111232	9.826/28.487
M_MCFL_Tri_MED	Triangular	4	554252/27908	26.242/57.452
M_MCFL_Hybr_HR	Curvilinear in MC, triangular in FL	20	145700/86073	6.716/40.381
M_MCFL_Hybr_MED	Curvilinear in MC, triangular in FL	10	34692/20828	13.710/79.438
<b>Sharp river meander (main channel &amp; floodplains case)</b>				
Name	Grid shape	Number of grid cells across MC	Number of elements/nodes	Min./max. cell edge length
S_MCFL_Cur_HR	Curvilinear	20	299880/301727	1.024/29.330
S_MCFL_Cur_MED	Curvilinear	10	74970/75894	3.005/58.48
S_MCFL_Hybr_HR	Curvilinear in MC, triangular in FL	20	155421/91003	6.472/42.450
S_MCFL_Hybr_MED	Curvilinear in MC, triangular in FL	10	39826/23576	12.938/81.433
S_MCFL_Tri_HR	Triangular	8	221970/112544	8.903/29.880
S_MCFL_Tri_MED	Triangular	4	55136/28350	18.588/59.625

### C.3 Close-up locally refined grids

- (a) Locally refined curvilinear grid at the bend  
with almost no floodplains  
(Grensmaas\_Cur\_MED\_Loc\_Ref)
- (b) Locally refined triangular grid at the bend  
with wide floodplains  
(Grensmaas\_Tri\_MED\_Loc\_Ref)



- (c) Locally refined triangular grid at the bend  
with wide floodplains  
(Grensmaas\_Tri\_MED\_Loc\_Ref)

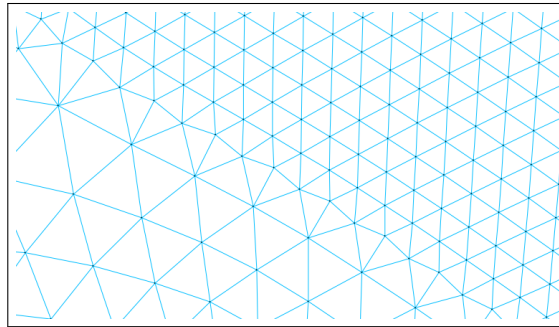


Figure C.1: Close-up for the three locally refined grids for the case study in the river bend (area of interest) with almost no floodplains (see Figure 2.2). The close-up is focused on the transition between the medium and locally refined bend, which is upstream of river bend. The names of the grids are given between brackets: Cur, Tri and Hybr for respectively curvilinear (as much as possible), triangular and hybrid; HR and MED for high and medium resolution respectively; and Loc and Ref for locally and refined respectively.

## C.4 Grids case study

Table C.3: Properties of the constructed grids for the Grensmaas river. Regarding the names: Grensmaas stands for the Grensmaas river; Cur, Tri and Hybr for respectively curvilinear (as much as possible), triangular and hybrid; HR and MED for high and medium resolution respectively; and Loc and Ref for locally and refined respectively. Furthermore, min/max stands for minimum and maximum respectively; and transitions for the shift between the medium resolution variant and local refinements.

Grensmaas				
Name	Grid shape	Number of grid cells across MC	Number of elements/nodes	Min./max. cell edge length
Grensmaas_Cur_HR	Curvilinear in MC, quadrilateral in FL of sharp bends	Min. 16	403489/405878	0.937/71.601
Grensmaas_Cur_MED	Curvilinear in MC, quadrilateral in FL of sharp bends	Min. 8	99919/101383	6.631/132.568
Grensmaas_Cur_MED_Loc_Ref	Curvilinear in MC, quadrilateral in FL of sharp bends and transitions, triangular at transitions	Min. 8 & (Min. 16 loc. ref.)	403489/405878	4.470/71.601
Grensmaas_Hybr_HR	Curvilinear in MC, triangular in FL	20	129263/130554	3.486/130.034
Grensmaas_Hybr_MED	Curvilinear in MC, triangular in FL	10	235961/129844	4.447/75.293
Grensmaas_Hybr_MED_Loc_Ref	Curvilinear in MC, triangular in FL and at transitions	10 & (20 loc. ref.)	370333/187077	8.806/52.842
Grensmaas_Tri_HR	Triangular	Min. 6	606273/304838	9.133/53.253
Grensmaas_Tri_MED	Triangular	Min. 3	286504/145041	16.199/52.941
Grensmaas_Tri_MED_Loc_Ref	Triangular	Min. 3 & (Min. 6 loc. ref.)	606273/304838	9.133/53.253

## D Results: hypothetical river meanders

### D.1 Mild river meander (main channel case)

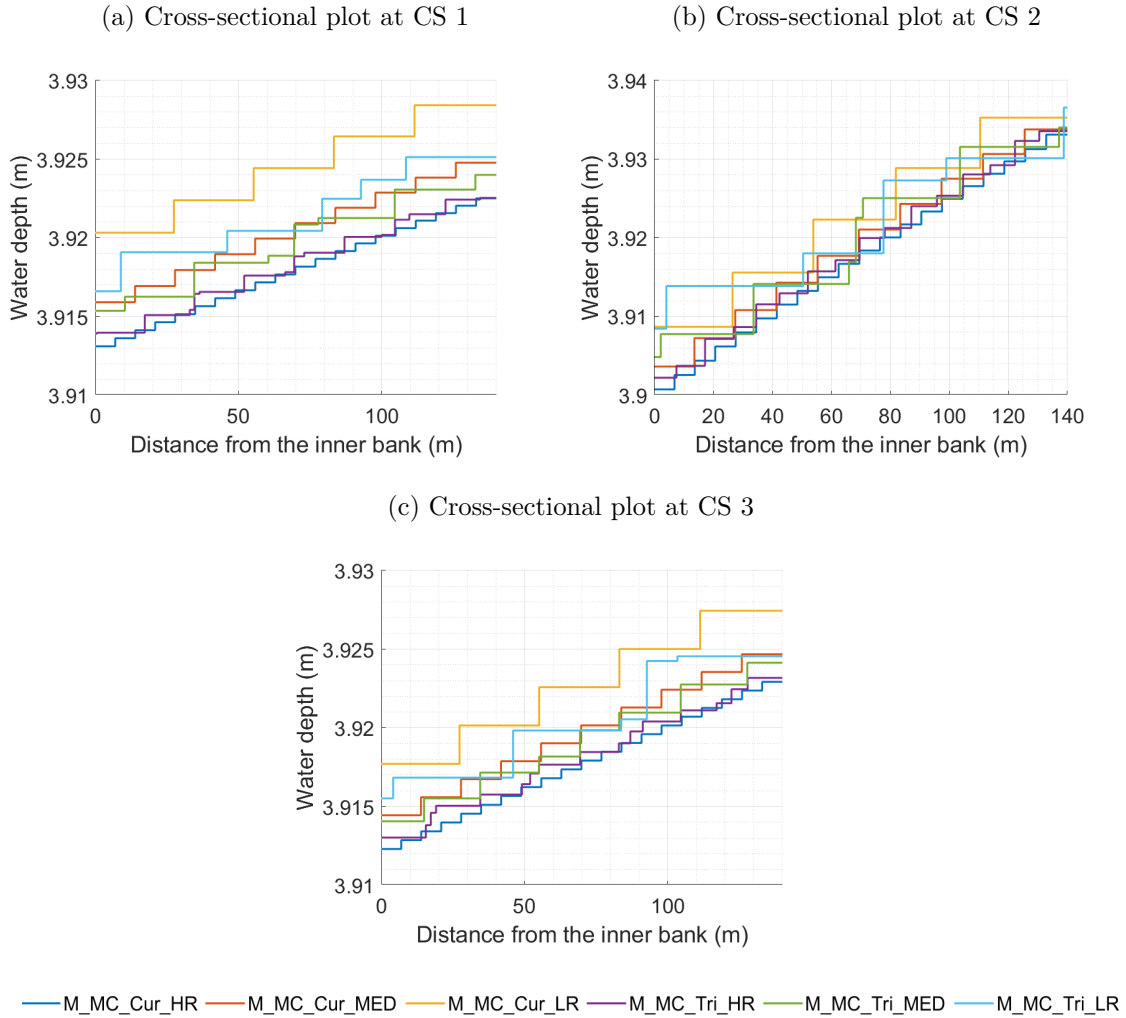


Figure D.1: Cross-sectional view of the simulated water depth for the mild river meander (main channel case) with the lowest discharge range at CS 1, CS 2 and CS 3 by the six considered grids. Regarding the names: M stands for mild; MC for main channel; Cur and Tri for respectively curvilinear and triangular; and HR, MED and LR for high, medium and low resolution respectively.

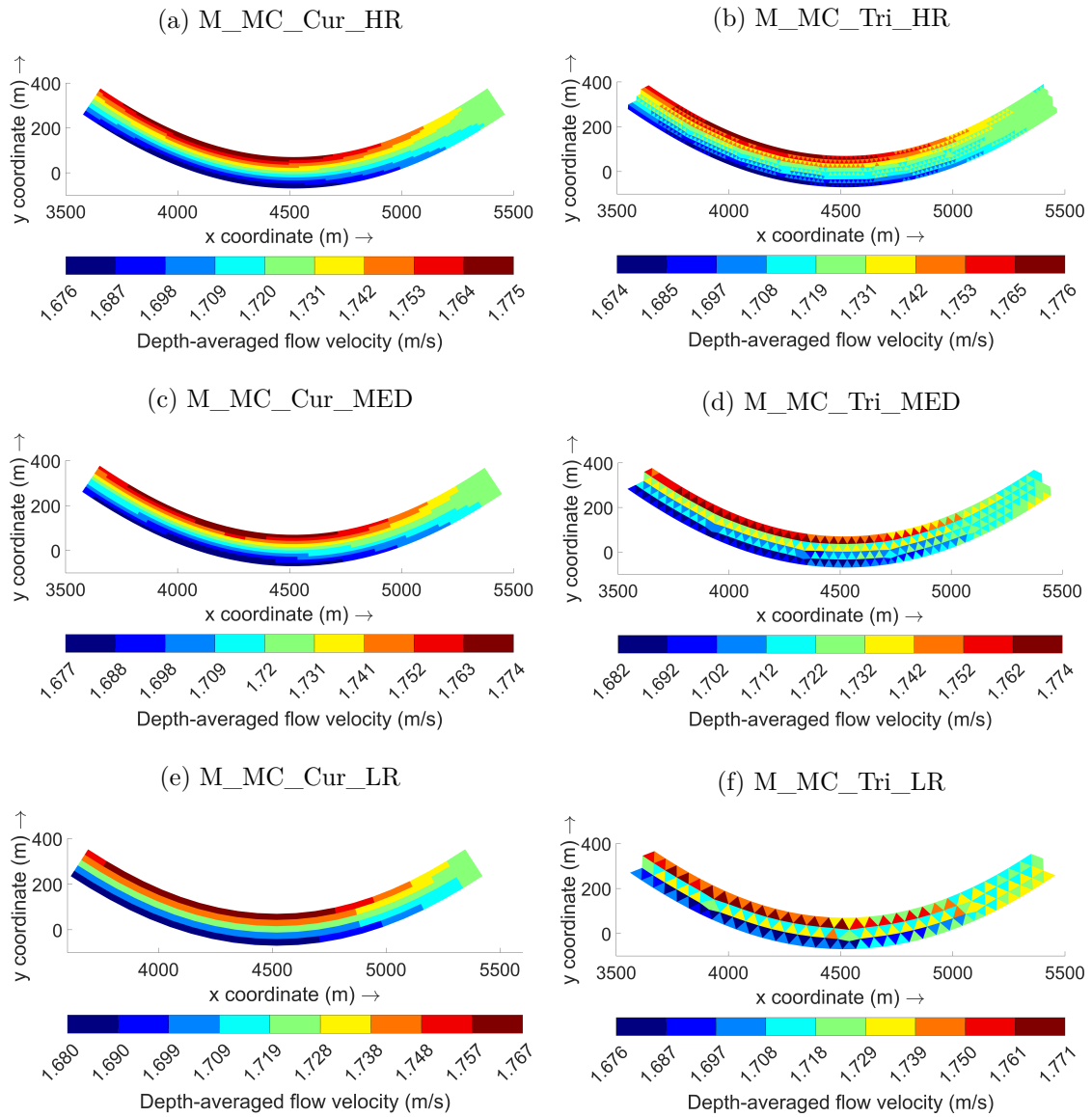


Figure D.2: Map-plots of the simulated depth-averaged flow velocities for the mild river meander (main channel case) with the lowest discharge range by the six considered grids. Regarding the names: M stands for mild; MC for main channel; Cur and Tri for respectively curvilinear and triangular; and HR, MED and LR for high, medium and low resolution respectively.

## D.2 Sharp river meander (main channel case)

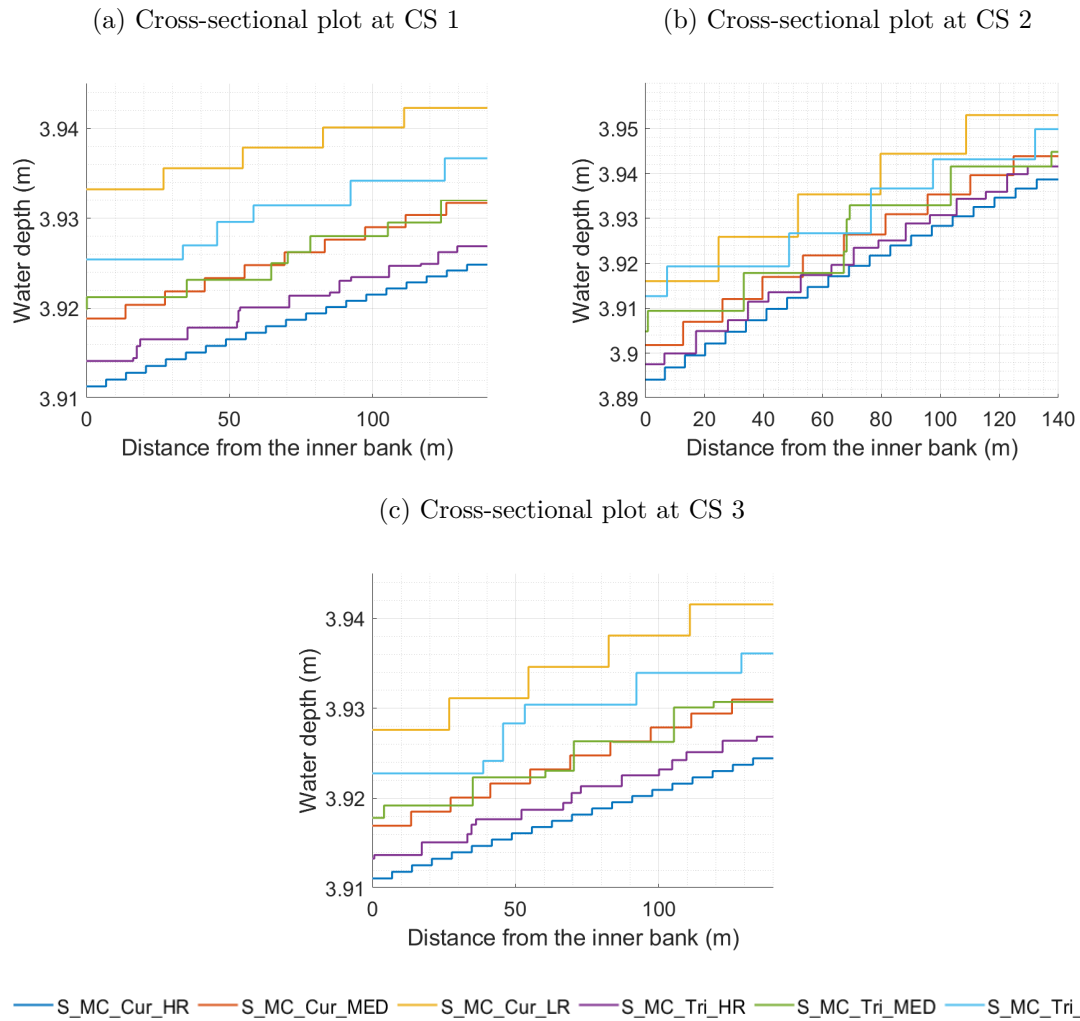


Figure D.3: Cross-sectional view of the simulated water depth for the Sharp river meander (main channel case) with the lowest discharge range at CS 1, CS 2 and CS 3 by the six considered grids. Regarding the names: S stands for sharp; MC for main channel; Cur and Tri for respectively curvilinear and triangular; and HR, MED and LR for high, medium and low resolution respectively.

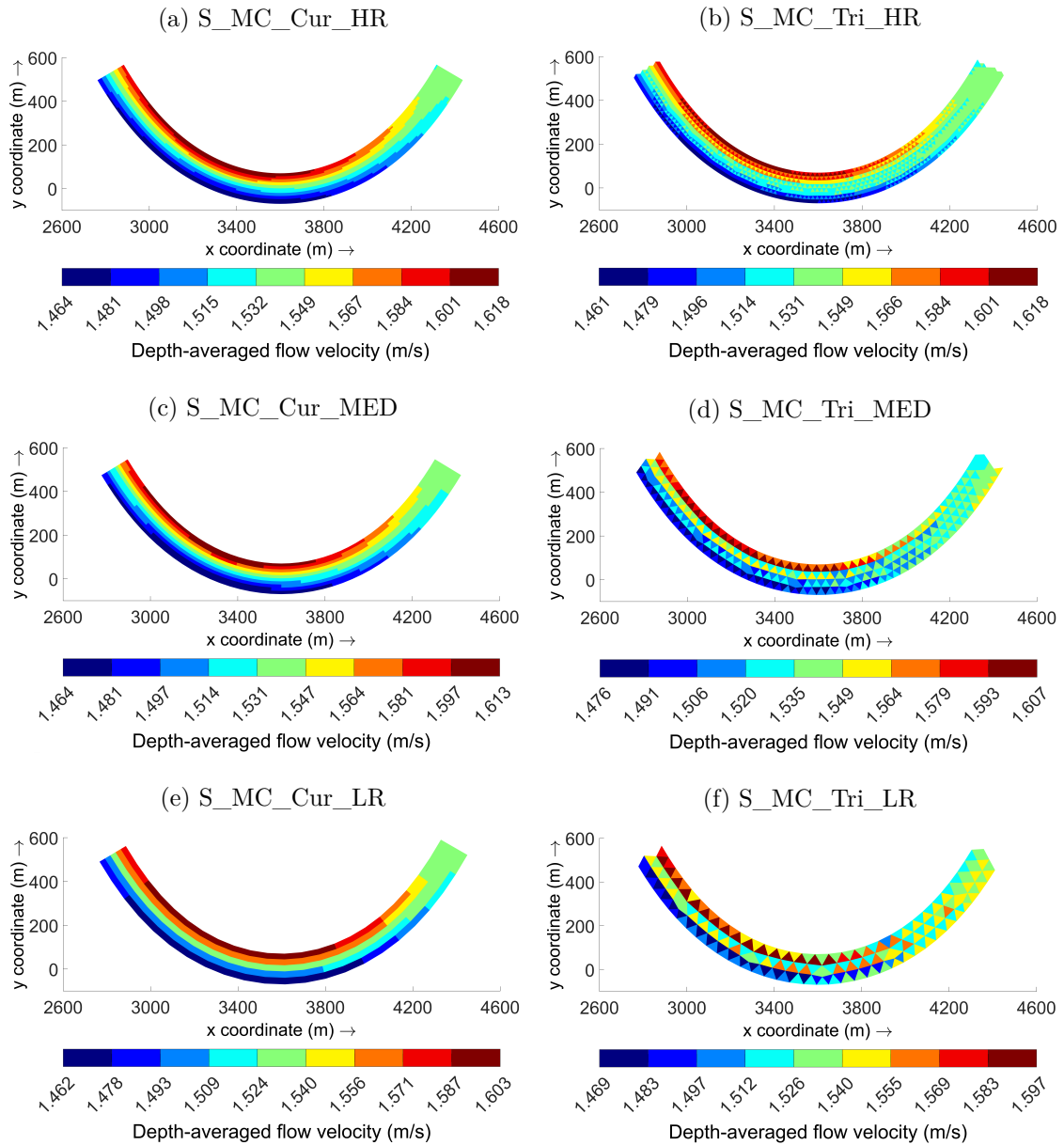


Figure D.4: Map-plots of the simulated depth-averaged flow velocities for the Sharp river meander (main channel case) with the lowest discharge range by the six considered grids. Regarding the names: S stands for sharp; MC for main channel; Cur and Tri for respectively curvilinear and triangular; and HR, MED and LR for high, medium and low resolution respectively.

### D.3 Mild river meander (main channel and floodplain case)

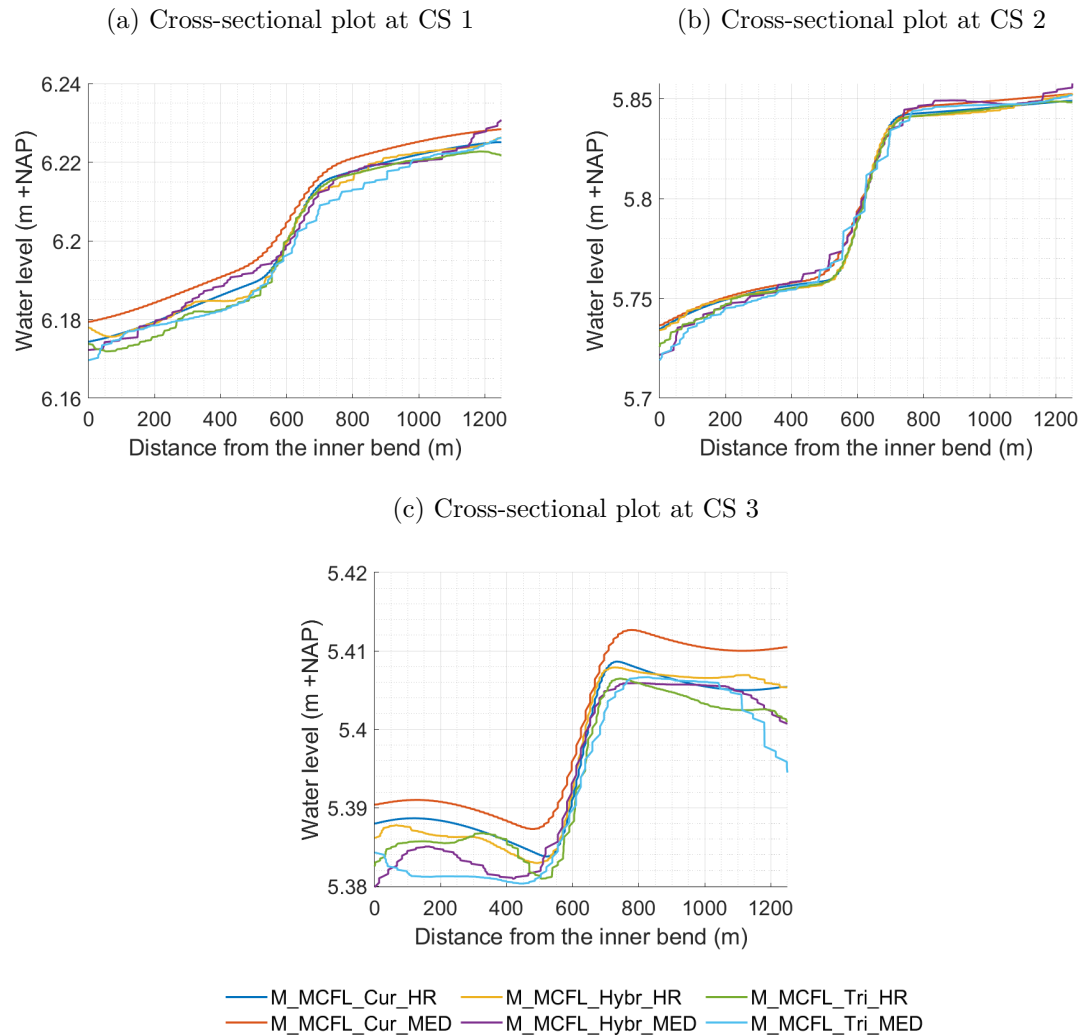


Figure D.5: Cross-sectional view of the simulated water level in the mild river meander (main channel and floodplain case) for the highest discharge range at CS 1, CS 2 and CS 3 by the six considered grids. Regarding the names: M stands for mild; MCFL for main channel & floodplains; Cur, Tri and Hybr for respectively curvilinear, triangular and hybrid; and HR and MED for high and medium resolution respectively.

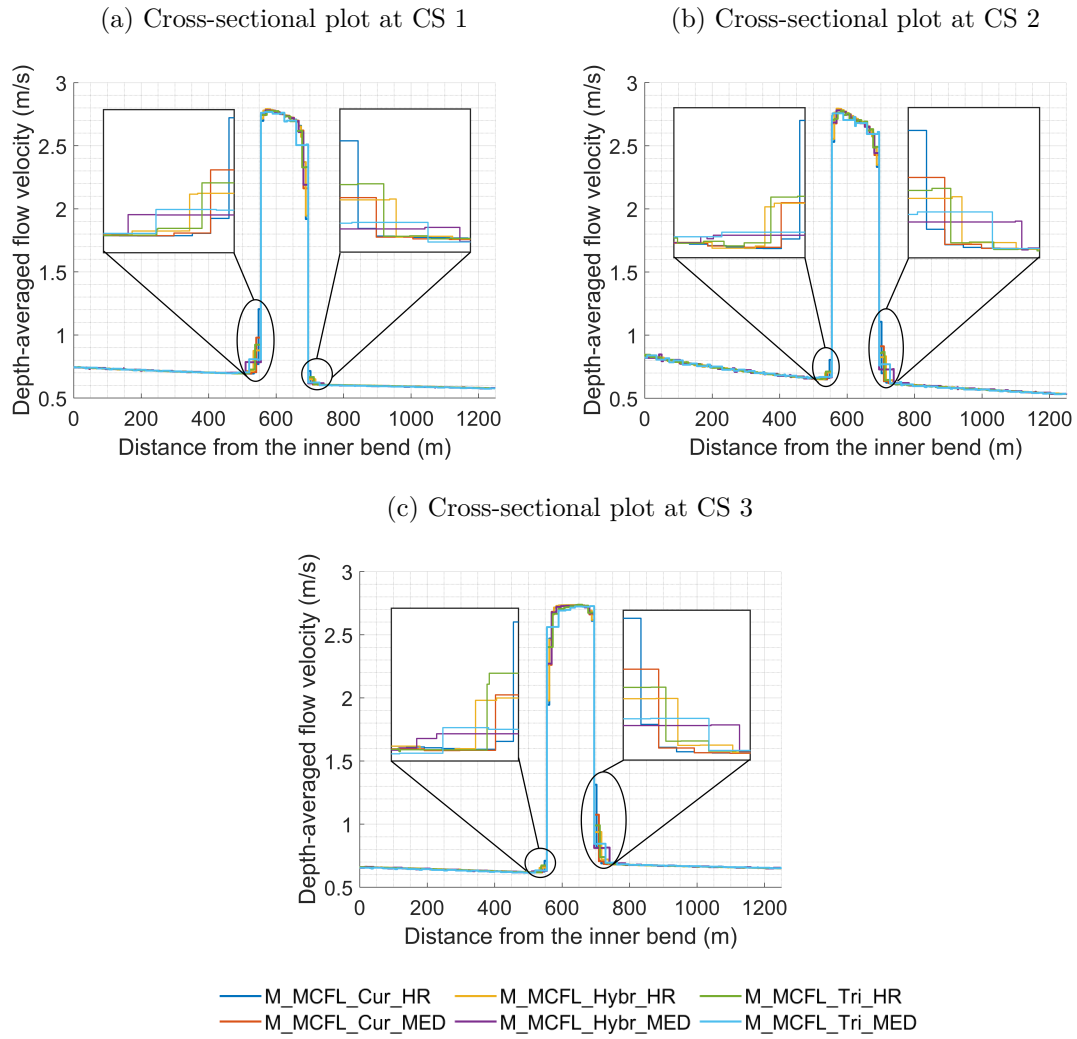


Figure D.6: Cross-sectional view of the simulated depth-averaged flow velocity in the mild river meander (main channel and floodplain case) for the highest discharge range at CS 1, CS 2 and CS 3 by the six considered grids. Regarding the names: M stands for mild; MCFL for main channel & floodplains; Cur, Tri and Hybr for respectively curvilinear, triangular and hybrid; and HR and MED for high and medium resolution respectively.

## E Results: case study

### E.1 River bend (small floodplain areas)

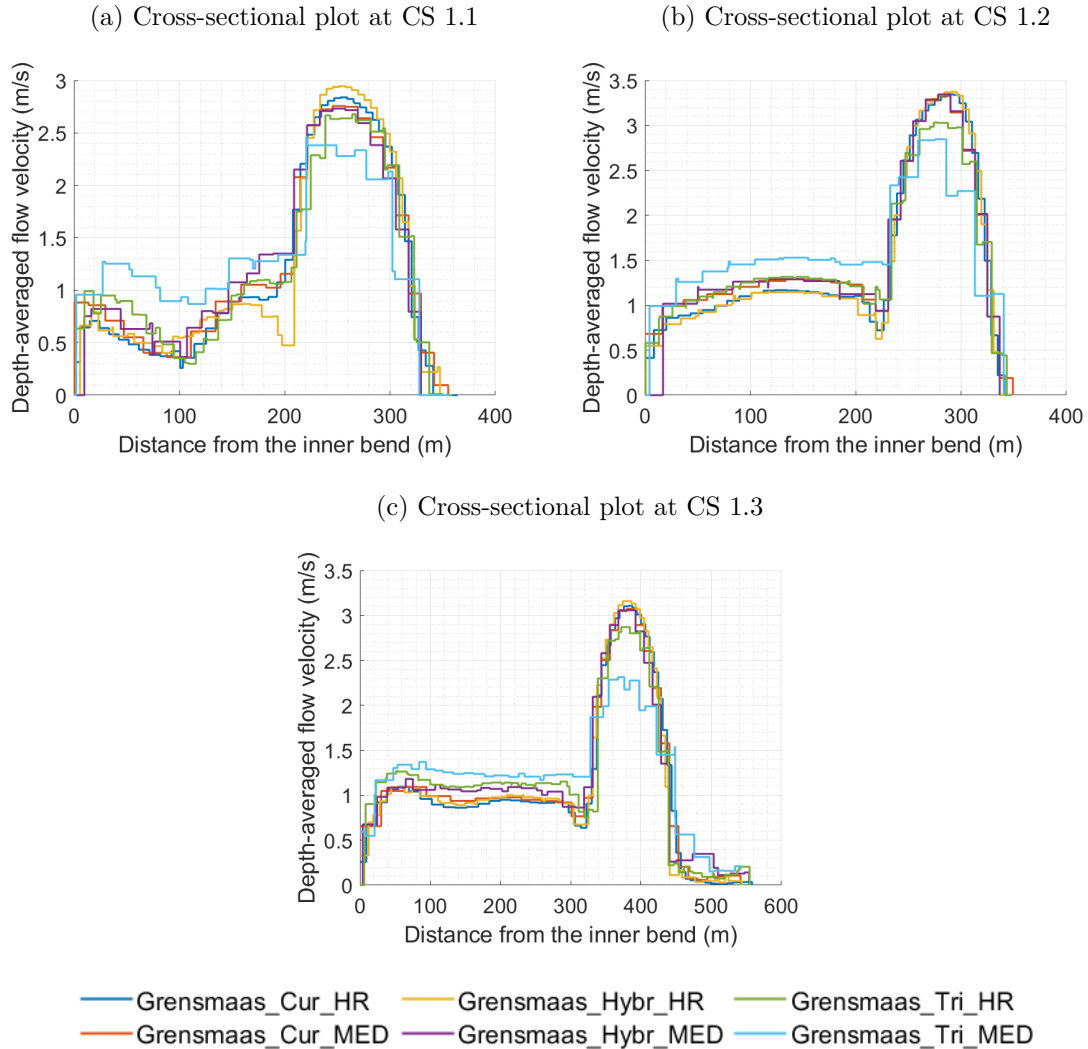


Figure E.1: Cross-sectional view of the simulated depth-averaged flow velocities for the medium discharge range of the six grids for the case study at CS 1.1, CS 1.2 and CS 1.3. Regarding the names: Grensmaas stands for the Grensmaas river; Cur, Tri and Hybr for respectively curvilinear (as much as possible), triangular and hybrid; and HR and MED for high and medium resolution respectively.

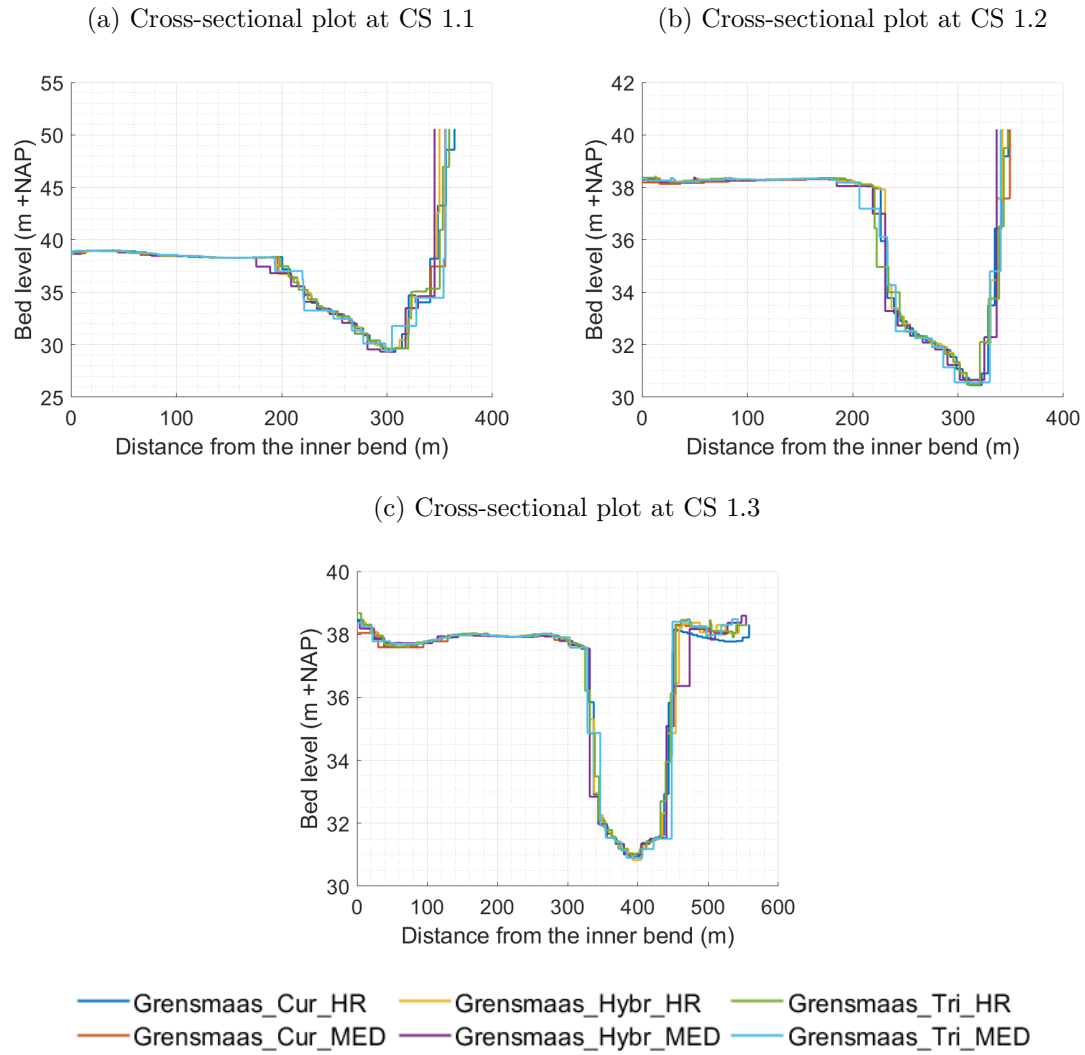


Figure E.2: Cross-sectional view of the bathymetry of the six grids for the case study at CS 1.1, CS 1.2 and CS 1.3. Regarding the names: Grensmaas stands for the Grensmaas river; Cur, Tri and Hybr for respectively curvilinear (as much as possible), triangular and hybrid; and HR and MED for high and medium resolution respectively.

## E.2 River bend (wide floodplain areas)

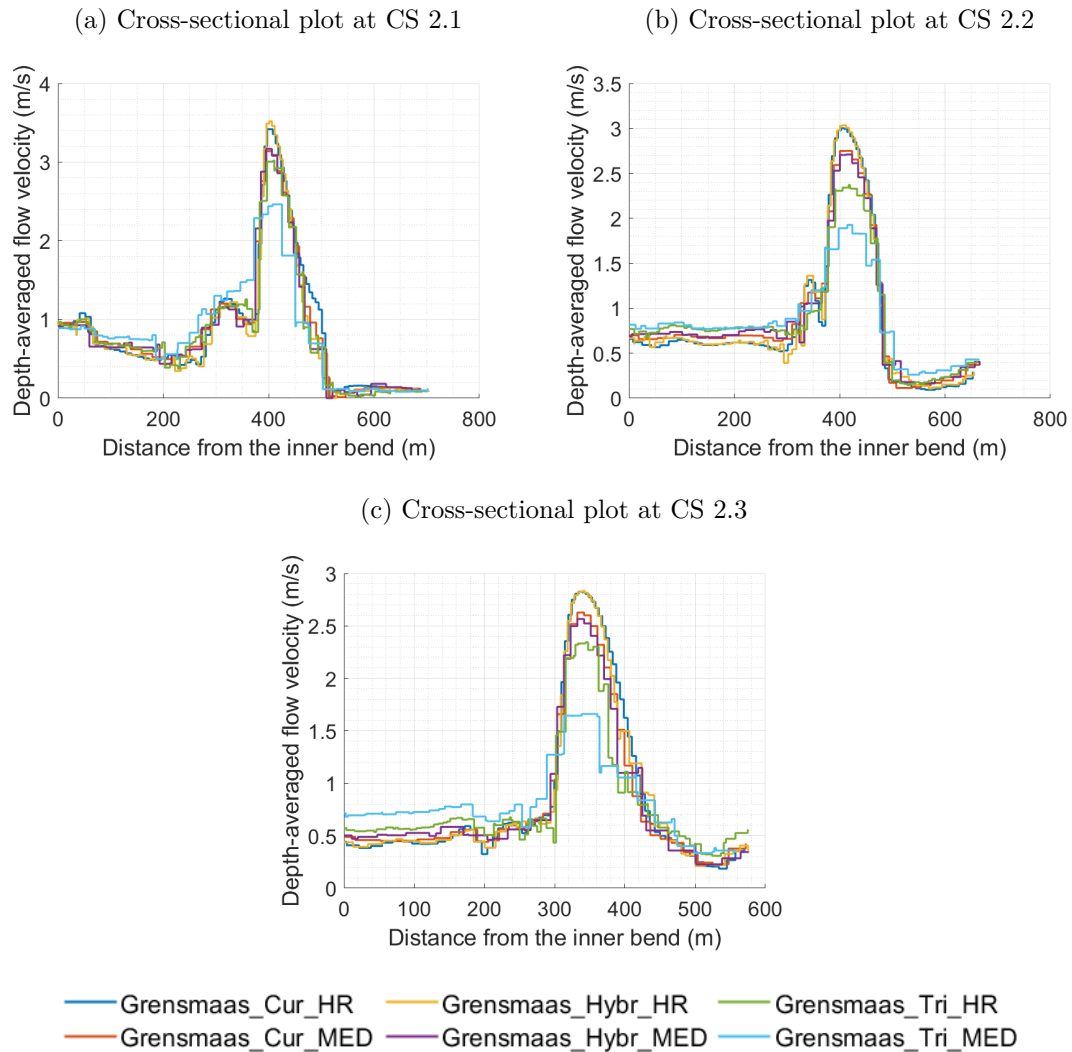


Figure E.3: Cross-sectional view of the simulated depth-averaged flow velocities for the medium discharge range of the six grids for the case study at CS 2.1, CS 2.2 and CS 2.3. Regarding the names: Grensmaas stands for the Grensmaas river; Cur, Tri and Hybr for respectively curvilinear (as much as possible), triangular and hybrid; and HR and MED for high and medium resolution respectively.

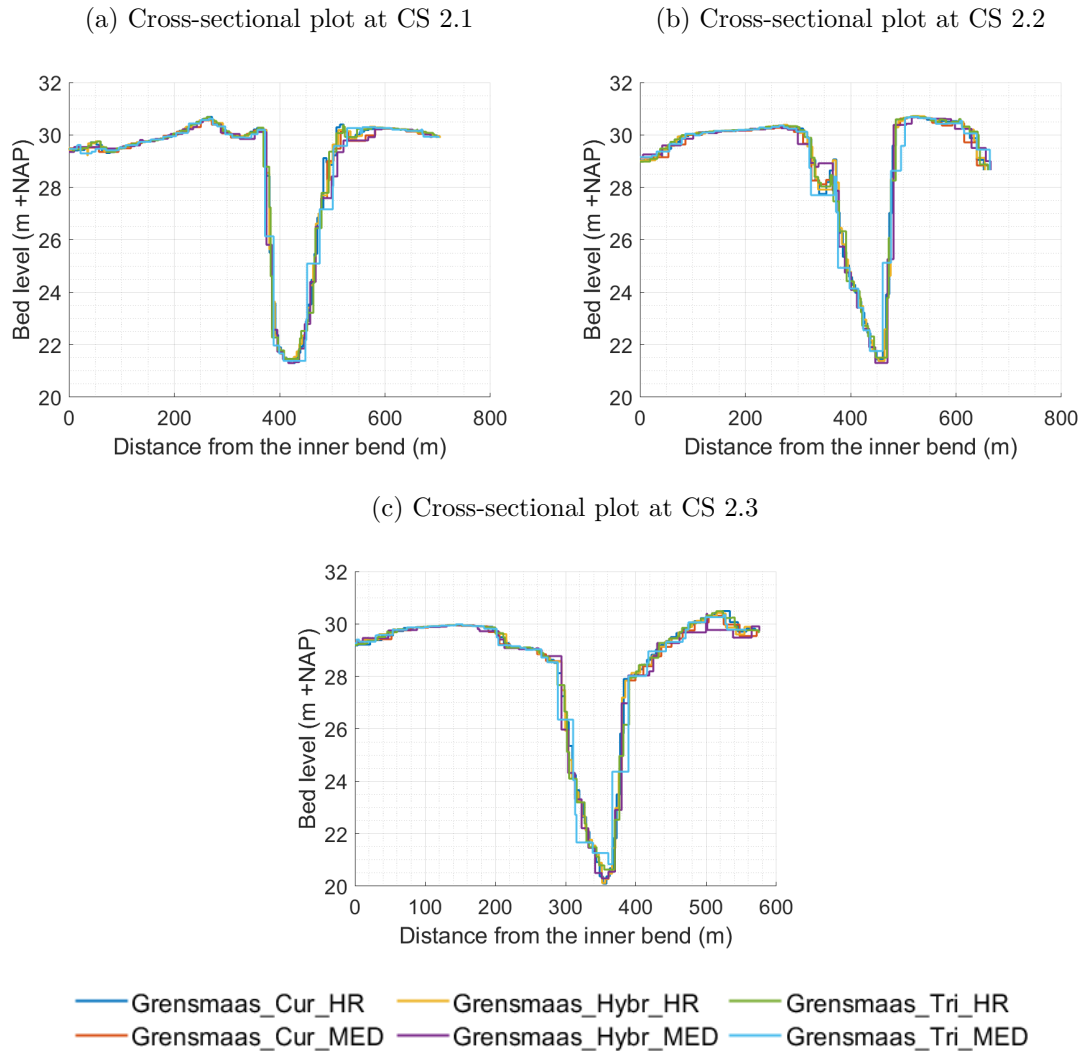


Figure E.4: Cross-sectional view of the bathymetry of the six grids for the case study at CS 2.1, CS 2.2 and CS 2.3. Regarding the names: Grensmaas stands for the Grensmaas river; Cur, Tri and Hybr for respectively curvilinear (as much as possible), triangular and hybrid; and HR and MED for high and medium resolution respectively.